

# **ENE417-G 23H**

## **Hydrogen and Fuel Cell Technologies**

Submitted By,



Md Iftekher Hossain

Mail: [mdih@uia.no](mailto:mdih@uia.no)



Opy Das

Mail: [opyd@uia.no](mailto:opyd@uia.no)



Anfaj Islam

Mail: [anifaji@uia.no](mailto:anifaji@uia.no)

Date  
23rd of November, 2023

# Table of Contents

Table of Contents .....	i
List of Figures .....	iii
<b>Chapter 1: PEM Stack &amp; Testing.....</b>	<b>1</b>
1.1    describing the 10 cell stack .....	1
1.1.1    Description for the stack and all of the components .....	1
1.1.2    Stacking Process to Make Up the 10 Cells.....	7
1.1.3    Function of the Channels in the Plates .....	9
1.1.4    Sealing of Plates to Avoid Gas Crossover and Leaks .....	11
1.2    Measuring the iv characteristics .....	12
1.2.1    Characterization PEM Introduction to Testing the Horizon 10 Cell PEM Stack .....	12
1.2.2    Characterization PEM Measuring the IV Behaviour of the Horizon 10 cell PEM Stack with Manual Measurement.....	15
1.2.2.1    Experimental setup .....	15
1.2.2.2    Experimental Data.....	16
1.2.2.3    IV Curve Based on Experimental Data.....	16
1.2.2.4    IP Curve Based on Experimental Data .....	17
1.2.2.5    Mode of Control .....	17
1.2.2.6    Power Density Curve (I-P Curve) .....	19
1.2.3    Characterization PEM Measuring the IV Behaviour of the Horizon 10 cell PEM Stack with LabVIEW.....	21
1.2.3.1    Comparison with Manual Measurements .....	24
1.2.4    Characterization PEM Measuring the IV Behaviour of the Horizon 10 cell PEM Stack with Zahner System .....	25
1.2.4.1    Hysteresis in the I-V Plot.....	26
<b>Chapter 2: SOFC Single Cell Setup and Testing by EIS .....</b>	<b>29</b>
2.1 SOFC Setting up .....	29
2.1.1    Characterization Techniques - SOFC Setup For Single Cell Testing.....	29
2.1.2    Characterisation Techniques - Setting up the SOFC for EIS Spectroscopy.....	38
2.2 EIS equivalent circuit board.....	40
2.3 Zahner EIS method .....	44
2.4 EIS spectrum obtained (Nyquist and bode plot) .....	51
<b>Chapter 3: EIS on an Electrochemical Equivalent Circuit with real lab measurements .....</b>	<b>53</b>
3.1    Describe The Method to Use Eis (Electrochemical Impedance Spectroscopy) To Determine The Characteristics For The Electrochemical Equivalent Circuit .....	53
3.2    Introduction of the Topic .....	55

3.3	Background Theory .....	59
3.4	The Real Lab Experiment Using The Iviumstat Eis Equipment.....	69
3.5	Results and Discussion.....	74
3.5.1	Anode and Cathode Contact.....	74
3.5.2	Electrolyte .....	74
3.5.3	Capacitor.....	75
3.5.4	Inductor.....	76
3.5.5	Inductor and Capacitor.....	77
3.5.6	Anode and cathode reaction .....	78
3.5.7	Complete cell reaction.....	79
3.5.8	Determining the value of components from Ivium Software .....	83
<b>Chapter 4:</b>	<b>Final Project.....</b>	<b>87</b>
4.1	Introduction .....	87
4.2	Theoretical Background .....	89
4.2.1	Electrochemical Aspects .....	89
4.2.2	I-V Curve and Power Density Curve .....	92
4.3	Methodology .....	93
4.3.1	Design Process: SolidWorks Steps .....	93
4.3.2	Fabrication and Assembling .....	96
4.3.2.1	Base .....	96
4.3.2.2	Screw .....	97
4.3.2.3	Carbon Paper .....	98
4.3.2.4	Nickel Foam .....	99
4.3.2.5	Nafion .....	100
4.3.2.6	Gasket .....	101
4.3.3	Experimental setup.....	102
4.4	Result and analysis .....	106
4.5	Conclusion .....	109
<b>Chapter 5:</b>	<b>References.....</b>	<b>111</b>
<b>Chapter 6:</b>	<b>Acknowledgement .....</b>	<b>113</b>

# List of Figures

Figure 1.1. Main housing of PEM 10 stack fuel cell (bottom part).....	2
Figure 1.2. Both surfaces of end plate (a) bottom surface that remains in contact with main housing (b) Upper surface that contains architecture.....	3
Figure 1.3. Bipolar plate (a) Serpentine shaped architecture for H <sub>2</sub> fuel (b) Straight channel architecture for air. ....	4
Figure 1.4. Membrane Electrode Assembly (MEA) that is responsible for the conversion of chemical energy into electrical energy.....	5
Figure 1.5. Fan assembly to supply air in the stack and current leads to collect generated current. ....	6
Figure 1.6. The overall unit-wise structure of the fuel cell. ....	8
Figure 1.7.Clamped compact whole stack of Fuel cell. ....	9
Figure 1.8. The embedded channels on bipolar plates (a)serpentine for H <sub>2</sub> fuel, (b) straight parallel channel on the air side.....	10
Figure 1.9. Sealing of plates to avoid gas crossover and leaks (a) Gasket to refrain overflow of gases (b) silicon over-ring rubber over the gas flow path to stop gas cross over. ....	11
Figure 1.10. Test setup of PEM stack.....	12
Figure 1.11. General Layout of the setup with stack in the background and the resistance box and DVMs in the foreground. ....	15
Figure 1.12. IV behaviour of the Horizon 10 cell PEM stack. ....	16
Figure 1.13. IP behaviour of the Horizon 10 cell PEM stack.....	17
Figure 1.14. IV Characteristic curve for PEM stack.....	17
Figure 1.15. Power density curve for stack. ....	20
Figure 1.16. IV and Ip curve of PEM cell based on Experimental Data. ....	20
Figure 1.17. Automatically plotted I-V curve and I-P curve from Potential..	21
Figure 1.18. Temporary increment in voltage due to increased resistance. ....	22
Figure 1.19. Smoother I-V curve. ....	23
Figure 1.20. I-V behaviour curve of PEM stack with active region and ohmic region.....	24
Figure 1.21. IV Characteristic curve for PEM stack.....	25

Figure 1.22. Hysteresis in I-V curve due to various losses. ....	26
Figure 2.1. (a) The housing of SOFC, (b) Placement of Mica seal with help of scotch tape.....	30
Figure 2.2. (a) Utilization of syringe with the help of air pump to implant glass sealant, (b) Implanted glass sealant (white material) along the circumference.....	30
Figure 2.3 Electrical connectivity at the anode side of the cell with Nickel mesh current collector.....	31
Figure 2.4 Single cell unit of SOFC (a) Cathode side of the single cell, (b) Anode side of the single cell. ....	31
Figure 2.5 Applying weight on the arrangement to provide another layer of glass sealant. ....	32
Figure 2.6 (a) Additional insulation layer of Aluminum felt on top of the arrangement, (b) Cathode current collector.....	33
Figure 2.7 (a) Installation of thermocouple to measure temperature, (b) Final piece of insulation sheet placed on top of thermocouple. ....	34
Figure 2.8 The top housing of SOFC. ....	34
Figure 2.9 Utilization of tie rods to secure the whole assembly of the fuel cell. ....	35
Figure 2.10 (a) Securely fastening the screws of the springs and accurately aligning the tie rods, (b) Twisting of contact wires to minimize noise. ....	35
Figure 2.11 The whole setup of SOFC in upside down position. ....	36
Figure 2.12 (a) oven or furnace, manufactured by Rohde group, (b) The entire setup placed at the oven to heat it up to operating temperature. ....	37
Figure 2.13 Mass flow controller at the top left-hand side of the fume hood. ....	37
Figure 2.14 Flow chart of setting up the SOFC.....	38
Figure 2.15 The complete set up with the connecting leads for the measurement. ....	39
Figure 2.16 (a) The back side of the Zahner system, (b) The human- machine interface to operate the experiment. ....	39
Figure 2.17 Electrochemical Equivalent Circuit .....	40
Figure 2.18 The ear side of the Electrochemical equivalent Circuit .....	41
Figure 2.19 Impedance spectroscopy of the screen.....	45

Figure 2.20 Main Screen of Software.....	45
Figure 2.21 Control Potentiostat Bar .....	46
Figure 2.22 Open Circuit Voltage of the SOFC.....	47
Figure 2.23 Selection of frequency .....	48
Figure 2.24 The frequency and amplitude set at required value .....	49
Figure 2.25 The whole window of setting the EIS spectroscopy. ....	49
Figure 2.26 The Recording Bar.....	50
Figure 2.27 Bode plot of Impedance.....	51
Figure 2.28 The Nyquist plot of impedance of SOFC fuel Cell .....	52
Figure 3.1 Ivium Equivalent Circuit Evaluator .....	54
Figure 3.2 EIS equivalent circuit .....	56
Figure 3.3 Nyquist Plot of RC circuit .....	57
Figure 3.4 Bode Plot of RC Circuit.....	58
Figure 3.5. Charge double layer at the cathode surface of a fuel cell.....	61
Figure 3.6. A representation of the equivalent circuit of electrochemical system.....	63
Figure 3.7. Nyquist, Bode magnitude and phase angle plots of some model circuits. $R1 = 1k \Omega$ .....	65
Figure 3.8. Nyquist, Bode magnitude, and phase angle plots of some model circuits. .....	68
Figure 3.9. Impedance mode at <b>IVIUMSTAT software</b> .....	70
Figure 3.10. Submenu for selection of the Current .....	71
Figure 3.11. Frequency selection panel .....	72
Figure 3.12. Anode and cathode contact resistances (a) Anode contact Nyquist plot (b) Cathode contact Nyquist plot.....	74
Figure 3.13. Nyquist plot for the electrolyte of the electrolyser.....	75
Figure 3.14. Nyquist plot for the $1000\mu F$ capacitor.....	75
Figure 3.15. Nyquist plot for the $150\mu H$ inductor.....	76
Figure 3.16. Nyquist plot for the series combination of inductor and capacitor. ....	77
Figure 3.17. Nyquist plot for (a) Anode reaction, (b) Cathode reaction, bode plot – Real part of impedance for (c) Anode (d) cathode, Bode plot – Imaginary part of impedance for (e) Anode (f) cathode. ....	78

Figure 3.18. (a) Nyquist plot for the complete cell (b) Bode plot of real impedance (c) Bode plot of imaginary portion of impedance for the complete cell. ....	80
Figure 3.19. Circuit behaviour at low and high experimental frequency condition. ....	80
Figure 3.20. Complete equivalent representation of the electrochemical system.....	82
Figure 3.21 Determined value of resistance from Nyquist plot of Anode Contact. ....	83
Figure 3.22 Determined value of resistance from Nyquist plot of Anode Reaction.....	83
Figure 3.23 Determined value of resistance from Nyquist plot of Cathode Reaction.....	84
Figure 3.24 Determined value of resistance from Nyquist plot of Cathode Contact. ....	84
Figure 3.25 Determined value of resistance from Nyquist plot of Complete cell. ....	84
Figure 3.26 Determined value of resistance from Nyquist plot of Electrolyte. ....	85
Figure 3.27 Determined value of resistance from Nyquist plot of Capacitor. ....	85
Figure 3.28 Determined value of resistance from Nyquist plot of Inductor. ....	85
Figure 3.29 Complete Circuit measured resistance value by Ivium Software .....	86
Figure 4.1. A typical single PEMFC schematic. ....	90
Figure 4.2. I-V Curve and Power Density Curve. ....	92
Figure 4.3. Distinguishable structures of the housing of PEM cell.....	95
Figure 4.4. Artillery Sidewinder X2 3D Printer. ....	97
Figure 4.5. Different views of 3D printed base. ....	97
Figure 4.6. M-6 screw. ....	98
Figure 4.7. (a) 5% Nafion Resin and PTC 40% (b) 2-Propoanol (c) Mixer of 5% Nafion Resin and PTC 40% (d) Platinum Catalyst Coating of Carbon Paper.....	99
Figure 4.8. Current collector, Nickel Foam, Carbon Paper from left to right. ....	100

Figure 4.9. (a) Humidification process of Nafion (b) Nafion after humidification.....	101
Figure 4.10. Gasket.....	102
Figure 4.11. Complete structure of the PEM cell.....	102
Figure 4.12. Hydrogen Fuel Tank .....	103
Figure 4.13. Hydrogen and Oxygen Inlet.....	103
Figure 4.14. Control of H <sub>2</sub> and O <sub>2</sub> flow to the PEM cell.....	104
Figure 4.15. PEM fuel cell anode and cathode contact. ....	104
Figure 4.16. Experimental Setup.....	105
Figure 4.17. Humidification of Fuel Cell. ....	105
Figure 4.18. IV characteristics of the PEM cell under three different test cases. ....	107
Figure 4.19. I-P characteristics of the PEM cell under three different test cases. ....	109



# Chapter 1: PEM Stack & Testing

---

## 1.1 DESCRIBING THE 10 CELL STACK

### 1.1.1 Description for the stack and all of the components

Because a fuel cell functions at a low voltage (i.e., well below 1 V), it is customary to build up the voltage to the desired level by electrically connecting cells in series to form a ‘stack’. There are a number of different designs of fuel cell, but in each case the unit cell has certain components in common. The given disassembled parts contribute to a horizontal PEM fuel cell that consists of 10 identical stacks. The entire compact configuration can be labelled into five distinguishable parts such as:

1. **Main Housing:** As shown in Figure 1.1, the Main Housing of the PEM fuel cell is a crucial component that incorporates four electrically isolated tie rods. By preventing any potential short circuits between the electrodes, these tie rods contribute to the overall reliability and performance of the fuel cell stack. The gold-plated inner surface of the main housing serves as an excellent conductor of electricity, facilitating the efficient flow of electrons within the fuel cell. This gold plating enhances the electrical conductivity of the housing, further optimizing the overall performance of the PEM fuel cell. To establish a secure and reliable connection between the main housing and the associated end plate, a portion of the gold-plated surface is covered with graphite tape. This graphite tape acts as a bridge, providing a firm and stable contact point that helps maintain a consistent electrical pathway and minimize resistance. The combination of the gold-plated inner surface and the graphite tape ensures not only electrical conductivity but also mechanical stability within the fuel cell. This robust connection between the main housing and the end

plate contributes to the overall structural integrity of the fuel cell stack, allowing it to withstand various mechanical stresses and vibrations encountered during operation.

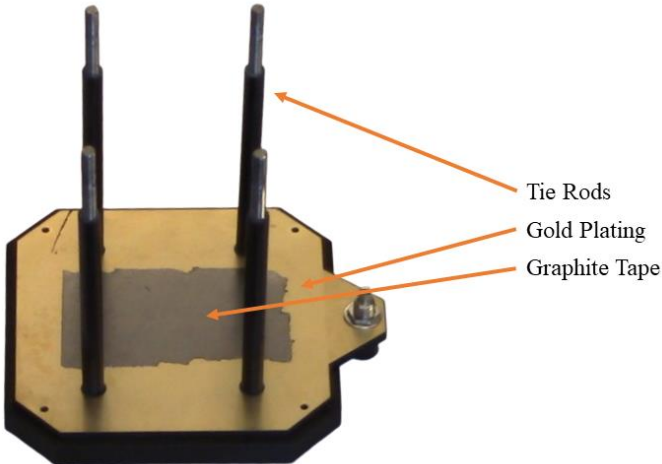


Figure 1.1. Main housing of PEM 10 stack fuel cell (bottom part).

**2. End Plate:** The End Plate is an essential component of the PEM fuel cell, serving multiple functions to ensure proper functioning and gas circulation within the cell. On one side, the end plate features a smooth surface that establishes contact with one of the end plates, creating a secure connection (Figure 1.2(a)). The other surface of the end plate is designed with distinct architectures that govern the circulation of hydrogen (bottom plate) and air (upper plate) within the immediate cell vicinity (Figure 1.2 (b)) To prevent any gas leakage, the end plate incorporates a rubber ring seal. This seal is specifically manufactured to fit easily within the groove of the architectural surface, providing an effective barrier against gas leaks.

During assembly, the end plate is carefully positioned over the main housing using the tie rods. This ensures proper alignment and connection between the end plate and the main housing, creating a robust and reliable structure. At the upper side of the end plate structures, there are two separate channels dedicated to the flow of hydrogen. These channels are strategically placed

directly over the extruded holes of the Membrane Electrode Assembly (MEA) and bipolar plates, allowing for efficient and controlled hydrogen flow within the fuel cell.

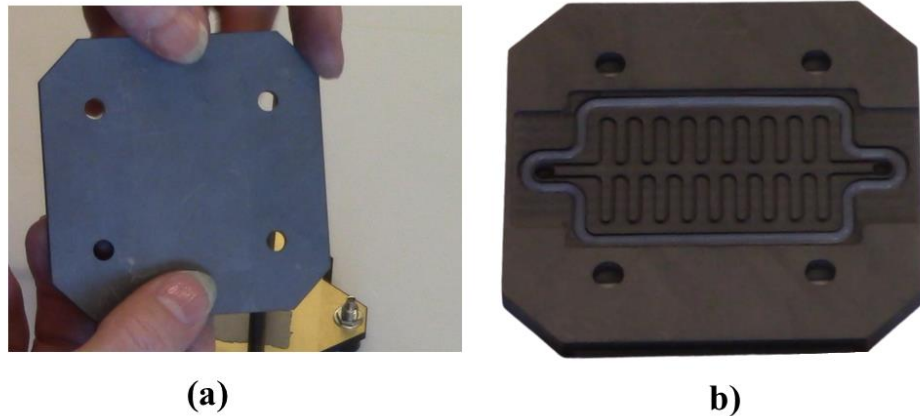


Figure 1.2. Both surfaces of end plate (a) bottom surface that remains in contact with main housing (b) Upper surface that contains architecture.

The design and placement of the end plate plays a crucial role in optimizing gas circulation, maintaining gas tightness, and facilitating the smooth operation of the PEM fuel cell. These features contribute to the overall performance and reliability of the fuel cell system, making it a viable and efficient energy conversion solution.

**3. Bipolar Plate:** The bipolar plates in a fuel cell are similar in structure to the end plates, with both surfaces containing specific architectures. However, unlike the end plates, the bipolar plates are positioned between the Membrane Electrode Assembly (MEA) layers.

The bipolar plates are designed with channels or architectures that enable the smooth flow of gas through the fuel cell stack, ensuring the delivery of reactants to all electrodes. The wall through which Hydrogen gas is needed to be flown the embedded channels are made serpentine whereas, it is straight parallel channel on the air side, as presented in Figure 1.3(a)-(b). These channels are intricately sculpted into the walls of the bipolar plates, ensuring

that there is no gas mixture trapped inside the cell. Additionally, this design allows for the recirculation of fuels among the electrodes, ensuring efficient utilization of all the fuel. By facilitating proper gas distribution and fuel recirculation, the bipolar plates significantly enhance the overall efficiency of the fuel cell.

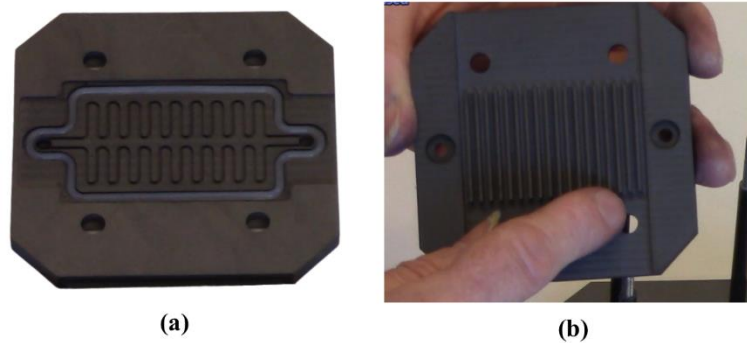


Figure 1.3. Bipolar plate (a) Serpentine shaped architecture for H<sub>2</sub> fuel (b) Straight channel architecture for air.

**4. Membrane Electrode Assembly (MEA):** Illustrated in Figure 1.4, At the heart of these fuel cells lies the Membrane Electrode Assembly (MEA), a critical component responsible for the conversion of chemical energy into electrical energy. The PEM MEA is compressed between two graphite plates which have been catalyst coated. Also, it is equipped with holes over both ends of the MEA. Holes are carefully positioned to feed the reactants into the channels that run over the surface of the electrodes. The air side of MEA has two silicon o-ring rubber so that the gas cannot cross over. Another striking feature of MEA is that on both sides small holes are embedded through the MEA to percolate the reactants through the electrodes. Point to be noted, the holes in the air circulation side are bigger in diameter, whereas the holes in the hydrogen side are finer. It should be noted that the hydrogen side of the MEA is oriented at the hydrogen face of bipolar plate. The MEA is composed of

three essential layers: the catalyst layer, the proton exchange membrane, and the gas diffusion layer.

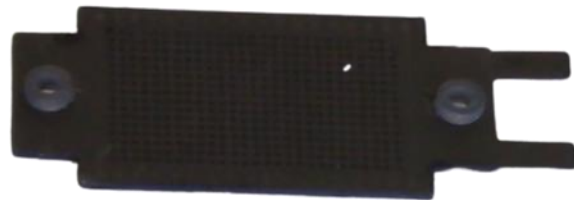


Figure 1.4. Membrane Electrode Assembly (MEA) that is responsible for the conversion of chemical energy into electrical energy.

- a) **Catalyst Layer:** The catalyst layer consists of finely dispersed catalyst particles, typically platinum-based, supported on carbon material. This layer facilitates electrochemical reactions, acting as a catalyst for the fuel cell's anode and cathode reactions.
- b) **Electrolytes:** An electrolyte medium that conducts ions. This may be a porous solid that contains a liquid electrolyte (acid, alkali or fused salt) or a thin solid membrane that may be a polymer or a ceramic. The membrane must be an electronic insulator as well as a good ionic conductor and must be stable under both strong oxidizing and strong reducing conditions. In PEM, the proton exchange membrane is used as electrolyte, usually made of a perfluoro sulfonic acid polymer such as Nafion, separates the anode and cathode compartments while allowing the passage of protons.
- c) **Gas Diffusion Layer:** The gas diffusion layer aids in the distribution of reactants and facilitates the removal of products. Normally the gas diffusion layers are of two types depending on the reaction that takes place on them.
  - i. **Anode:** A negative fuel electrode (anode) that incorporates an electrocatalyst, which is dispersed on an electronically conducting

material. The electrode is fabricated so that the electrocatalyst, the electrolyte and the fuel come into simultaneous contact at a three-phase boundary.

**ii. Cathode:** A positive electrode (cathode), also with a triple-point electrocatalyst, at which the incoming oxygen (either alone or in air) is reduced by uptake of electrons from the external circuit.

5. **Fan:** For the optimum air circulation through the stack a fan is connected to the cathode (as shown in Figure 1.5) in such a way that air can flow through the channels maintaining sufficient flow pressure created through the distinct structure of bipolar plates.



Figure 1.5. Fan assembly to supply air in the stack and current leads to collect generated current.

A stack also has current collectors that are located at the two ends of the stack and are connected by end-plate assemblies.

During the operation of a PEM fuel cell, hydrogen gas enters the anode compartment, where it dissociates into protons and electrons. The protons pass through the proton exchange membrane, while the electrons are forced to travel through an external circuit, generating electrical current. At the cathode, oxygen gas combines with protons and electrons to produce water molecules. The MEA plays a crucial role in facilitating these reactions by

providing a platform for efficient catalyst utilization, proton conduction, and gas diffusion.

### 1.1.2 Stacking Process to Make Up the 10 Cells

Generally, the flat plate is by far the preferred geometry for fuel cells, and one way of assembling such cells in series is to connect the edge of each negative electrode to the positive of the next cell through the string. However, the problem with this method is that the electrons must flow across the face of the electrode to the current collection point. That's why the electrodes might be quite good conductors because if each cell is only operating at about 0.7 V, even a small voltage drop can be significant. Consequently, this type of stack design is not used unless the current flows are very low or the electrodes are particularly good conductors, and the dimensions of the stack are small.

A much better method of cell interconnection for planar fuel cells is to use a 'bipolar plate'. This is an electrically conducting plate that contacts the surfaces of the positive electrode of one cell and the negative electrode of the next cell, hence it is known as 'bipolar' plate. At the same time, the bipolar plate serves as a means of feeding oxygen to the negative anode and fuel gas to the positive cathode of the adjacent cells. This is achieved by having channels machined or moulded on either side of the plate along which the gases can flow and the products (i.e., pure water in the case of hydrogen fuel) can exit. Various designs of channel geometry have been proposed to maximize the access of gases and the removal of water, e.g., pin-type, series-parallel, serpentine, integrated and interdigitated flow-fields. The arrangement of the channels (also known as the 'flow-field') leads the bipolar plate to be also known as the flow-field plate. Bipolar plates must also be relatively impermeable to gases, sufficiently strong to withstand stack assembly and easily mass produced. They are made of a good electronic conductor such as graphite or stainless steel.

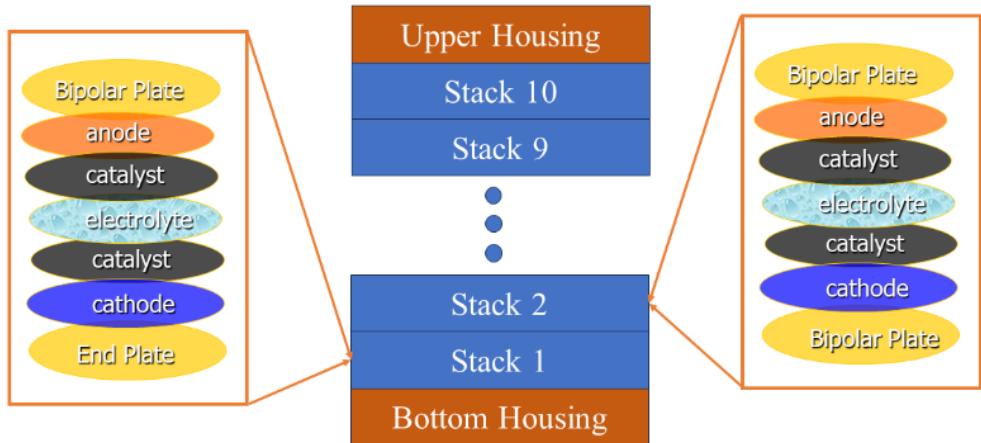


Figure 1.6. The overall unit-wise structure of the fuel cell.

The overall structure of the fuel cell unit-wise is depicted in Figure 1.6. At the bottom side of the structure there remains the main housing which is equipped with four tie rods that hold the 10 stacks together. The stack begins with an end plate from both sides, where one surface of the plate is flat that connects the main working portion of the cell with the current collectors in both side and the other surface is sculptured with architectures. To connect several cells in series, anode–electrolyte–cathode assemblies have to be prepared which is also to be known as MEA. These are then ‘stacked’ together with bipolar plates placed between each pair of cells. The stack has serpentine channels for feeding hydrogen over the anodes and horizontal channels for feeding oxygen (or air) over the cathodes. The result is a solid block, in which the electric current passes efficiently more or less straight through the cells, rather than over the surface of each electrode one after the other. The process of stacking together is repeated for 10 consecutive cells. After placing the stacks one by one on the housing, over the end plate at the top, a current collector is stacked which also contains channels to flow the Hydrogen fuel within the cell. In the end, the whole structure is clamped together to give a strong and robust device as presented in Figure 1.7

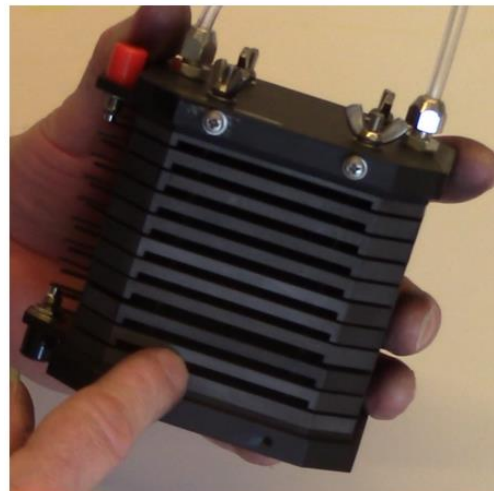


Figure 1.7.Clamped compact whole stack of Fuel cell.

### 1.1.3 Function of the Channels in the Plates

The architecture embedded over the bipolar or end plates are known as Flow Filed Plate (FFP). The FFP is an important component of the cell as it supplies fuel (hydrogen, H<sub>2</sub>), and oxidant (air, O<sub>2</sub>) to the MEA, removes water, and collects electrons produced. It also provides mechanical support for the MEA. The FFP has several roles, for example, it separates gases between the half cells and neighbouring cells in a stack; it provides sufficient rib area to provide an electronic conducting medium between the anode and cathode; it possesses a specific flow field design containing channels allowing even distribution of the reaction gases (low pressure drop for transport); it provides a solid structure for the MEA, and it facilitates water and heat management. In addition to that a good field should also prevent water condensation, remove water efficiently, and provide sufficiently high moisture content in the membrane. The design of FFP is influenced both by the plate material itself and by the adjoining Gas Diffusion Layer (GDL). The aim with any design of flow-field is to ensure that humidity is balanced throughout the cell and that gases can flow readily to and from each GDL.

In the assembled fuel cell, the surface through which Hydrogen gas is needed to be flown, the embedded channels are made serpentine whereas, it is straight parallel channel on the air side, as presented in Figure 1.8(a)-(b). The serpentine pattern is preferred by most PEMFC manufacturers. It offers a good compromise between the issues of pressure drop and water removal. The large number of turns in the flow path means that pressure drop is compromised, and this is overcome usually by employing multiple parallel serpentines rather than the single. Another reason for this kind of structure is to provide maximum surface area to make the H<sub>2</sub> to be able to impinge on the anode electrode as much as possible. Also, this architecture helps to avail the available H<sub>2</sub> on a recirculating manner thus reducing the loss of H<sub>2</sub> which in turn increases the overall efficiency of the cell. On the other hand, there are no such complexities associated with the flow of air. That's why a more fabrication friendly architecture can be used for the air side just to maintain uniform and constant flow of air over the electrodes.

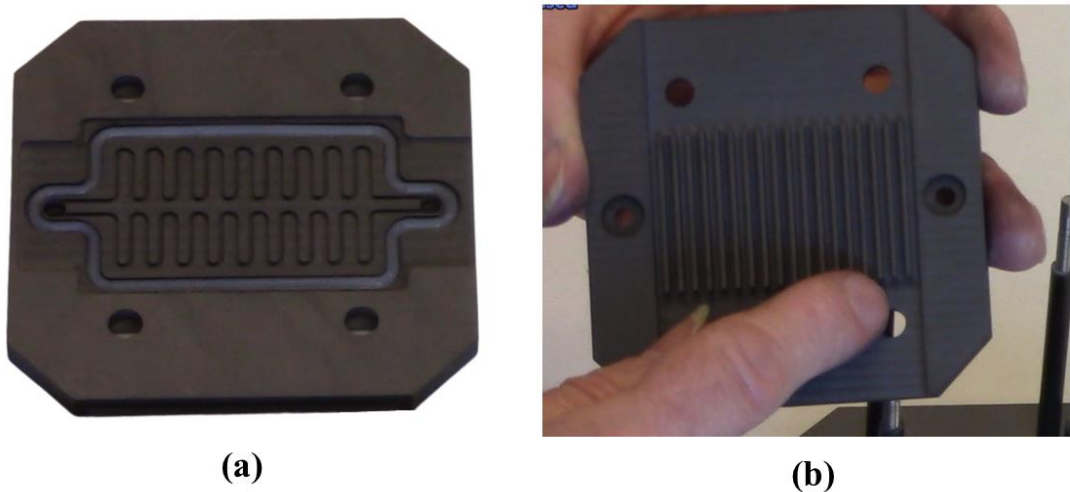


Figure 1.8. The embedded channels on bipolar plates (a)serpentine for H2 fuel, (b) straight parallel channel on the air side

#### 1.1.4 Sealing of Plates to Avoid Gas Crossover and Leaks

The construction of fuel-cell stacks through the application of bipolar plates gives very good electrical connection between one cell and the next. On the other hand, the use of bipolar plates necessarily means that there are many vulnerable holes or connecting points with the potential for causing leakage of both reactant gas and cooling fluid. The supply of reactant gas to each and every positive electrode has to be kept separate from that to each and every negative electrode. The entire edge of each anode and cathode is also respectively subject to leakage. Seals that keep the gases apart and also prevent cell-to-cell seepage of liquid electrolyte, which otherwise would give rise to partial short-circuits.

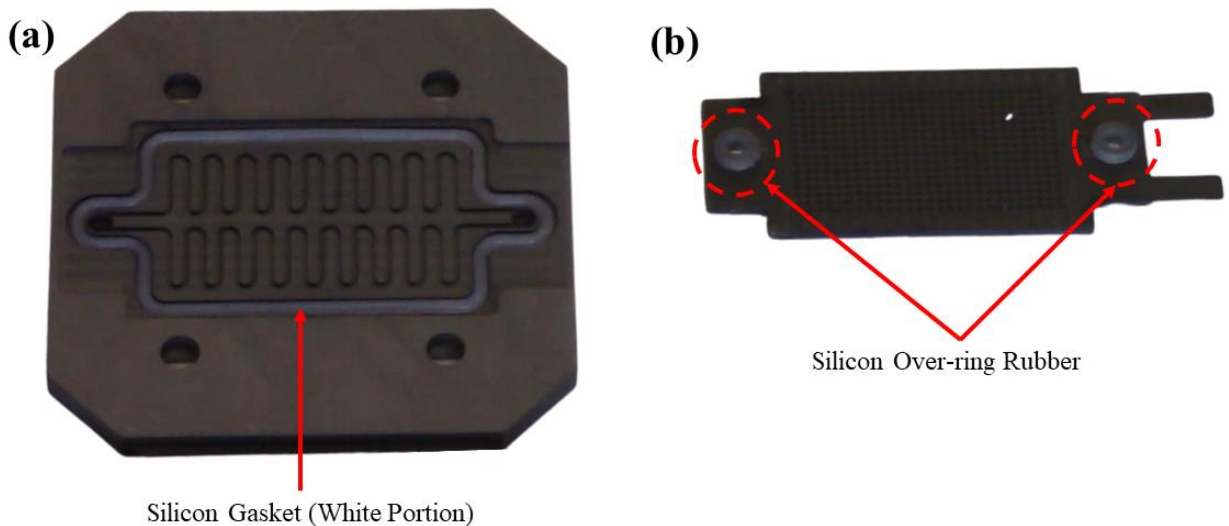


Figure 1.9. Sealing of plates to avoid gas crossover and leaks (a) Gasket to refrain overflow of gases (b) silicon over-ring rubber over the gas flow path to stop gas cross over.

Because the electrodes must be porous (to permit the access of gas), they allow leakage of the gas through their edges. Consequently, the edges must be sealed. This is done through 'Gasket' which is made of Silicon rubber that prevents leakages of gases and liquids. Sometimes sealing is done by making the electrolyte compartment within the bipolar plates slightly larger than the electrodes and fitting a gasket around each electrode, as presented in Figure 1.9(a). Such assemblies can then be made into a stack in which the fuel and

oxygen can then be supplied to the electrodes using a separate flow path. Holes are carefully positioned to feed the reactants into the channels that run over the surface of the electrodes. Also, the air side of MEA has two silicon over-ring rubber over the gas flow path so that the gas cannot cross over, as shown in Figure 1.9(b). With this arrangement, the hydrogen should only come into contact with the anodes. Similarly, the oxygen (or air) fed horizontally through the stack should only contact the cathodes and certainly not the edges of the anodes.

## 1.2 MEASURING THE IV CHARACTERISTICS

### 1.2.1 Characterization PEM Introduction to Testing the Horizon 10 Cell PEM Stack

A set up to test PEM fuel cell is presented at Figure 1. The main parts of this set up described briefly in the following section.

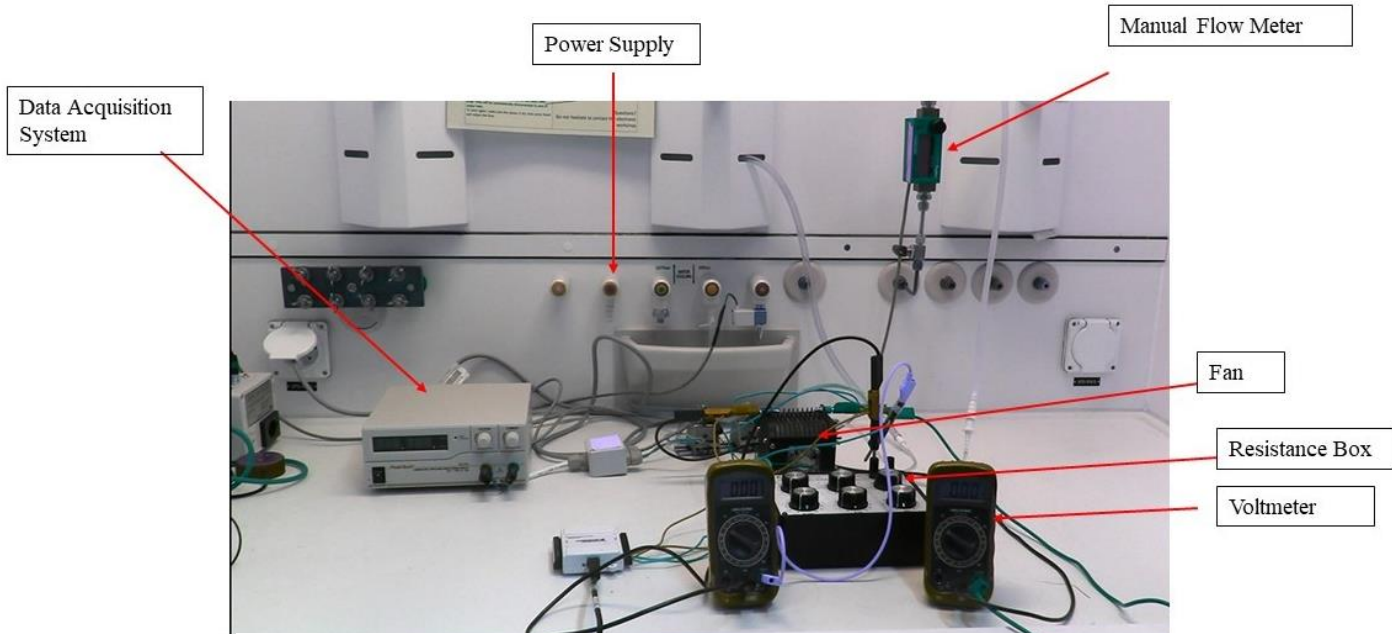


Figure 1.10. Test setup of PEM stack.

**Manual Flow Meter:** Manual flow meter that controls the Input Hydrogen fuel to the stack. The stack is composed of 10 cells. Flow Measurement: Manual flow meters play a pivotal role in the evaluation of PEM fuel cell stacks. They are

connected to both the inlet and outlet lines of the fuel cell stack. These lines are responsible for supplying hydrogen and oxygen (or air) to the fuel cell stack and removing exhaust gases.

1. **Flow Control:** Manual flow meters offer precise control over the flow rates of hydrogen and oxygen. Operators can adjust these flow rates using knobs or valves, a critical step in optimizing the fuel cell stack's performance and ensuring the correct proportions of reactants.
2. **Monitoring:** Manual flow meters often feature displays or scales that indicate flow rates in units like liters per minute (LPM) or cubic centimetres per minute (CCM). This real-time monitoring allows operators to continuously track and adjust gas flow.
3. **Calibration:** To ensure accurate flow measurements, manual flow meters require calibration. This process involves setting the flow meter to a known standard, typically using a calibration gas with a known flow rate.
4. **Safety:** Safety is of paramount importance when working with hydrogen gas due to its high flammability. Operators must strictly adhere to safety protocols and guidelines when handling manual flow meters and conducting tests on PEM fuel cell stacks.
5. **Data Collection:** During testing, various parameters such as flow rates, voltage, current, and other critical data are collected. These data points are vital for assessing the performance and efficiency of the PEM fuel cell stack. The readings from the manual flow meter are an integral part of this comprehensive data collection process.

**Air Supply:** In a 10-stack hydrogen fuel cell system, a continuous supply of oxygen is crucial to drive the electrochemical reactions within the fuel cells, enabling them to combine hydrogen and produce electricity. To achieve this, a strategically positioned fan draws in ambient air and directs it to the air side of the fuel cell stack. This fan is powered by an external electrical source, typically

located at the rear of the fuel cell setup. Its speed and airflow rate are carefully controlled to ensure that the fuel cells receive the precise amount of oxygen required for efficient electricity generation.

**Resistance Box:** Linked to the hydrogen fuel cell stack is a resistance box. This component facilitates the alteration of electrical resistance across the stack, permitting manual or LabVIEW-controlled adjustments to load conditions. This is vital for generating the Current-Voltage (IV) curve, an essential analytical tool for assessing the fuel cell's performance across various electrical loads

**Two Voltmeters:** Voltage loss refers to the reduction in electrical potential that occurs as the electric current traverses the connecting lines and the resistance box. The utilization of two separate voltmeters, one for measuring potential across the resistance and the other across the fuel cell stack, serves the purpose of precisely quantifying this voltage loss. This measurement provides the means to calculate the extent of voltage dissipation within the setup due to electrical resistance and related factors.

**Data Acquisition System:** A Data Acquisition System (DAS) is employed to automate the generation of I-V (Current-Voltage) curves in hydrogen fuel cell testing:

1. **Sensor Integration:** The DAS interfaces with various sensors to precisely measure current and voltage.
2. **Rapid Data Sampling:** It continuously samples sensor data in real-time to capture current and voltage variations.
3. **Data Conversion:** Analog sensor signals are converted into digital format for computer processing.
4. **Data Storage:** Digital data is stored for analysis and historical reference.

5. **Control and Automation:** Software controls the DAS, automating resistance adjustments and system parameters.
6. **I-V Curve Generation:** The DAS creates I-V curves by recording current and voltage data while adjusting load conditions.
7. **Real-Time Monitoring:** The system provides real-time monitoring of curve generation.
8. **Data Analysis:** Software conducts data analysis, including power output and efficiency calculations.
9. **Results Presentation:** Finally, it presents graphical representations for performance analysis.

### **1.2.2 Characterization PEM Measuring the IV Behaviour of the Horizon 10 cell PEM Stack with Manual Measurement**

#### **1.2.2.1 Experimental setup**

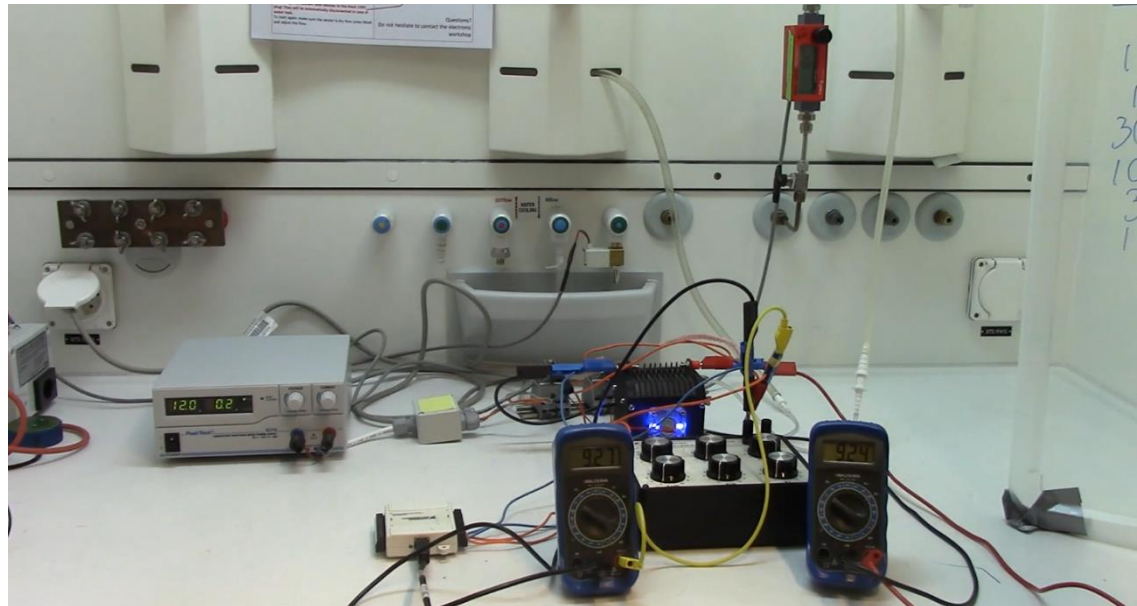


Figure 1.11. General Layout of the setup with stack in the background and the resistance box and DVMs in the foreground.

### 1.2.2.2 Experimental Data

Table 1.1 Experimental data for IV behaviour of PEM stack.

<b>R (<math>\Omega</math>)</b>	<b>V (volts)</b>	<b>I (amps)</b>
$\infty$	9.27	0
<b>10000</b>	9.17	9.17e-5
<b>1000</b>	8.79	8.79e-4
<b>300</b>	8.43	0.0281
<b>100</b>	8.04	0.0804
<b>30</b>	7.47	0.249
<b>10</b>	6.96	0.696

### 1.2.2.3 IV Curve Based on Experimental Data

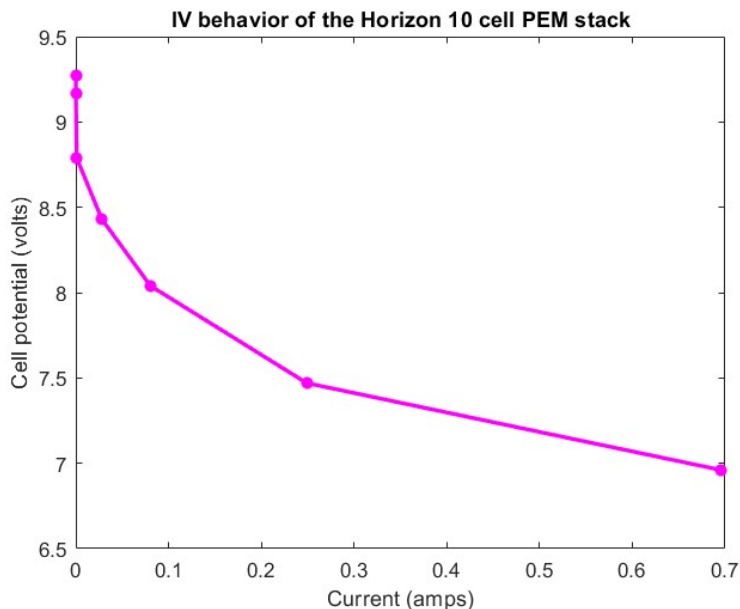


Figure 1.12. IV behaviour of the Horizon 10 cell PEM stack.

#### 1.2.2.4 IP Curve Based on Experimental Data

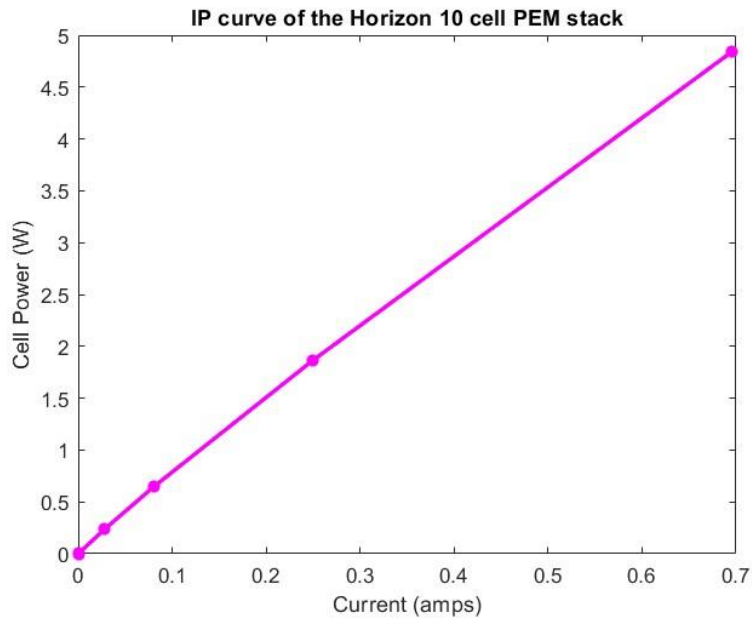


Figure 1.13. IP behaviour of the Horizon 10 cell PEM stack.

#### 1.2.2.5 Mode of Control

There are three distinct regions of a fuel cell IV curve:

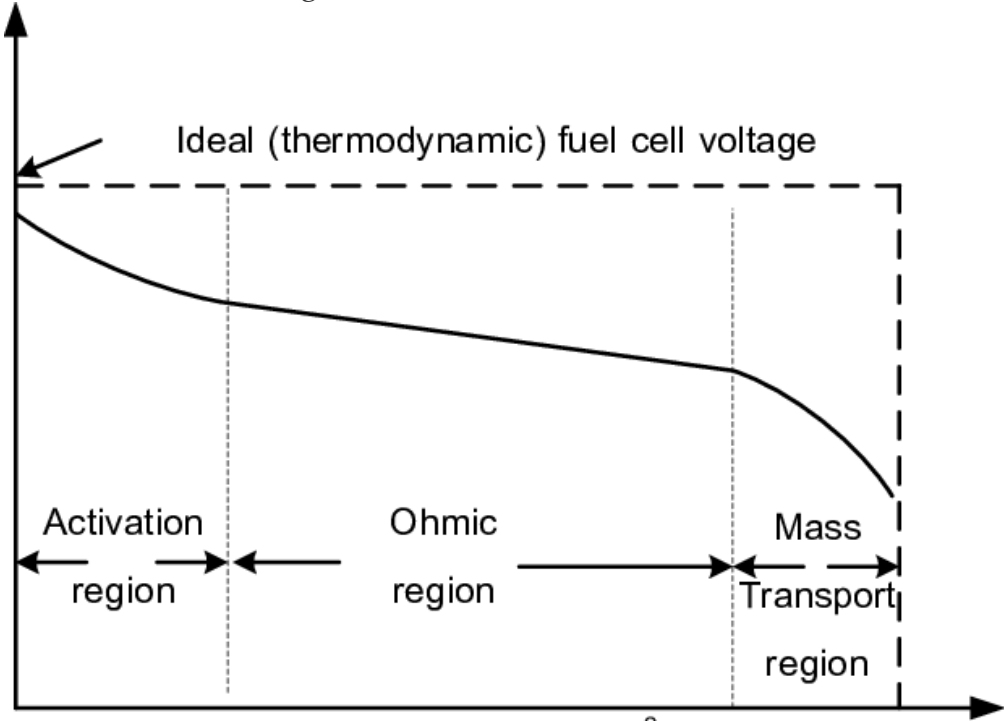


Figure 1.14. IV Characteristic curve for PEM stack.

- At low current densities, the cell potential drops as a result of the activation region.
  - At moderate current densities, the cell potential decreases linearly with current due to ohmic region.
  - At high current densities, the cell potential drop departs from the linear relationship with current density as a result of a more pronounced mass transport region.
- a) Activation losses:** Activation losses arise from the slowness of the chemical reactions occurring at the electrode surfaces. A fraction of the generated voltage is lost in facilitating the electron transfer during these chemical reactions. This impact on the voltage exhibits a distinctly non-linear behaviour. This form of losses prevails as the primary source of losses at low current density and serves as an indicator of the catalyst's efficiency under specific temperature conditions. It presents a complex three-phase interface problem, where gaseous fuel, the solid metal catalyst, and the electrolyte must all interact. Although the catalyst lowers the activation barrier's height, there remains a voltage loss due to the slowness of the oxygen reaction.
- b) Ohmic Losses:** Conductors possess an inherent resistance to the flow of electric charge, leading to a decrease in cell voltage. Ohmic losses, characterized by a direct voltage drop, result from the inherent resistance encountered by electrons as they traverse the electrode materials, interconnections, and the resistance to ion flow within the electrolyte. It arises from the electrical resistance inherent in various components of the cell. The elements contributing to this electrical resistance encompass the electrolyte, the catalyst layer, the gas diffusion layer, bipolar plates, interface contacts, and terminal connections. Internal ohmic losses within

the fuel cell predominantly govern the reduction in voltage, encompassing both electronic and ionic components of fuel cell resistance. This voltage reduction exhibits a linear relationship with current density, earning it the alternate name of "resistive losses".

- c) **Mass Transport Losses:** For a fuel cell to generate electricity continuously, a constant supply of fuel and oxidant is required. Simultaneously, the products must be removed to achieve optimal fuel cell efficiency. The examination of mass transfer involving uncharged species holds great significance, as inadequate comprehension can result in substantial performance declines within the fuel cell. Fuel cell performance depends on the concentrations of reactants and products within the catalyst layer. To mitigate concentration losses, it is crucial to optimize mass transport within the fuel cell electrodes and their associated flow structures. Mass-transport losses, arises from fluctuations in the reactant concentrations at the electrode surfaces during fuel consumption. This form of irreversibility is occasionally termed "concentration losses" due to its impact on voltage, given that reactant concentration directly influences it. Another synonymous term, "mass-transport losses," is employed because these losses arise from an insufficient transport of reactants to the electrode surface.

#### **1.2.2.6 Power Density Curve (I-P Curve)**

The Figure 1.15 displays a graph depicting the relationship between voltage, power, and current for a PEM fuel cell. Notably, as the current density increases, there is a corresponding reduction in the open circuit voltage.

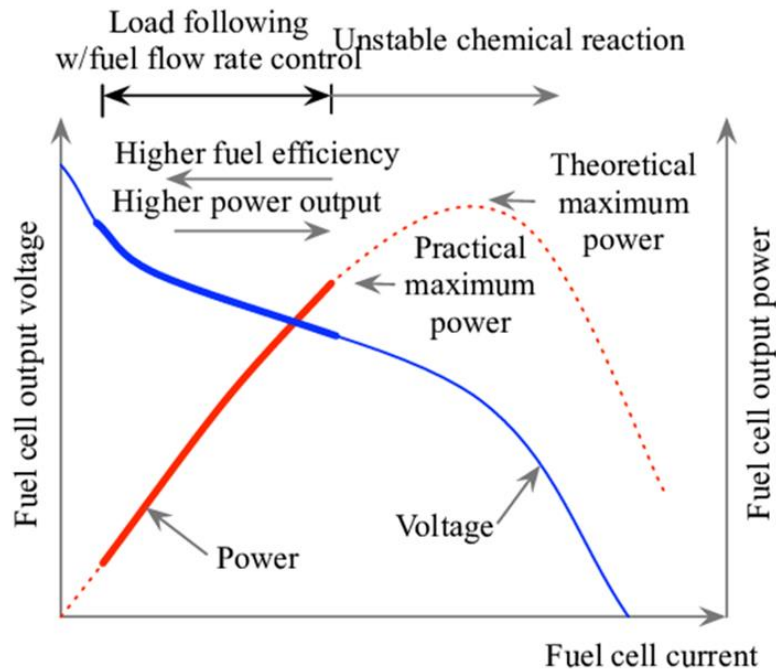


Figure 1.15. Power density curve for stack.

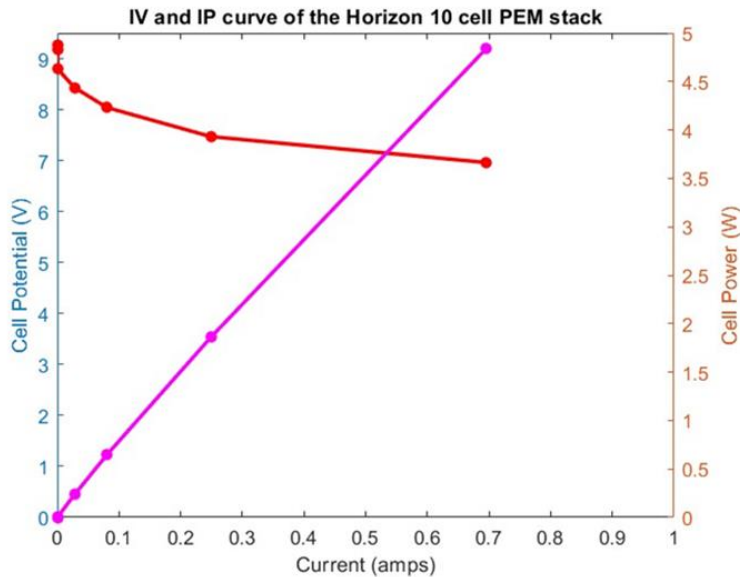


Figure 1.16. IV and Ip curve of PEM cell based on Experimental Data.

The maximum output current of the fuel cell is depending on the current density of the membrane multiplied by the membrane's surface area. Simultaneously, the fuel cell's output voltage is determined by the voltage of a single cell multiplied by the total number of stacked cells.

Furthermore, it's crucial to recognize that the fuel cell's power output can be adjusted within a specified range, known as the load-following region, by regulating the rate of fuel flow. The power output of the fuel cell is intricately linked to factors such as temperature, pressure, and humidity. Consequently, dynamic control of these parameters is imperative to achieve optimal efficiency in fuel cell operation.

### 1.2.3 Characterization PEM Measuring the IV Behaviour of the Horizon 10 cell PEM Stack with LabVIEW

In this part we will discuss how the I-V curve will be plotted using Data acquisition in LabVIEW. It's the same setup as previously described. We will plot the data on the screen. We can see the potential across the stack and the resistance.

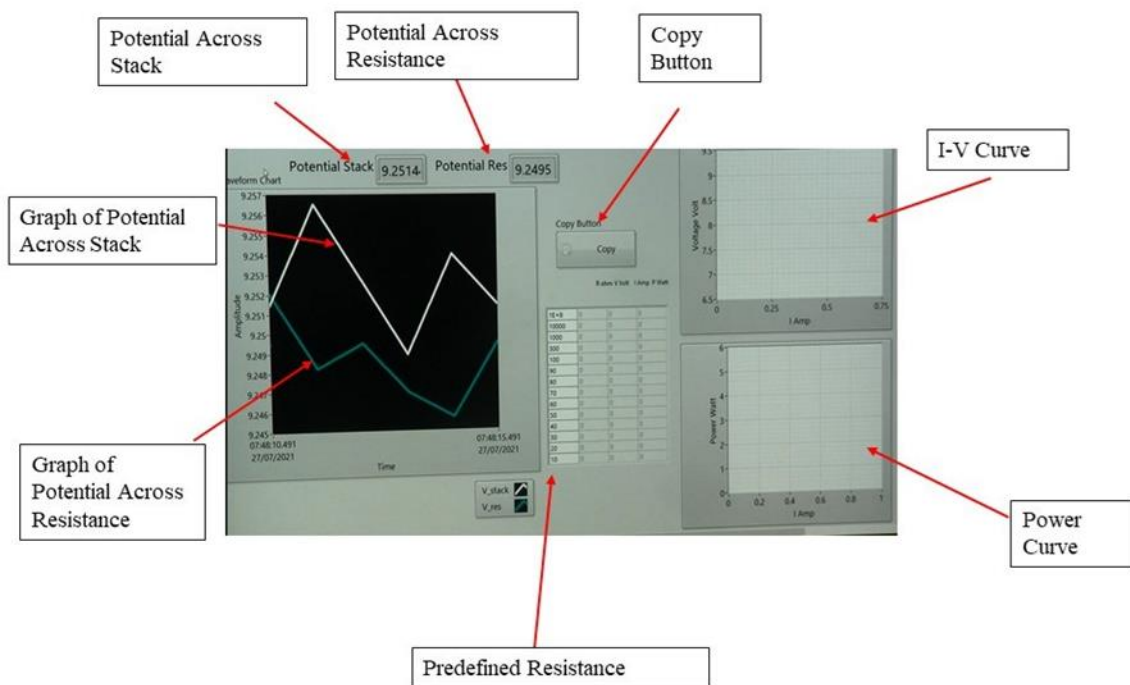
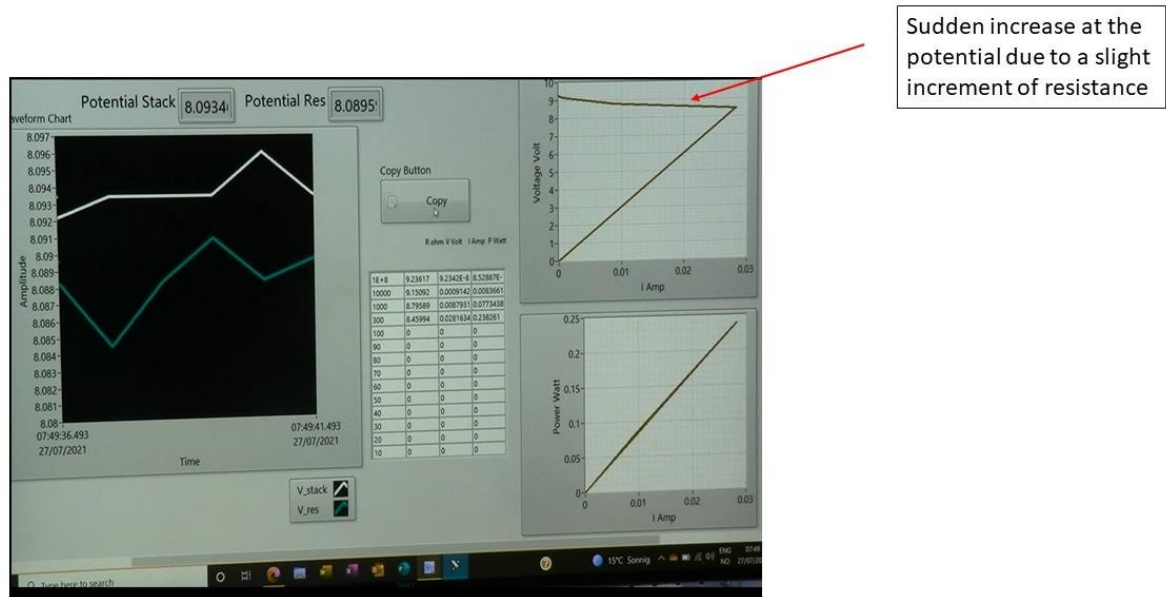


Figure 1.17. Automatically plotted I-V curve and I-P curve from Potential.

On the right side of the screen the respected I-V curve and power curve will be plotted automatically from the potentials which will be shown on the left side

as shown in Figure 1.17. We have preselected some resistance on the which is shown on the middle of the screen. When we are satisfied with both potential, we will select copy. Then the voltage we measured will be copied and using the resistance the respective current value and power will also be calculated automatically.



We can observe that at the last two values there was a transient in the resistance. So, we had to wait a little more until the graph settled down.

At the end we got an almost smooth I\_V curve as shown is Figure 1.19.

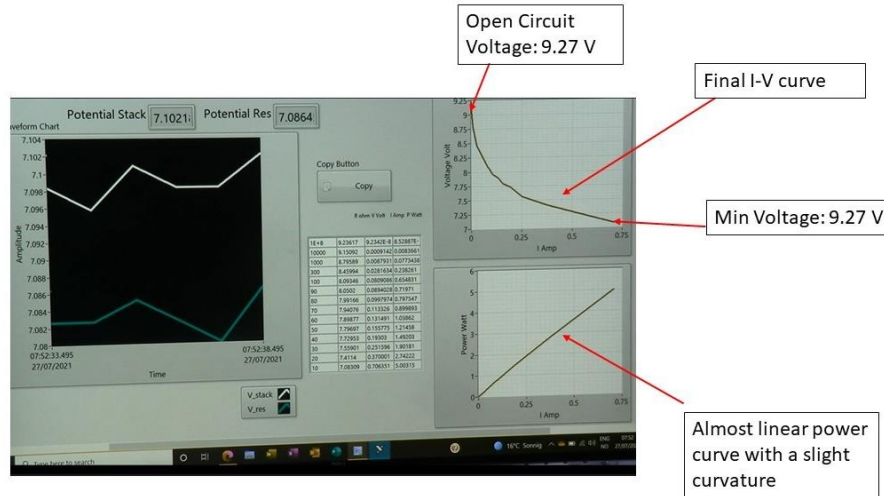


Figure 1.19. Smoother I-V curve.

The max value of voltage: 9.23

The max value of voltage: 7.06.

The power curve has a small curvature. However, we are far away from maximum value. That also indicated that we are in an ohmic region now. Because the power curve can be gained before the mass limiting mass limiting region.

At zero current the voltage is approximately 9.27 which is called open circuit voltage. An the from the current will increase as the cell is discharged and the chemical energy is converted into electrical energy with higher and higher current density and more electrical power. Then cell terminal voltage drops. No matter what type of cell we use (e.g. AFC, PEM, SOFC) the characteristics is almost similar in all cases.

In Figure 1.20, the activation region is represented by the red portion of the image. Also known as the minimal current density region. A rapid initial decrease in potential is caused by the activation of the electrode or the activation of the kinetics of the electrode. In Figure 1.20, yellow box represents the ohmic

region. This is also called medium current density region. This is a linear region which is limited by ohmic resistance by electrolyte ohmic resistance or IR loss. In this figure the graph is far from Mass Transfer Region. At the higher current we can see that the curve bend down with sharper shape which means the potential will drop further because the reaction is limited by the supply of reactant and the transporter way of product that's mass transfer limitation. In the mass transfer region, we will observe a rapid decrease in potential and a high current flow for the shortest amount of time. As there is a sufficient movement of reactants, we have not yet reached the region of mass transfer.

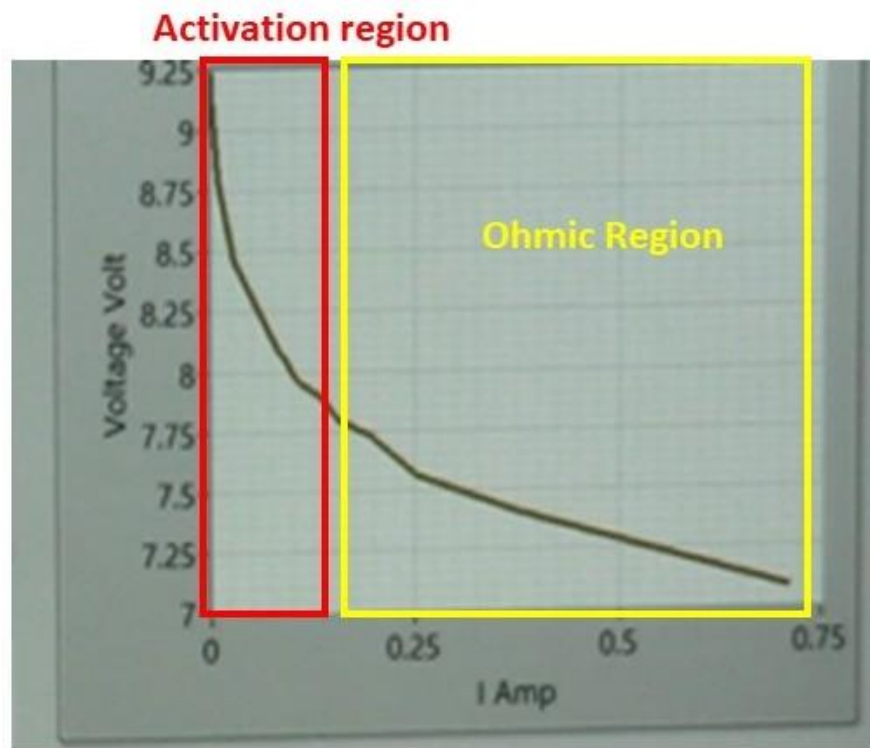


Figure 1.20. I-V behaviour curve of PEM stack with active region and ohmic region.

#### 1.2.3.1 Comparison with Manual Measurements

It is evident that the I-V curves obtained from both manual measurements and LabVIEW measurements demonstrate a substantial amount of similarity. In each case, the upper limit is around 9.2 V, while the lower limit is approximately

7 V. Both times, the electrode's first activation caused a quick change in potential, which was followed by a period of stable potential in the ohmic area

#### 1.2.4 Characterization PEM Measuring the IV Behaviour of the Horizon 10 cell PEM Stack with Zahner System

In this experimental section, IV curve is measured for the horizon 10 cell stack with the Zahner system. In Zahner system the stack is connected to the laptops. A software named cyclic Voltammetry has been used to perform this experiment by changing the potential in a cyclic manner.. Recording parameter is started at 9.3 volts going down to 5.8 volts and then back up to 9.3 volts. This is done at the speed of 50mV/s.

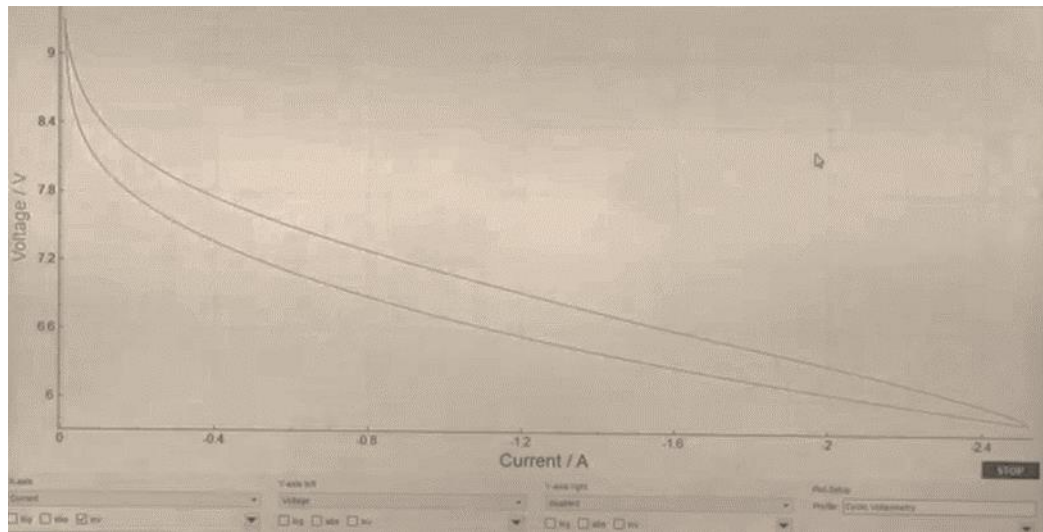


Figure 1.21. IV Characteristic curve for PEM stack.

Figure 1.21 shows the complete IV curve. The plot starts at 9.3 volts, at OCV (open circuit voltage). Initially the plot is in charge limiting region and slowly transitions to the ohmic region where the curve is slowly flattening. The end voltage is selected as 5.8 volts because it is right before the mass limiting region which can be a problem as it has an adverse behaviour. So, the plot has to be stopped right before it. As soon as the curve has hit the minimum voltage limit, the plot goes backward. There is a difference between forward and backward

line because of some hysteresis of the system. Finally, the curve reached again to the OCV through ohmic and charge limiting region.

#### 1.2.4.1 Hysteresis in the I-V Plot

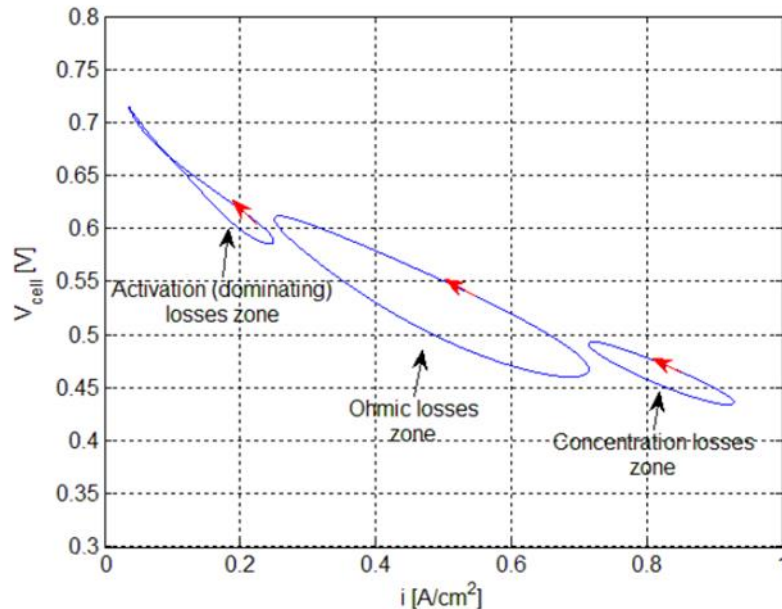


Figure 1.22. Hysteresis in I-V curve due to various losses.

The IV curve is useful for troubleshooting issues in the fuel cell stack. If the IV curve is recorded while increasing and decreasing the current, it may show hysteresis. This typically indicates a change in fuel cell conditions, such as drying or flooding of the membrane. Hysteresis can be attributed to several factors. One of these factors is the double layer capacitor effect, which interacts with activation losses. Another significant contributor to hysteresis is the management of water within the cells. For example, various studies have employed electrochemical impedance spectroscopy (EIS) to measure membrane resistance and have demonstrated that, at low power densities, this impedance is higher during increasing current than when decreasing it. Consequently, variations in membrane moisture serve as one explanation for the observed hysteresis effect. Additionally, in-depth investigations using a one-dimensional transient fuel cell model have uncovered a hysteresis effect at very low frequencies. This particular

phenomenon arises from inadequate liquid water content at high current densities, resulting in pore flooding.



# **Chapter 2: SOFC Single Cell Setup and Testing by EIS**

---

## **2.1 SOFC Setting up**

### **2.1.1 Characterization Techniques - SOFC Setup For Single Cell Testing**

A solid oxide fuel cell (SOFC) is a type of fuel cell that converts chemical energy from a fuel, such as hydrogen or natural gas, into electrical energy through an electrochemical process. SOFCs operate at high temperatures, typically between 500 and 1000 degrees Celsius, which allows for efficient conversion of fuel into electricity.

SOFCs consist of three main components: an anode, a cathode, and an electrolyte. The fuel, such as hydrogen or natural gas, is supplied to the anode, where it undergoes oxidation, releasing electrons. The electrons then flow through an external circuit, generating electrical power. At the cathode, oxygen from the air reacts with electrons and any remaining fuel to produce water or carbon dioxide.

In this article, the installation process of a single solid oxide fuel cell (SOFC) within its housing is described. Initially, the housing is positioned upside down, as depicted in Figure 2.1(a). The housing itself is made up of Inconel which is nickel chromium based super alloy often utilized in extreme environments where components are subjected to high temperature, pressure, and mechanical loads. It's also oxidation and corrosion resistant. Subsequently, the cell components are assembled, and the necessary attachments are completed. Once this is done, the entire setup is inverted and placed into a furnace, where it undergoes heating to reach the designated operating temperature.

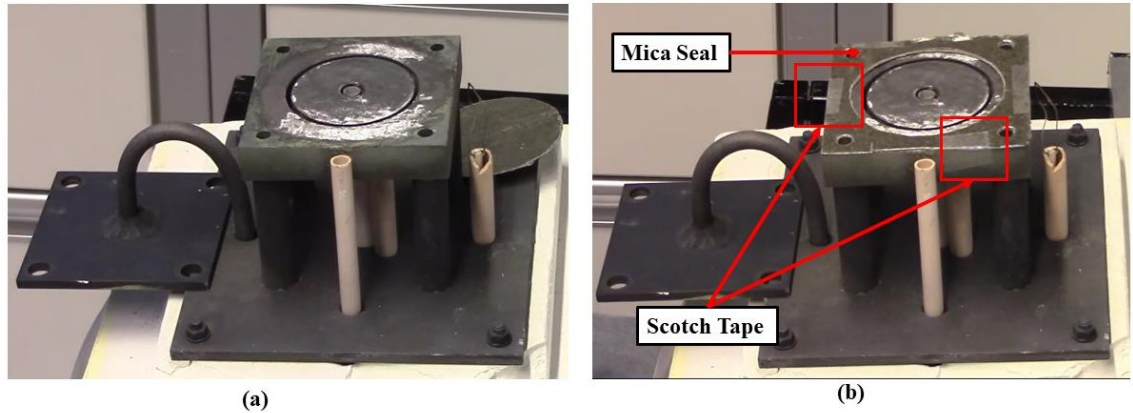


Figure 2.1. (a) The housing of SOFC, (b) Placement of Mica seal with help of scotch tape.

The initial element to be inserted into the housing is a mica seal. The seal will be secured in place using scotch tape to maintain its fixed position as illustrated in Figure 2.1(b).

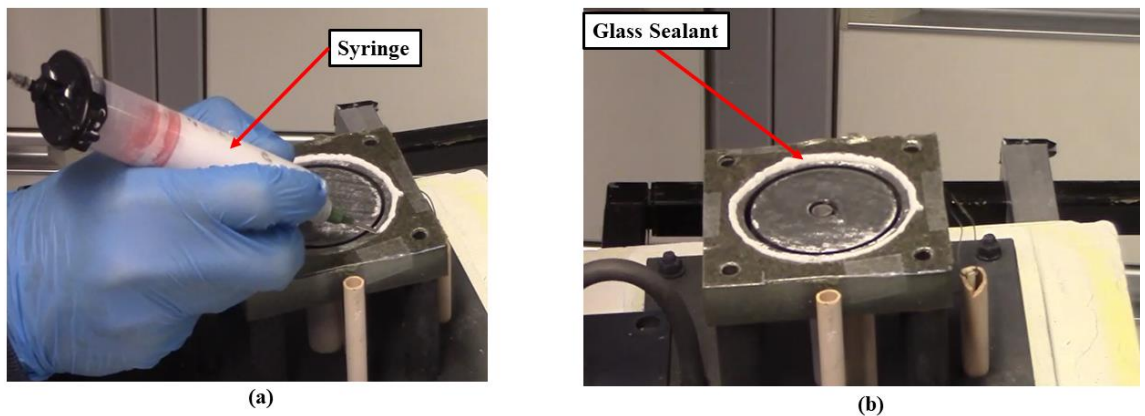


Figure 2.2. (a) Utilization of syringe with the help of air pump to implant glass sealant, (b) Implanted glass sealant (white material) along the circumference.

Subsequently, a glass sealing will be applied along the edges to prevent any leakage, as the test will be conducted in a sealed environment. An air pump is utilized to exert pressure on the syringe as shown in Figure 2.2(a), thereby facilitating the deposition of a thin layer of glass sealant around the

circumference where the cell will be positioned. Hence, the white substance in Figure 2.2(b) denotes the glass sealant.

Subsequently, a Nickel mesh current collector, equipped with a gold wire as illustrated in Figure 2.3, is positioned along the inner edge of the glass sealant and pressed downward. This arrangement ensures that the Nickel foam comes into direct contact with the housing, establishing electrical connectivity at the Anode side of the cell.

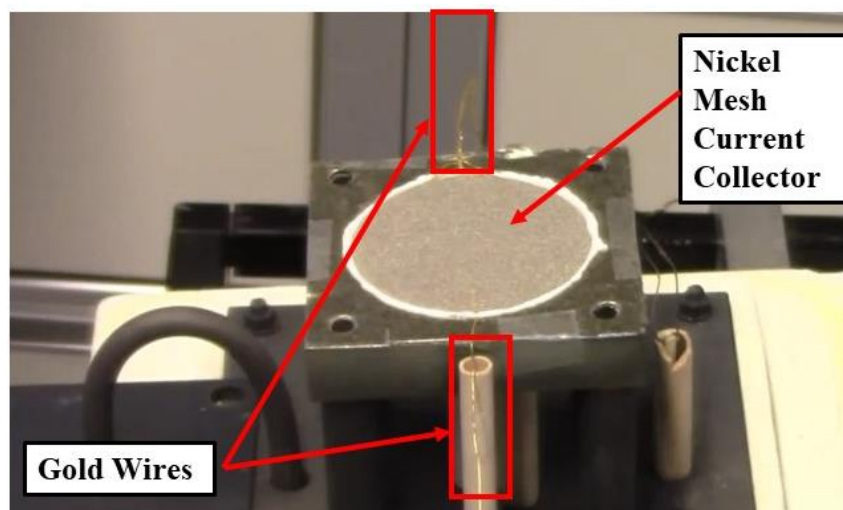


Figure 2.3 Electrical connectivity at the anode side of the cell with Nickel mesh current collector.

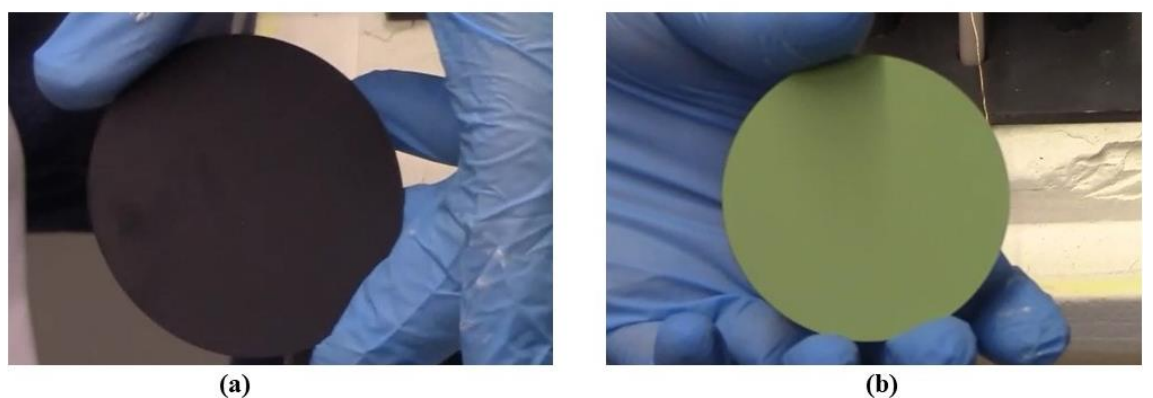


Figure 2.4 Single cell unit of SOFC (a) Cathode side of the single cell, (b) Anode side of the single cell.

Furthermore, the single cell needs to be placed on top of the anode current collector. The cathode side of the single cell is black in color Figure 2.4(a), conversely, the Anode side of the cell, characterized by a green hue as shown in Figure 4(b), is indicative of Nickel Oxide. Conversely. The green side is placed directly onto the Nickel foam current collector. The individual cell is then positioned directly above the current collector, within the perimeter defined by the glass sealant.

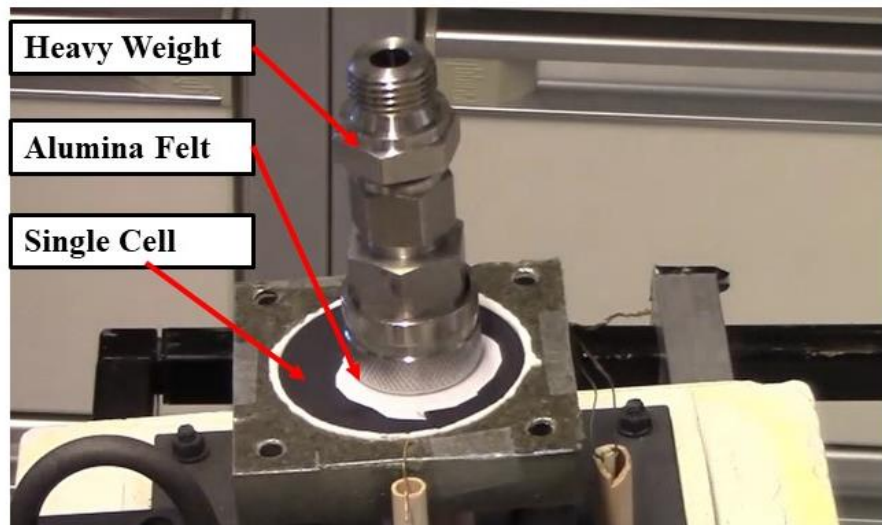


Figure 2.5 Applying weight on the arrangement to provide another layer of glass sealant.

Following the placement of the single cell, a sheet of alumina felt is positioned on top and pressed down using a weight as shown in Figure 2.5. This weight is carefully chosen to generate sufficient pressure, ensuring the components remain securely in place. The purpose of the alumina felt is to provide protection for the single cell during the weight application. Subsequently, a gentle pressure is applied to firmly secure the cell against the glass sealant. A second layer of glass sealant, typically in the form of liquefied organic powder, is then applied. This sealant will solidify when subjected to the appropriate oven temperature. To achieve a gas-tight assembly, the glass sealant

is compressed so that it completely covers the edge of the fuel cell. This step is crucial to ensure an airtight structure while the assembly undergoes heating in the oven. Finally, the weight and a smaller portion of the alumina felt are removed. Next step is applying an additional layer of aluminum felt is employed as insulation to electrically isolate the top housing from the bottom housing Figure 2.6(a). This insulation is essential to prevent any electrical interaction between the two parts. The aluminum felt is carefully positioned and secured in place using scotch tape.

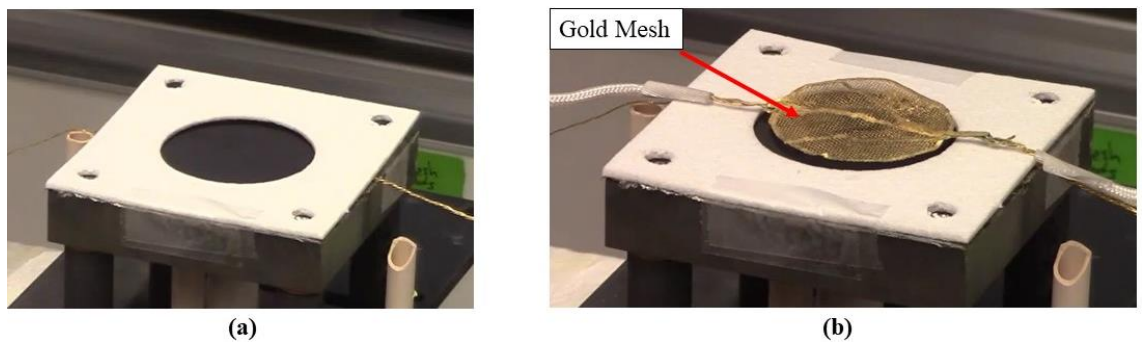


Figure 2.6 (a) Additional insulation layer of Aluminum felt on top of the arrangement, (b) Cathode current collector.

For the cathode current collector, a gold mesh is utilized as shown in Figure 2.6(b). Gold is chosen as the material for its inert properties, ensuring it does not undergo oxidation even when exposed to high temperatures. The gold mesh features two gold wires, one on each side, for voltage and current measurements. This configuration enables a classic four-wire measurement setup, with two wires connected to the anode and two wires connected to the cathode.

Above the cathode current collector, an additional circular aluminum felt is positioned as an insulator. This circular felt incorporates a central hole to allow the passage of fuel, ensuring that air is applied at the center of the cathode.

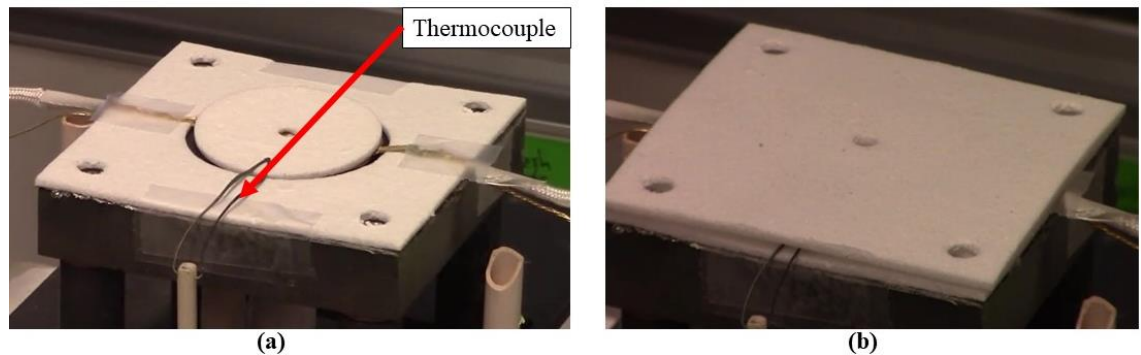


Figure 2.7 (a) Installation of thermocouple to measure temperature, (b) Final piece of insulation sheet placed on top of thermocouple.

Before installing the top housing, a thermal couple is employed to measure the temperature as shown in Figure 2.7(a). The thermocouple passes through a twin-pole alumina shield and is placed at the edge of the cathode. Its purpose is to measure the temperature on the cathode side of the cell. A square-shaped aluminum felt, serving as the final piece of insulation, is placed above the thermocouple. The insulations are held together using scotch tape as illustrated in Figure 2.7(b).

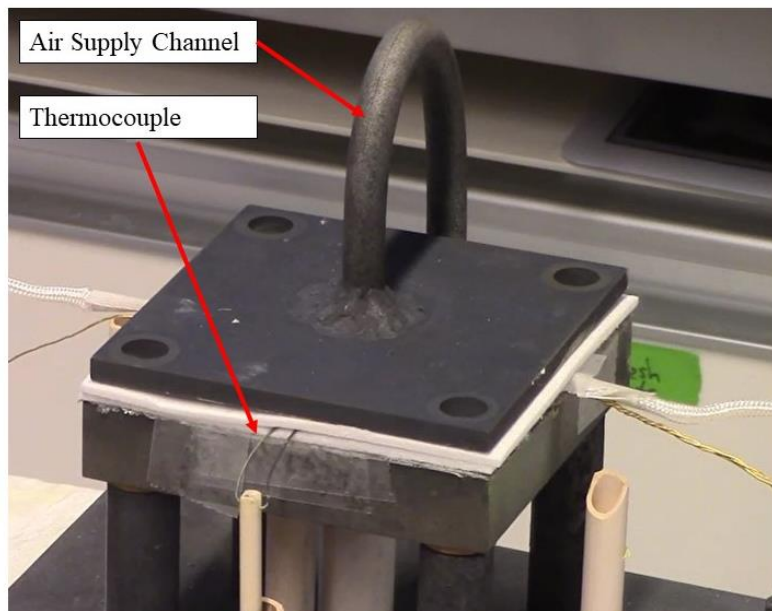


Figure 2.8 The top housing of SOFC.

Next, the top housing, made of inconel material, is positioned as displayed in Figure 2.8. This top housing features a central tube for the supply of air, which is placed at the center of the cell.

To secure the entire assembly, four tie rods are utilized. These tie rods serve as both structural support and insulators. A brown ring, composed of a material known as stramin, is employed to electrically isolate the tie rods from the cathode. This electrical isolation is necessary as the anode plate and cathode plate must be electrically isolated. It should be noted that the anode itself is connected to an anode plate, which is maintained at ground potential.

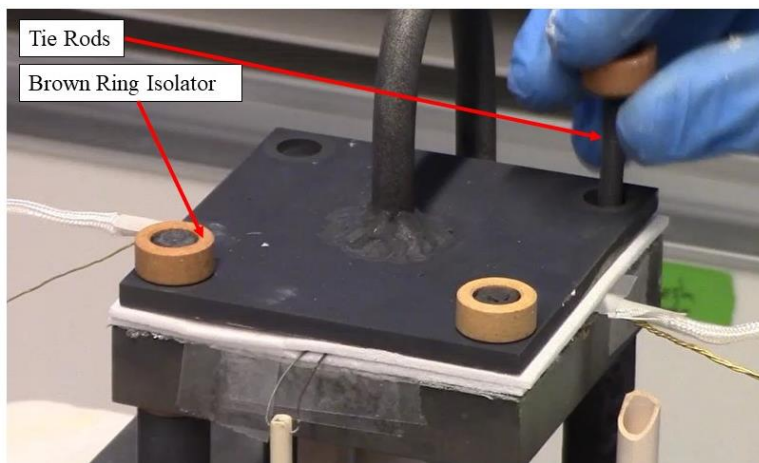


Figure 2.9 Utilization of tie rods to secure the whole assembly of the fuel cell.

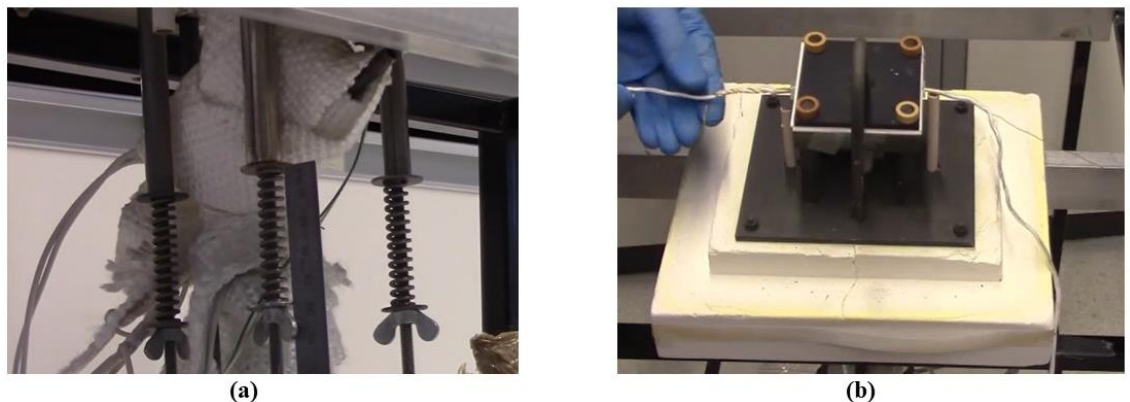


Figure 2.10 (a) Securely fastening the screws of the springs and accurately aligning the tie rods, (b) Twisting of contact wires to minimize noise.

Lastly, springs are applied to the tie rods to hold the housing together while in an inverted position. By tightening the screws of the springs and correctly positioning the tie rods, the springs are compressed to a position of precisely 43 mm, as indicated by rotating wing plates. This ensures that the springs are extended to a length of 43 mm.

The assembly of the cell is now complete. A contact wire is placed around the ceramic shield, passing through the housing. The contact wire is then twisted to minimize noise during impedance or EIS spectroscopy measurements as shown Figure 2.10(b). With this, the setting up SOFC is completed, and it's displayed in Figure 2.11.

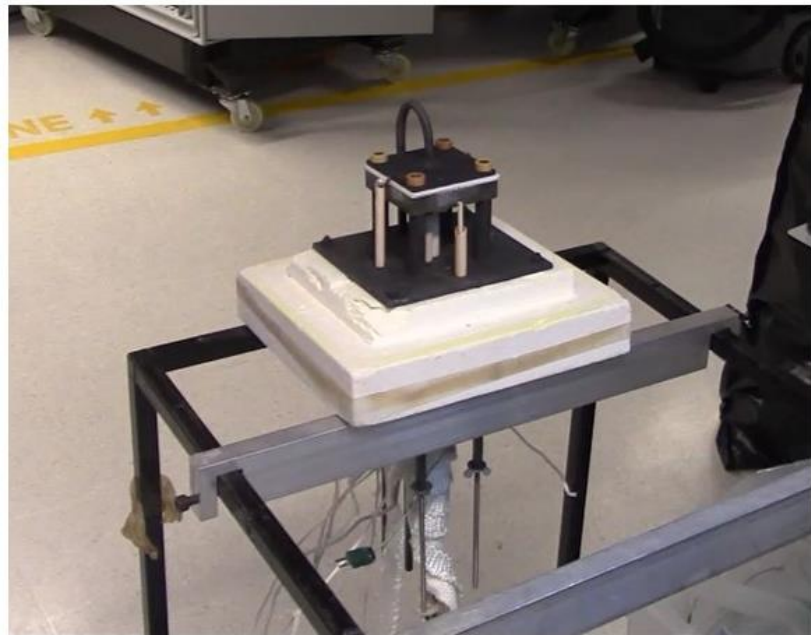


Figure 2.11 The whole setup of SOFC in upside down position.

The assembled setup is then transferred to an oven or furnace, specifically the one manufactured by Rohde as shown in Figure 2.12(a), to be heated up to a temperature of 180°C. The entire setup is positioned on the top of the oven, utilizing the available opening, and maintained at the desired operating temperature. The setup can now be observed within the oven in Figure 2.12(b).

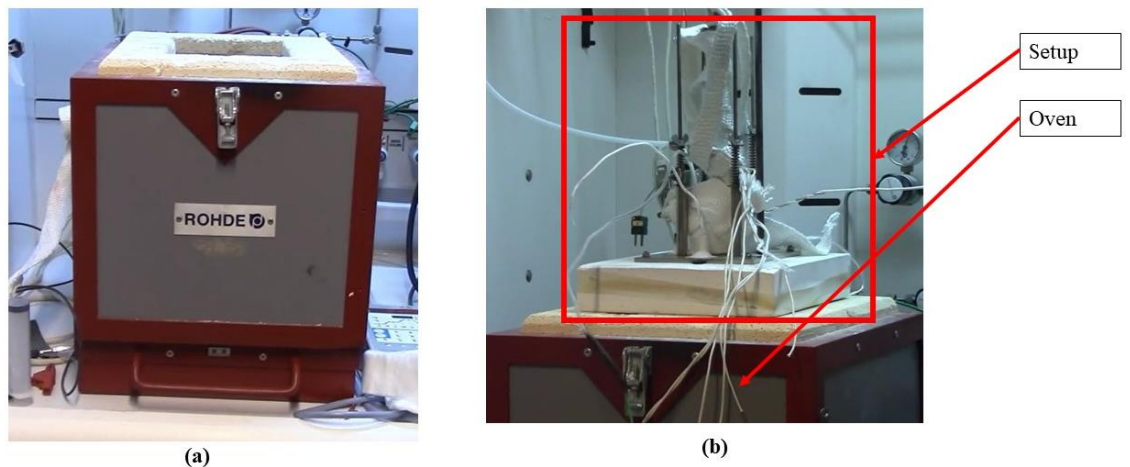


Figure 2.12 (a) oven or furnace, manufactured by Rohde group, (b) The entire setup placed at the oven to heat it up to operating temperature.

Next, the gases required for operation, namely air and fuel, are connected. These gases are supplied through a mass flow controller. The mass flow controller, located at the top left-hand side of the fume hood, is responsible for controlling the flow rate of the gases as depicted in Figure 2. 13.



Figure 2.13 Mass flow controller at the top left-hand side of the fume hood.

A logging system is attached, which includes thermocouple measurements and utilizes a tight casing for accurate temperature monitoring of the oven. Electric probes are connected to the contact wires. To prevent any electrical leakage and avoid short circuits, ample insulation is utilized throughout the setup.

With these steps completed, the entire setup is now ready to be heated to its designated operating temperature. The overall steps are summarized through the flow chart illustrated in Figure 2.14.

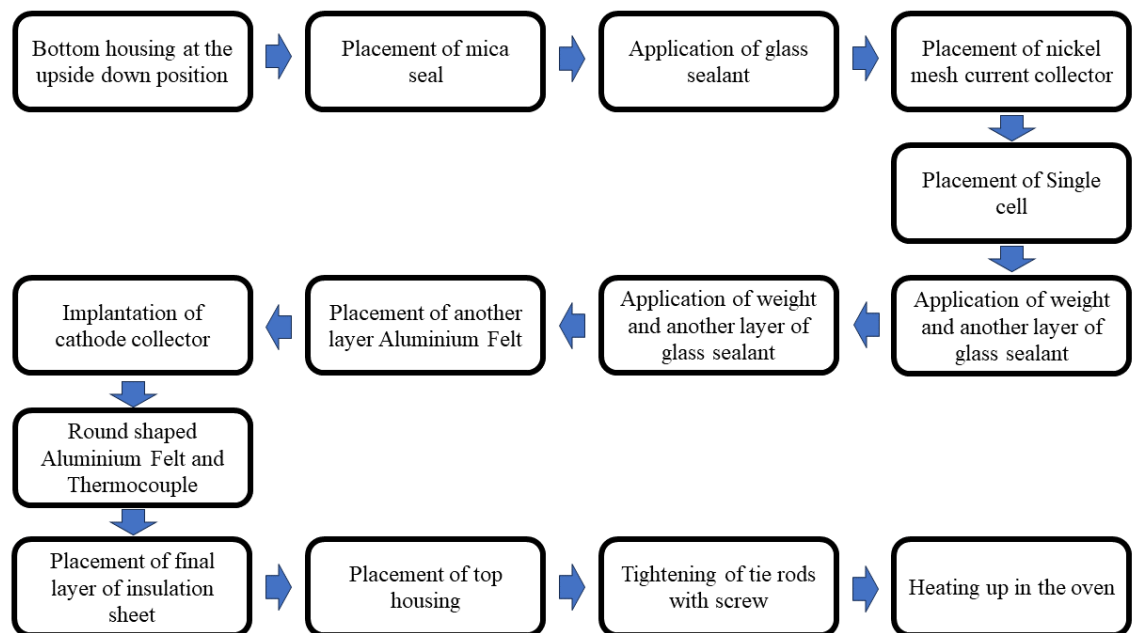


Figure 2.14 Flow chart of setting up the SOFC.

### 2.1.2 Characterisation Techniques - Setting up the SOFC for EIS Spectroscopy

The experimental measurement of impedance spectroscopy for the previously established Solid Oxide Fuel Cell will be conducted using a Zahner system. All the leads necessary for the experiment are connected to the system as shown in Figure 2.15.

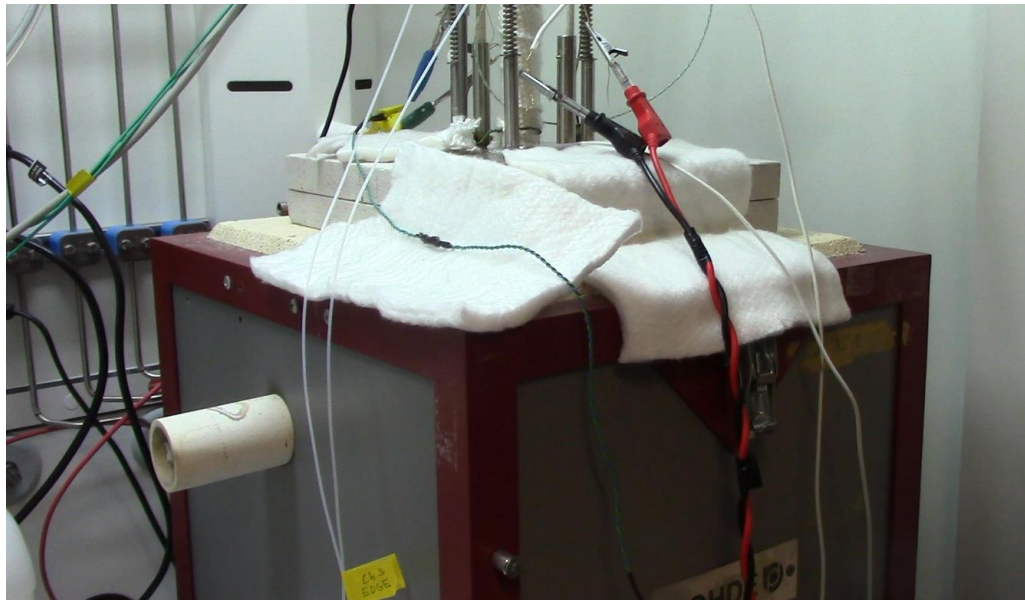


Figure 2.15 The complete set up with the connecting leads for the measurement.

To maintain the Solid Oxide Fuel Cell at its operating temperature, it is heated within an oven. Adjacent to the cell, an impedance separator is positioned. Figure 2.16(a) depicts the back side of Zahner system, rendering the front side invisible. Additionally, a laptop as shown in Figure 2.16(b), equipped with the necessary software for impedance measurement serves as the human-machine interface.

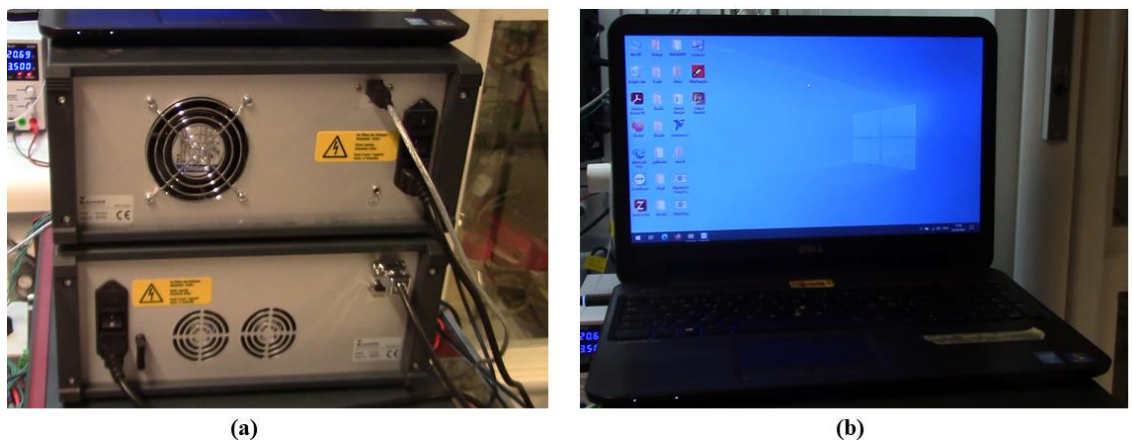


Figure 2.16 (a) The back side of the Zahner system, (b) The human-machine interface to operate the experiment.

## 2.2 EIS equivalent circuit board

In this part we are going to look at electrochemical equivalent circuit which is mainly used for analysing any fuel cell or any electrolyser or any other kind of electrochemical process from the point of a model that is made of electrical components. The whole mechanism of this equivalent circuit is described in the following sections:

In this part we are going to look at electrochemical equivalent circuit which is mainly used for analyse any fuel cell or any electrolyser or any other kind of electrochemical process from the point of a model that is made of electrical components. In this case, electrical components are normally combination of resistance and capacitors that represents physical process of electrochemical phenomenon. This will assist to understand the whole process in more convenient way which itself is a complex process.

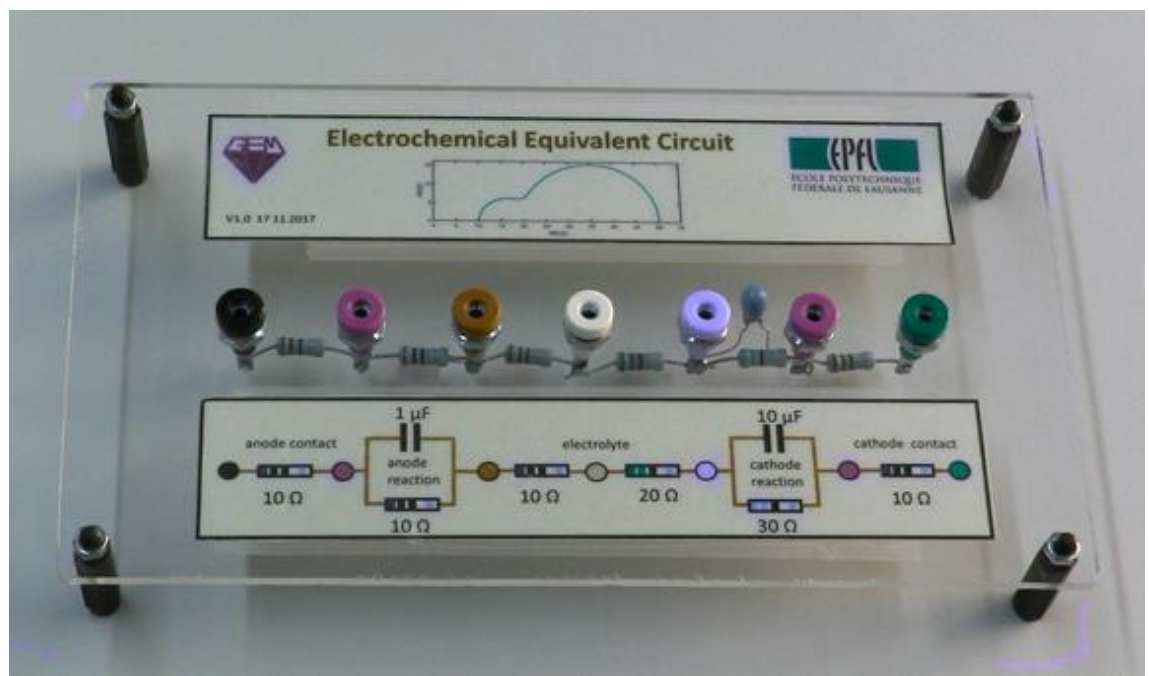


Figure 2.17 Electrochemical Equivalent Circuit

In this case, we have a plastic board consist of combination of resistor and capacitors in the rear side. This can be observed in Figure 2.18.



Figure 2.18 The ear side of the Electrochemical equivalent Circuit

The electrical components are labelled that normally represents the equivalent resistance of the process they are referring to.

From left to right, we can see some sections that are :

Anode contact:  $10 \Omega$ .

Anode reaction:  $10 \Omega$  R in parallel with  $1\mu F$  capacitor.

Electrolyte resistance:  $10 \Omega$  resistor and 20-ohm resistor.

Cathode reaction:  $30 \Omega$  R in parallel with  $10\mu F$  capacitor.

Cathode contact:  $10 \Omega$ .

The objective is to determine these values of impedance of the equivalent circuit as a function of frequency using electrochemical impedance spectroscopy. The response generated by the procedure resembles the red trace displayed on the board. These values were meticulously selected so that we might observe some separation of events within the impedance spectrum. Consequently, the

anode reaction capacitor is 1uF and the cathode reaction capacitor is 10uF; this indicates that the two reactions have different time constants.

The result of the analytical examination of parallel resistance combinations is a semicircle. In an electrochemical impedance spectroscopy (EIS) measurement, the impedance plot of a parallel combination of a capacitor and resistor usually appears as a semicircle within the Nyquist plot. As a result of the components' frequency-dependent behaviour, this semicircular shape results. The real component ( $Z'$ ) of the impedance is represented along the x-axis in the Nyquist plot, while the imaginary component ( $Z''$ ) is depicted along the y-axis. The impedance of a resistor and capacitor connected in parallel can be mathematically represented as:

$$Z=R \parallel \frac{1}{j\omega C}$$

Where:

$Z$  is the impedance

$R$  is the resistance

$C$  is the capacitance

$j$  is the imaginary unit

$\omega$  is the angular frequency

The angular frequency  $\omega$  approaches zero at very low frequencies. In this instance, the term  $\frac{1}{j\omega C}$  approaches infinity, which causes the capacitor's impedance to increase significantly. As a result, the impedance's imaginary part predominates, and the impedance is situated at a certain location along the Nyquist plot's y-axis.

The capacitor's impedance drops with increasing frequency. Because the resistor's impedance is frequency independent, it maintains a constant value simultaneously. The resistor's impedance is significantly higher than the

capacitor's at high frequencies. As a result, the resistor rules and establishes the parallel combination's impedance.

The semicircular shape in the Nyquist plot is formed by the change from the capacitor-dominated region to the resistor-dominated region. The impedance grows with frequency along a semicircle, initially on the y-axis (which is completely imaginary) and progressively becoming closer to the resistance value (which is purely real) as the frequency rises to extremely high levels.

The resistance and capacitance values in the Nyquist plot which is again related to time constant dictate the radius of the semicircle. A wider semicircle is the result of a higher resistance or capacitance.

**Time Constant:** The concept of time constant is conventionally linked to the procedure of capacitor charging or discharging in a direct current circuit. The frequency can cause variation in the impedance of an AC circuit component, such as a capacitor or resistor.

The impedance in AC circuits is frequency-dependent and is denoted by a complex number which combines information regarding both magnitude and phase. It is possible to express the impedance of a component as a function of frequency, and to analyse its behaviour using methods such as impedance spectroscopy or frequency response analysis. The time constant of a parallel combination of a resistance and capacitance in an RC circuit is given by the product of the resistance and the equivalent capacitance. It can be calculated using the formula:

$$\text{Time Constant } (\tau) = R \times C_{eq}$$

Where:

$\tau$  is the time constant

R is the resistance

$C_{eq}$  is the equivalent capacitance of the parallel combination of capacitors.

Here in our equivalent circuit the anode reaction is represented by the smaller semicircle on the impedance chart. In contrast, the cathode reaction is represented by the larger semicircle, which possesses greater values of C and R which increased the time constant. Additionally, the cathode reaction produces an output at a reduced frequency. Nonetheless, there is some intentional overlap that won't be expected to be observed in practise. They will invariably overlap since the processes are to be separated.

### 2.3 Zahner EIS method

Electrochemical Impedance Spectroscopy (EIS) is a versatile technique used in various fields, including electrochemistry, materials science, and battery research. EIS allows for the characterization of the dynamic electrical behaviour of conductive materials and systems. In this section we will explore the Zahner EIS method for a SOFC fuel cell. In the following part the whole process is describe briefly:

1. Zahner made AC impedance equipment is connected to the Zahner Symon electrochemical workstation. The Zahner EIS system refers to the electrochemical impedance spectroscopy (EIS) measurement capabilities provided by Zahner, a manufacturer of high-precision potentiostats and electrochemical workstations. EIS is a technique used to study the electrical properties of electrochemical systems by applying small amplitude AC signals and measuring the resulting impedance response Zahner's EIS system allows for clean impedance measurements at high voltages.

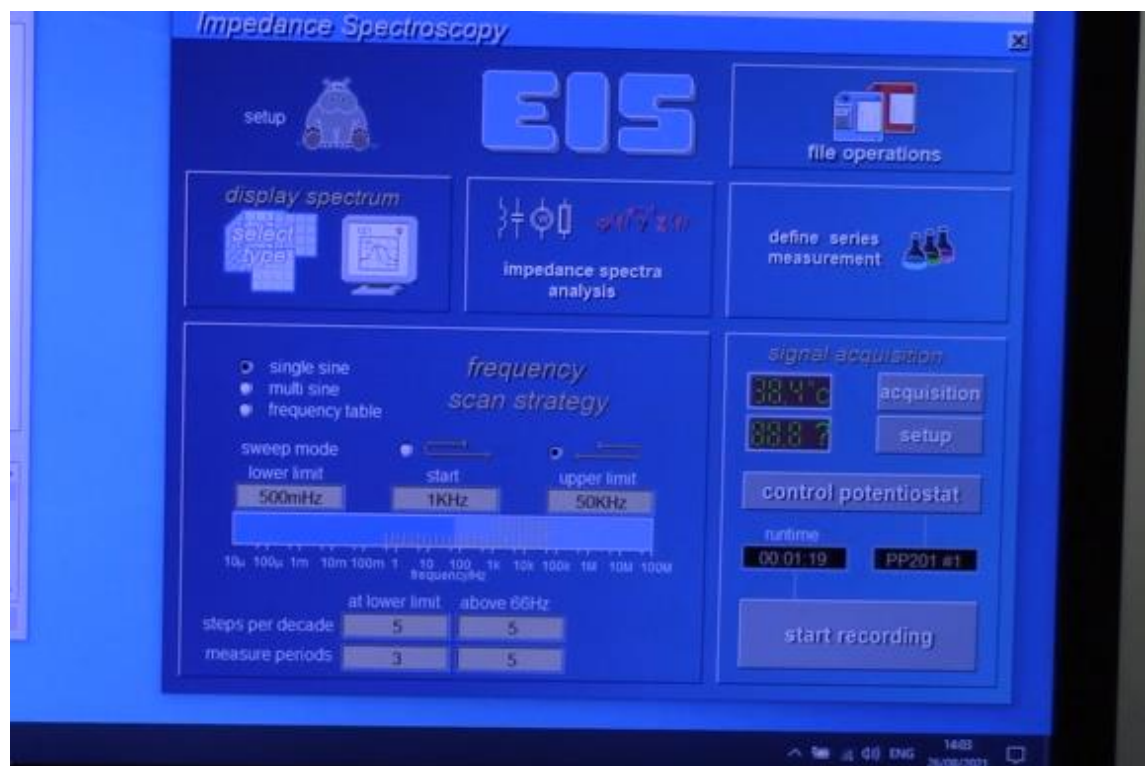


Figure 2.19 Impedance spectroscopy of the screen



Figure 2.20 Main Screen of Software

2. We have opened the EIS spectroscopy software. The spectroscopy software opened in Impedance spectroscopy initially. We can also open it from the main screen of the software which contains other mechanism like IV scanning and many more. But we will use EIS as we are measuring Impedance. Vs Frequency

3. We have to select some parameters initially. First of all we have to select control potentiostat from the right side of the screen.

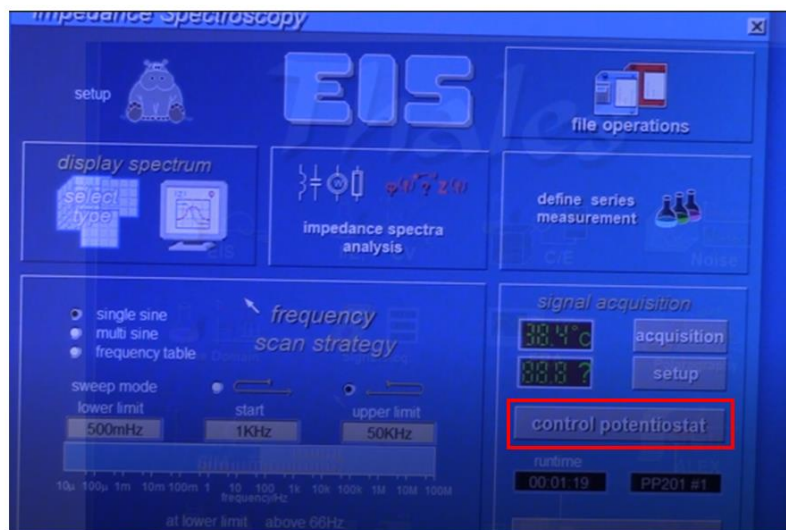


Figure 2.21 Control Potentiostat Bar

4. We need to choose the operating point of the system where we want to do the impedance spectroscopy. The following are a few varieties of EIS spectroscopic techniques:

**Frequency Sweep:** The most used EIS technique, frequency sweep, involves applying a sinusoidal voltage signal to the system across a range of frequencies. At every frequency, the impedance is computed and the ensuing current response is monitored. This technique can disclose a variety of electrochemical processes and provides information about the system's response at various frequencies.

**Potentiostatic EIS:** Using this technique, a little sinusoidal disturbance is introduced while the system is maintained at a constant potential. The

impedance is ascertained by measuring the current response that results. When examining systems under certain electrochemical circumstances, potentiostatic EIS is helpful.

**Galvanostatic EIS:** In this case, a little sinusoidal disturbance is delivered while the system is maintained at a constant current. The impedance is computed, and the voltage response is measured as a result. Galvanostatic EIS is frequently used to study systems in which the ability to control current is crucial.

We can choose potentiostatic mode and galvanostatic mode. But Galvanostatic mode is preferred for this experiment.

6. As the galvanostat mode is turned off, so the dc voltage is showing the OCV voltage which is 1.236 volt that is expected for a conventional SOFC cell at 80-20 fuel composition (80% H<sub>2</sub>, 20 % N<sub>2</sub>).



Figure 2.22 Open Circuit Voltage of the SOFC

6. If we go to the potentiostat and select 0.8 volt which is typical operating point of fuel cell with a suitable safety margin for any low voltage lower limit. And current amplitude is set at 0. And when the potentiostat mode is on, the Dc current jumps up to -7.8 Amp that accounts for desired 0.8 voltage.

This is a way to measure how much load we must put so that we can achieve the voltage we are looking for.

7. But we want to perform impedance spectroscopy in galvanostat mode, the potentiostat is turned off and we have to move to the Galvano stat mode. So the current is set to -7.85 Amp.

8. The next step is to set up the amplitude of the impedance spectroscopy. For that we need an amplitude at optimum amplitude to noise ratio so that the noise can't dominate the measurement.

Noise to Signal Ratio: The noise-to-signal ratio (NSR) is a measure that compares the level of unwanted noise to the level of the desired signal in a system. It is commonly used in various fields, including communication, imaging, and signal processing, to assess the quality and reliability of a signal. The NSR is typically expressed as a ratio or in decibels (dB), where a higher ratio or dB value indicates a better signal quality with less interference from noise.

But also the amplitude should not be too high as we want to operate at the linear region. The amplitude is chosen to 500mA which should be in between of the 5 to 10 % of Dc bias value. So we have selected this value at 500m.

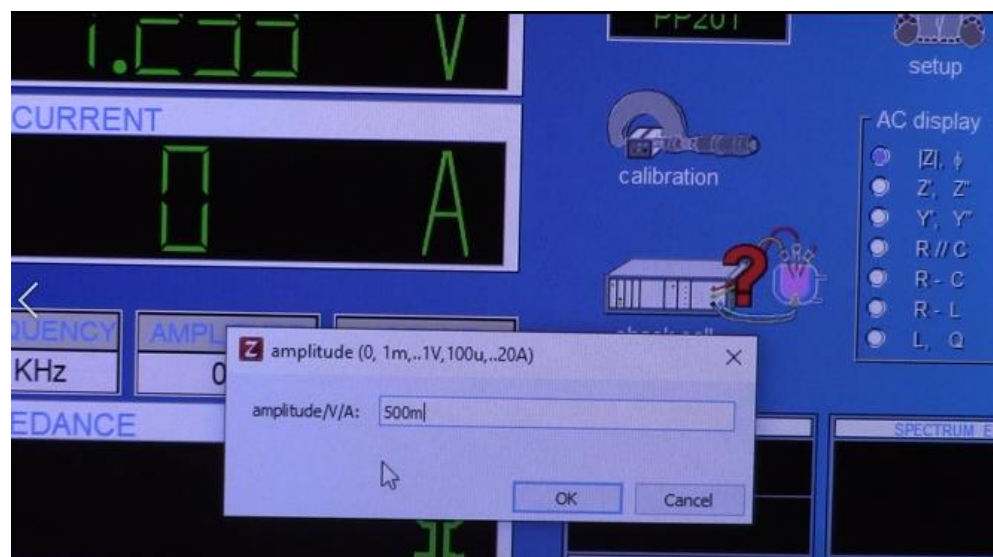


Figure 2.23 Selection of frequency

9. The frequency is constant is 1kHz. In the whole measurement all that matter is DC bias value and amplitude.

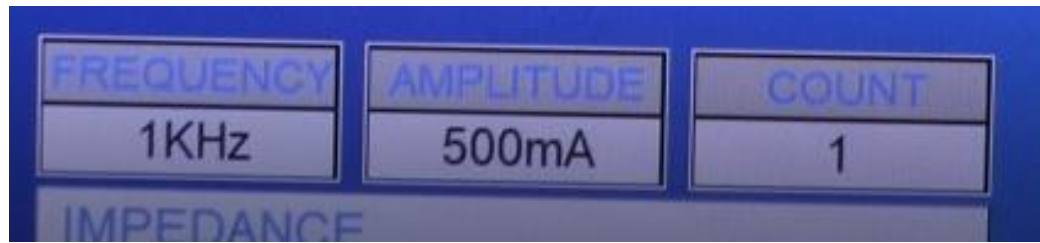


Figure 2.24 The frequency and amplitude set at required value

10. Next we have to set other parameters such as limit of frequency which goes from 10 micro to 100M. at this moment we are limiting the range between 500mHz to 50kHz. We can set the starting point, and the measurement goes to upper limit range than drops down to lower limit that is set manually. The whole operation is in the sweep mode. Also, the software can understand abbreviations like k that stands for thousand and etcetera.

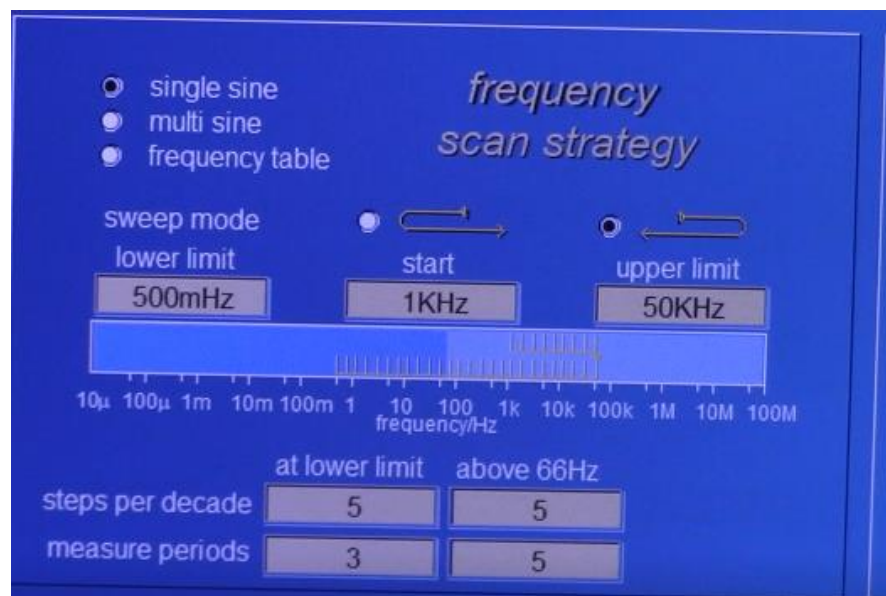


Figure 2.25 The whole window of setting the EIS spectroscopy.

11. Lastly, we have the option to choose the steps per decade, or the number of frequency points we desire per decade. The number of periods we desire for the entire procedure is set up at the measurement mode option. Every period, we take an average of the value, do impedance spectroscopy, and measure the impedance. As the number of periods increases, accuracy improves. Steps per decade often range from 10 to 15, indicating a higher amount of data points and therefore higher resolution. In order to increase measurement accuracy, the usual measure intervals are five to twenty.

12. After setting up the parameters, the estimated runtime is visualized. The estimated runtime is dependent upon the two params that has been set earlier. In this case it is 1mniate 19 secs,



Figure 2.26 The Recording Bar

13. The measurement commences by selecting the "Start Recording" option. We are able to observe real-time measurements. At this point, we can analyse several DC parameters like as impedance, phase, frequency, voltage, and current. The current parameter, now set at -7.85 Amps, needs to be continuously checked to maintain a constant value, while the voltage should be kept at the established value of 0.8 volts. Furthermore, we can observe the constant variation in frequency that essentially corresponds to the sweep mode we have

chosen. Also, we have the capability to analyse and determine both the magnitude and phase of the impedance at the specific position being measured.

## 2.4 EIS spectrum obtained (Nyquist and bode plot)

Here at the figure we are observing the bode plot of impedance.

### Bode Impedance Plot:

Bode plots depict the relationship between the impedance of a system and frequency, with frequency typically represented on a logarithmic scale. It consists mainly of variables such as magnitude and phase.

Commonly expressed in decibels (dB), the magnitude diagram illustrates how the impedance magnitude varies with frequency.

The phase angle of impedance varies with frequency, as indicated by the phase shift or time delay between voltage and current on the phase plot.

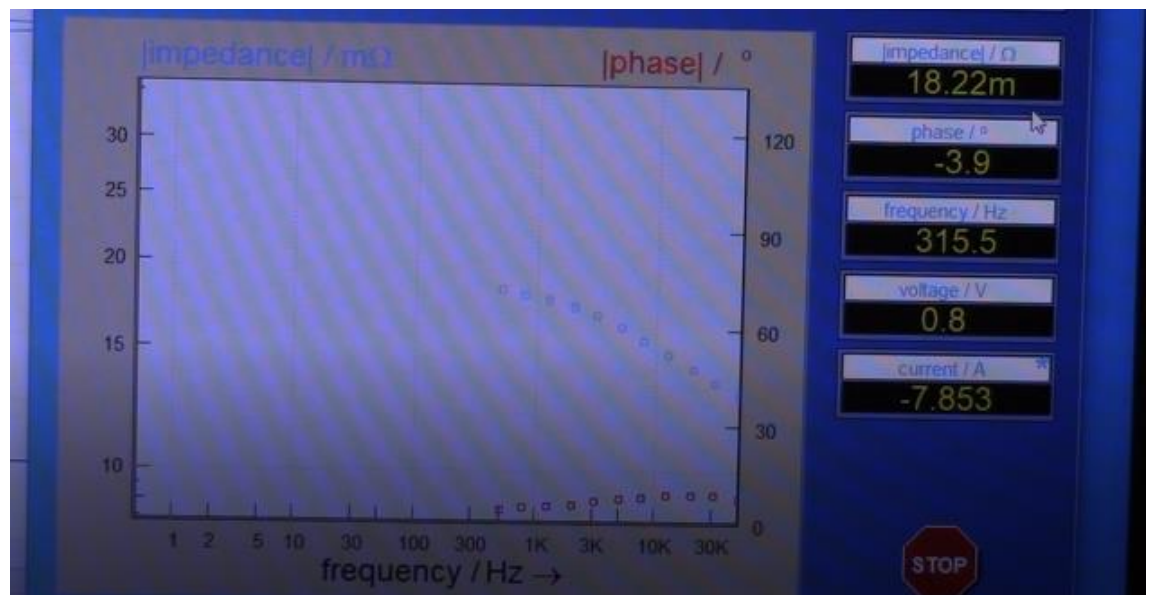


Figure 2.27 Bode plot of Impedance

**Nyquist Impedance Plot:** The Nyquist plot visualizes impedance (x axis real, y axis imaginary). As contrast to bode plot, a Nyquist plot depicts the impedance of a system in the complex plane graphically. Particularly in control

systems, it is employed to assess the frequency response and stability of a method.

The complex impedance (comprising real and imaginary components) is represented in a Nyquist plot as a function of frequency, usually achieved by varying the frequency across a range of values. As we have selected the frequency range 50m to 50k , so the impedance has been plotted in this range that is shown on Figure 2.28. We can observe that in Nyquist plot it reassembles the shape of semicircle.

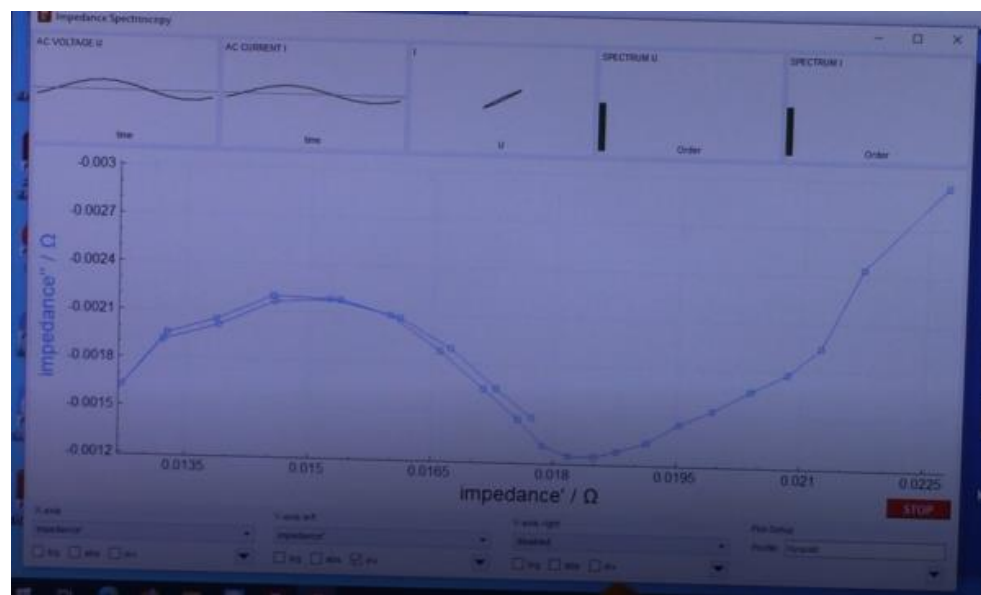


Figure 2.28 The Nyquist plot of impedance of SOFC fuel Cell

Finally, the software offers the option of different representation of data. Also, for each axis other parameters like voltage, current etc. Also, logarithmic, linear, or different types of scaling can be chosen as per the requirement. Most frequently, Nyquist or bode plot is observed to see what is happening.

The data can be saved or exported in different form like csv, text file etc.

# Chapter 3: EIS on an Electrochemical Equivalent Circuit with real lab measurements

---

## 3.1 Describe The Method to Use Eis (Electrochemical Impedance Spectroscopy) To Determine The Characteristics For The Electrochemical Equivalent Circuit

EIS Basic: Electrochemical Impedance Spectroscopy (EIS) serves as a robust analytical technique for studying complex electrochemical systems. EIS involves the measurement of a complex impedance spectrum across a broad spectrum of alternating current (AC) frequencies. However, the impedance at specific frequencies in the system typically reflects contributions from multiple cell components, leading to increased complexity in EIS spectrum analysis.

The most common method used to analyze EIS spectra is equivalent circuit modelling. This method involves the simulation of cell elements within the circuit. Each component's performance is subsequently characterized using conventional electrical elements, such as resistors, capacitors, and inductors plus a few specialized electrochemical elements.

The first step in the process involves making an initial estimation. The system elements predicted that will play a part in the cell's impedance. These elements are then incorporated into an Equivalent Circuit Model. The effective arrangement of these elements into logical series and parallel configurations is crucial for successful modelling. Each element within the model exhibits a well-defined impedance behaviour, determined by the element type and the specific value(s) of its parameter(s).

Upon creating the system model, typically, the parameter values for these elements are initially unknown. For instance, a painted metal surface possesses a coating capacitance, but the precise value of this capacitance remains undetermined.

**Graphical Model Editor:** The IviumStat is Ivium's high performance potentiostat/galvanostat/ZRA. It is well-suited for applications requiring a wide dynamic range, such as battery testing, corrosion measurements, and electrochemical research applications due to its broad current measurement capabilities and wide frequency range for impedance. The Iviumstat Electrochemical Impedance Spectroscopy Software includes a graphical Model Editor that can be used to build an equivalent circuit model. Figure 3.1 shows the Ivium equivalent circuit evaluator for anode reaction. This model represents one possible assignment of the circuit elements to physical phenomena.

The graphical Model Editor can be used to make up quite complicated circuits. One advantage of this approach is that we do not have to deal with the complex circuit descriptor codes that some older modeling programs use.

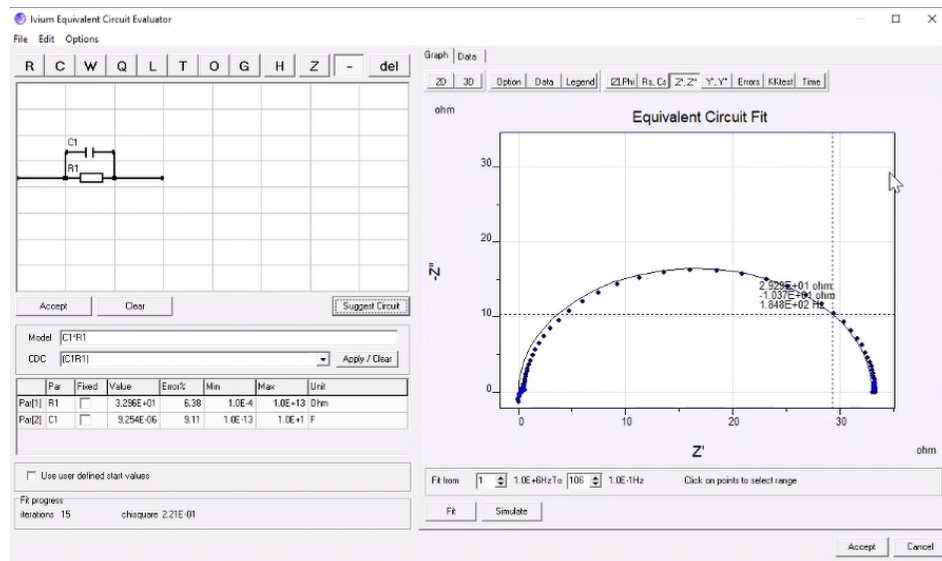


Figure 3.1 Ivium Equivalent Circuit Evaluator

**Fitting the Model to Experimental Data:** After modelling a system that represents the chemical system, a non-linear least square fitting program is used

to fit the model to the experimental data. This program attempts to minimize the deviation between the spectrum of the model and the experimental data spectrum.

One of the more difficult tasks in equivalent circuit modeling is determining the initial values for the model's parameters. The optimization program needs to start with values (often called seed values) for all parameters. If the initial values are far from the optimal values, the optimization program may be unable to find the best fit. In Ivium Electrochemical Impedance Spectroscopy Software, start values may be entered by the operator or will be calculated automatically and fit parameters may optionally be fixed. The software will calculate the best fitting set of parameters with the Levenberg-Marquardt technique.

**Determination of Component's Impedance :** By analyzing the best-fitted data obtained through EIS measurements, the impedance of each system element can be accurately determined. This pivotal aspect of EIS allow to gain a comprehensive understanding of the electrical and electrochemical behavior of the system, enabling insights into complex processes by breaking them down into individual components and their associated impedances. Ultimately, this information proves invaluable in various fields, from battery research to corrosion studies, providing a deeper understanding of the underlying mechanisms within electrochemical systems.

### 3.2 Introduction of the Topic

**Electrochemical Impedance Spectroscopy (EIS):** Electrochemical Impedance Spectroscopy (EIS) is a highly sensitive characterization technique that nondestructively examines the electrical behavior of chemical systems. EIS systems assess the time-dependent response of these systems using low-amplitude alternating current (AC) voltages across various frequencies. EIS provides quantitative measurements, enabling the analysis of small-scale

chemical processes at the electrode interface and within the electrolyte. As a result, EIS proves valuable for investigating diverse dielectric and electrical properties in research areas such as batteries and corrosion studies.

The significance of Electrochemical Impedance Spectroscopy (EIS) over alternative electrochemical methods lies in its unique capability to discriminate and, thus, provide extensive insights into the electrical, electrochemical, and physical phenomena occurring within a real electrochemical system. Notably, EIS measurements within an electrochemical system can be translated into an equivalent electrical circuit. This circuit comprises familiar passive components like resistors, capacitors, and inductors, as well as interconnected elements known as distributed elements. In essence, each of these processes can be represented as an equivalent electrical circuit, each characterized by distinct time constants.

When operating in the time domain, as is common in voltammetric techniques analyzing certain processes can be exceptionally challenging, if not outright impossible. In contrast, working in the frequency domain, over a broad range of frequencies, Electrochemical Impedance Spectroscopy (EIS) simplifies the complexity of electrochemical systems by breaking them down into individual processes with distinct time constants. This facilitates their straightforward analysis. Slower processes can be explored at lower frequencies, while faster processes can be studied at higher frequencies.

### EIS Equivalent Circuit:

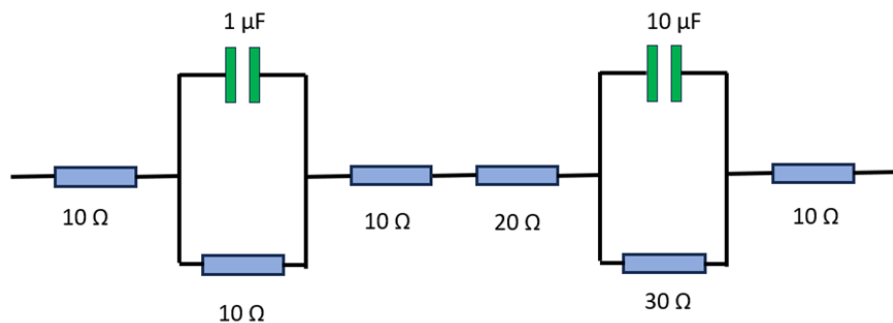


Figure 3.2 EIS equivalent circuit

Electrochemical processes associated with the electrolyte/interface are simulated/computed as an electric circuit (equivalent circuit) involving electrical components (resistors, capacitors, inductors). This equivalent circuit is designed and implemented to understand and evaluate the individual components of the EIS system. From left to right, the initial 10-ohm resistor denotes the anode contact, followed by a parallel network of a capacitor and resistor, representing the anode reaction. In the middle, two resistors signify the impedance of the electrolyte. Subsequently, the second parallel network consisting of a capacitor and resistor characterizes the cathode reaction. Finally, the last 10-ohm resistor serves to represent the cathode contact in the circuit.

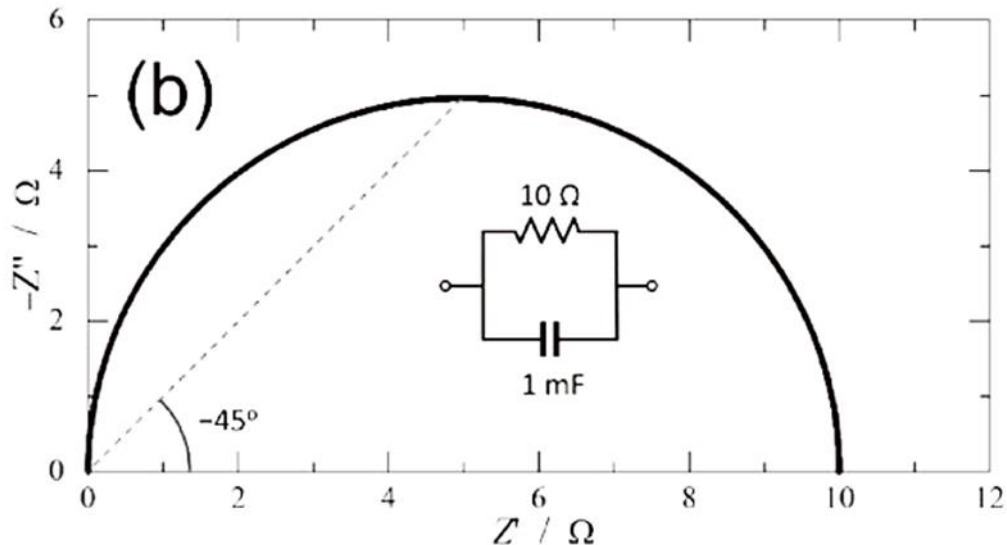


Figure 3.3 Nyquist Plot of RC circuit

**Data Presentation:** The impedance, denoted as  $Z$ , can be represented using two distinct methods: by its absolute value  $|Z(\omega)|$  and phase shift  $\theta(\omega)$ , or by its real part  $Z'(\omega)$  and imaginary part  $Z''(\omega)$ . These two representations of  $Z$  are visualized through two primary means: the Bode plot, which illustrates the logarithms of  $|Z(\omega)|$  and  $\theta(\omega)$  as functions of the logarithm of frequency, and the Nyquist plot, in which  $Z'(\omega)$  is represented on the horizontal axis, while  $-Z''(\omega)$  is displayed on the vertical axis. Two types of EIS representations, the Bode plot and Nyquist plot, convey the same information regarding impedance

(Z). Nevertheless, there are differences in the details acquired from these two visualizations.

Nyquist plots are a commonly employed method for assessing electrochemical impedance data. In these plots, the real impedance data is plotted on the x-axis, while the negative imaginary data is displayed on the y-axis. Nyquist plots utilize the electrical components defined by equivalent circuits to depict the frequency-dependent characteristics of impedance responses.

In the context of a parallel RC circuit, the impedance Z is determined by the equation  $1/Z = 1/ZR + 1/ZC$ . In parallel configuration, the behavior of the circuit element with the lower impedance takes precedence. Consequently, in the high-frequency range, impedance Z of the parallel RC circuit equals ZC, whereas in the low-frequency range, it equals ZR. In a Nyquist plot representing the parallel RC circuit, the locus of impedance, Z forms a semicircle, with the arc's diameter equivalent to R. The time constant for the parallel RC circuit is RC. At a frequency of  $\omega = 1/(RC)$ ,  $|ZR| = |ZC|$ , and  $\theta = -45^\circ$ , which corresponds to the vertex of the arc within the Nyquist plot.

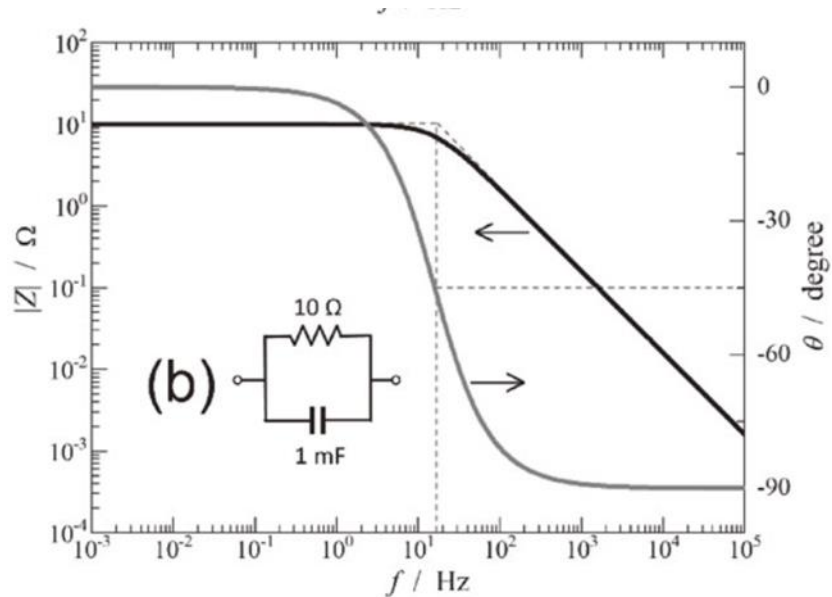


Figure 3.4 Bode Plot of RC Circuit

One notable limitation of Nyquist Plots is their inability to indicate the specific frequency at which data points were recorded. An alternative and widely used presentation method is the Bode Plot, which plots impedance against logarithmic frequency on the X-axis. On the Y-axis, it showcases both the absolute values of impedance ( $|Z| = Z_0$ ) and the corresponding phase shift, providing a more comprehensive representation of the data.

Examining the Bode magnitude plot, we observe that at extremely low frequencies, the magnitude of impedance ( $|Z|$ ) equates to  $R$ , while at significantly high frequencies,  $|Z|$  equals  $1/\omega C_1$ . Notably, the curve exhibits a change in slope, highlighted in Figure with a dotted-line circle, at the frequency corresponding to the system's time constant. This transition point marks a significant feature in the plot.

Examining the Bode magnitude plot, we observe that at extremely low frequencies, the magnitude of impedance ( $|Z|$ ) equates to  $R$ , while at significantly high frequencies,  $|Z|$  equals  $1/\omega C_1$ . Notably, the curve exhibits a change in slope, highlighted in Figure with a dotted-line circle, at the frequency corresponding to the system's time constant. This transition point marks a significant feature in the plot.

### 3.3 Background Theory

Valuable insights into the dynamic behavior of cells can be obtained by analyzing their response to step and impulse input. A simple yet highly effective model can be derived from a linear differential equation to accurately represent the cell's response to changes in load steps, specifically in relation to activation overvoltage. When the current undergoes stepwise changes, it takes a certain amount of time for the charge to accumulate or dissipate. In the activation loss region, the voltage does not immediately track the current like the ohmic voltage drop; instead, it gradually approaches its final equilibrium value. An approach to model this cell voltage response involves introducing an equivalent circuit. In

the equivalent circuit of a fuel cell or an electrolyzer, various components contribute to the series resistance, commonly referred to as the circuit's backbone. These components encompass charge transfer resistance, double layer capacitance, RC time constants, electrolyte resistance, and contact resistance.

### **Charge Transfer Resistance:**

Charge transfer resistance refers to the resistance encountered during the transfer of charge at the electrode-electrolyte interface. It represents the resistance to the electrochemical reactions taking place at the electrode surface. The charge transfer resistance is influenced by factors such as the nature of the electrode material, the kinetics of the electrochemical reactions, and the presence of any catalysts.

The probability of a reaction taking place depends on the density of the charges, electrons and ions on the electrode and electrolyte surfaces. Any collection of charge will generate a difference in electrical potential between the electrode and electrolyte — this is the 'activation overpotential'.

### **Double Layer Capacitance:**

The double layer capacitance is associated with the electrical double layer formed at the electrode-electrolyte interface. It arises due to the separation of charges between the electrode surface and the electrolyte. The double layer capacitance is a measure of the ability of the electrical double layer to store electrical charge. It depends on factors such as the surface area of the electrode and the properties of the electrolyte.

In electrochemical systems, the double-layer forms in part due to diffusion effects associated with the reactions between the electrons in the electrodes and the ions in the electrolyte, and also as a result of applied voltages. For example, the situation depicted in Figure 3.5 might arise at the cathode of a fuel cell with

an acid electrolyte. Electrons will collect at the surface of the electrode, and H<sup>+</sup> ions will be attracted from the bulk to the surface of the electrolyte. The electrons and ions, together with the oxygen supplied to the positive electrode, will take part in the reaction.

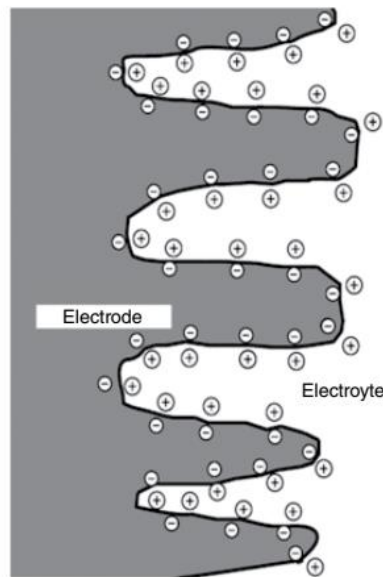


Figure 3.5. Charge double layer at the cathode surface of a fuel cell (*collected from [1]*).

The layer of charge on or near the electrode | electrolyte interface is a store of electrical energy, and as such behaves much like an electrical capacitor. If the current changes, it will take some time for the charge (and its associated voltage) to dissipate (if the current reduces) or build up (if there is a current increase). Consequently, unlike an ohmic loss in voltage, the activation overpotential does not immediately change with the current [1].

Consider now the combined effect of the overpotentials on two electrodes of a complete fuel cell. If the current through the fuel cell suddenly changes, the operating voltage will show an immediate change due to the internal resistance that is followed by a fairly slow progress to its final equilibrium value. The behavior can be modelled by using an equivalent circuit, with the double-layer represented by an electrical capacitor.

The capacitance of a capacitor,  $C$ , is given by the formula:

$$C = \epsilon \frac{A}{D}$$

where  $\epsilon$  is the electrical permittivity,  $A$  is the surface area and  $D$  is the separation of the plates. For a fuel cell,  $A$  is the real surface area of the electrode, which is several thousand times greater than its length  $\times$  width. The separation,  $D$ , is very small, i.e., typically only a few nanometers.

### **RC Time Constants:**

The RC time constants in the equivalent circuit of a fuel cell represent the time constants associated with the resistive and capacitive elements in the circuit. The resistive element ( $R$ ) represents the series resistance, while the capacitive element ( $C$ ) represents the double layer capacitance. The RC time constants determine the rate at which the circuit responds to changes in voltage or current. They are influenced by the values of resistance and capacitance in the circuit.

### **Electrolyte Resistance:**

The electrolyte resistance represents the resistance encountered by the ions as they move through the electrolyte. It depends on factors such as the conductivity of the electrolyte and the distance the ions need to travel. The electrolyte resistance is an important factor in determining the overall performance of the fuel cell, as it affects the efficiency of ion transport and the overall resistance of the circuit.

### **Contact Resistance:**

Contact resistance refers to the resistance encountered at the interfaces between different components of the fuel cell, such as the electrode-electrolyte interface or the electrode-current collector interface. It arises due to imperfect

contact between the components and can be influenced by factors such as surface roughness, contamination, and the presence of oxide layers. Contact resistance can significantly impact the overall performance of the fuel cell by affecting the flow of charge between the components.

These components, including charge transfer resistance, double layer capacitance, RC time constants, electrolyte resistance, and contact resistance, collectively make up the series resistance or the backbone of the equivalent circuit of a fuel cell. Understanding and optimizing these components is crucial for improving the performance and efficiency of fuel cells.

The connection between the double layered capacitances formed in the electrodes, the charge stored in it and the resulting activation overpotential leads to an equivalent circuit, as shown in Figure 3.6. The resistor  $R_{ac}$  and  $R_{kc}$  simulates the contact resistances from anode side and cathode side. A change in current gives an immediate change in the voltage drop across this resistor as represented by  $R_{elec}$ . The resistor  $R_a$  and  $R_k$  models the activation overpotential of anode and cathode respectively, and their associated capacitors 'smooths' any voltage drops across these resistor.

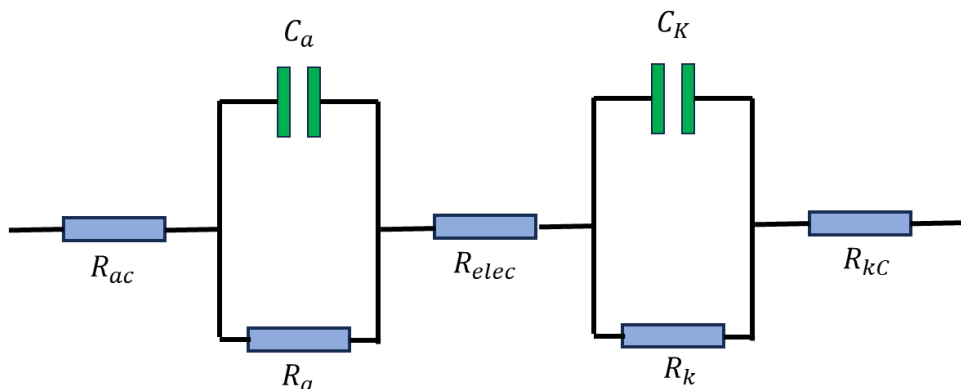


Figure 3.6. A representation of the equivalent circuit of electrochemical system. Electrochemical impedance spectroscopy (EIS) offers kinetic and mechanistic data of various electrochemical systems and is widely used in corrosion studies, energy conversion and storage technologies, etc. EIS is based on the perturbation

of an electrochemical system in equilibrium or in steady state, via the application of a sinusoidal signal (*ac* voltage or *ac* current) over a wide range of frequencies and the monitoring of the sinusoidal response (current or voltage, respectively) of the system toward the applied perturbation. Considering that the electrochemical system under study is a linear time-invariant system (that is, the output signal is linearly related to the input signal and the behaviour of the system is not changed over time), EIS is a “transfer function” technique that models the output signal (*ac* current or *ac* voltage) to the input signal (*ac* voltage or *ac* current) over a wide range of frequencies. The importance of EIS over other electrochemical techniques lies in its ability to discriminate and, thus, to provide a wealth of information for various electrical, electrochemical, and physical processes take place in a real electrochemical system. As mentioned above, a great advantage of EIS is the simulation of the data (an impedance spectrum) to an equivalent electrical circuit and in this way to retrieve numerical values for the components included in the circuit. The Nyquist and Bode plots for various simple electrical circuits containing a single passive element (R, C, or L) as well as combinations of them in different arrangements (in series or in parallel) are illustrated in Figure 3.7 and Figure 3.8, respectively to analyse their behaviours in electrochemical systems.

### R Circuit:

When the circuit contains only a resistor, Figure 3.7A, the equation of the impedance is  $Z = R1 + j0$ . The real part equals  $R1$ , while the imaginary part is zero. As a result, the Nyquist plot shows a single point lying in the real axis. That is, the impedance values at all the excitation frequencies are exactly the same and equal to the value of the resistance of the resistor. As a result, the Bode magnitude plot shows a straight line that crosses the left axis at  $|Z| = R1$ , as

$$Z = \sqrt{Z'^2 + Z''^2} = R1$$

while the Bode phase angle plot shows a straight line that crosses the right axis at  $\varphi = 0^\circ$ , as through a resistor, the voltage and current waveforms are “in-phase”.

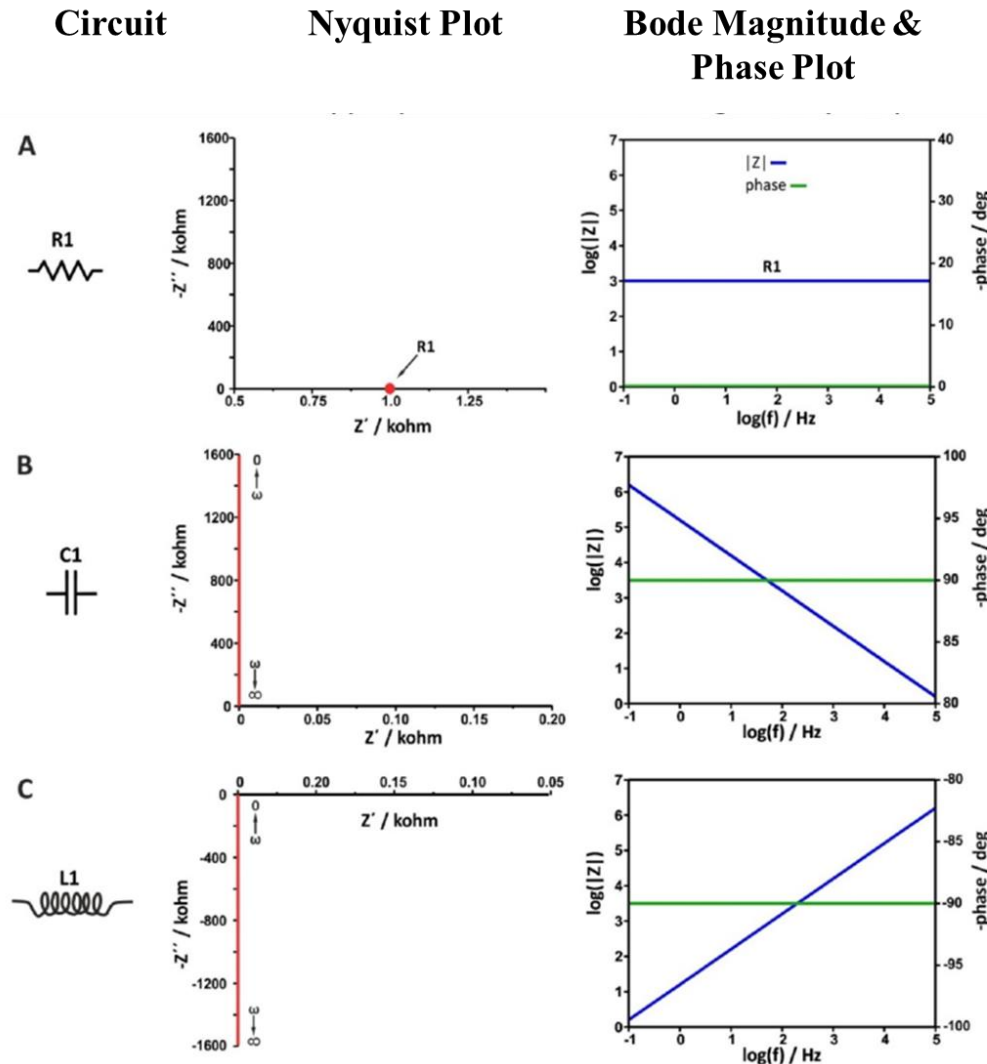


Figure 3.7. Nyquist, Bode magnitude and phase angle plots of some model circuits.  $R1 = 1\text{k}\Omega$  (*collected from [[2]]*).

### C Circuit:

When the circuit contains only a capacitor, Figure 3.7B, the equation of the impedance is  $Z = 0 + 1/j\omega C = 0 - j(1/\omega C)$ . The real part is zero, while the imaginary part is reversely proportional to the capacitance and frequency. As a result, the Nyquist plot shows a straight line lies in  $y$ -axis (the real impedance is zero). Values close to zero corresponds to high frequencies, while at lower frequencies

the impedance values are higher. The Bode magnitude plot shows a straight line with slope -1, while the Bode phase angle plot shows a straight line that crosses the right axis at  $\varphi = -90^\circ$ , as through a capacitor, the voltage and current waveforms are “out-of-phase” with  $\pi/2$ .

### L Circuit:

When the circuit contains only an inductor, Figure 3.7C, the equation of the impedance is  $Z = 0 + j\omega L$ . The real part is zero, while the imaginary part is proportional to the inductance of the coil and frequency. As a result, the Nyquist plot shows a straight line lies in  $y$ -axis, below the real axis, as in this case the phase difference between voltage and current is  $\varphi = 90^\circ$ . Values close to zero corresponds to low frequencies, while at higher frequencies the impedance values become higher. The Bode magnitude plot shows a straight line parallel to the frequency axis. At all the measurements the phase difference is  $90^\circ$ , where the voltage leading the current  $\pi/2$ .

### LC Series Circuit:

When the circuit contains a series combination of an inductor and a capacitor, the equation of the impedance is  $Z = 0 + jwL - jwC$ . The real part is zero, while the imaginary part is proportional to the effect of inductance and capacitance for a particular frequency. As a result, the Nyquist plot shows a straight line lies in  $y$ -axis, below and above the real axis, as in this case the phase difference between voltage and current is  $\varphi = 90^\circ$  and  $-90^\circ$  depending upon the frequency. The Bode magnitude and phase plot follows the trace given by the expression,

$$Z(w) = \sqrt{Z'^2 + Z''^2} = w(L - C)$$

So, Bode magnitude and phase plot follows the nature of the dominant component in the circuit.

### RC Parallel Circuit:

When the circuit contains a resistor and a capacitor connected in parallel as in Figure 3.8A, the equation of the impedance is,

$$Z(w) = \frac{1}{\frac{1}{R1} + jwC1} = \frac{R1}{1 + jwC1R1} = \frac{R1}{1 + (wR1C1)^2} - j \frac{wC1R1^2}{1 + (wR1C1)^2}$$

and the Nyquist plot corresponds to a semicircle. In this case, at very high frequencies the capacitive reactance tends to zero ( $\omega \rightarrow \infty, X_c \rightarrow 0$ ), and thus, all the current passes through the capacitor. The circuit acts as a short circuit and the impedance is zero. At very low frequencies, the capacitive reactance tends to infinity ( $\omega \rightarrow 0, X_c \rightarrow \infty$ ), and all the current passes through the resistor. The impedance contains only the real part and  $Z' = R$ . In response to the discussion above, when the  $\omega \rightarrow 0$  the current is constant. The constant current cannot flow through the capacitor, it flows only though the resistor. At intermediate frequencies, the current passes at the same time through the capacitor and the resistor, while the ratio of the respective currents is defined by the opposition of the current flow through each branch. Traversing from high to medium frequencies, the capacitive reactance becomes larger but remains still lower than the ohmic resistance ( $X_c < R1$ ), which causes more alternating current to go through the capacitor while less constant current goes through the resistor. However, there is a single characteristic frequency corresponding to equal values of reactance and resistance ( $X_c = R1$ ). At this frequency the imaginary part of the impedance is maximum ( $wZ_{immax}$ ). For which we can write,

$$wZ_{immax} = \frac{1}{T_1} = \frac{1}{R1C1}, \quad \text{here } w = 2\pi f$$

The value of the frequency for which imaginary part of the impedance is maximum can be easily determined from the Bode magnitude and phase plot.

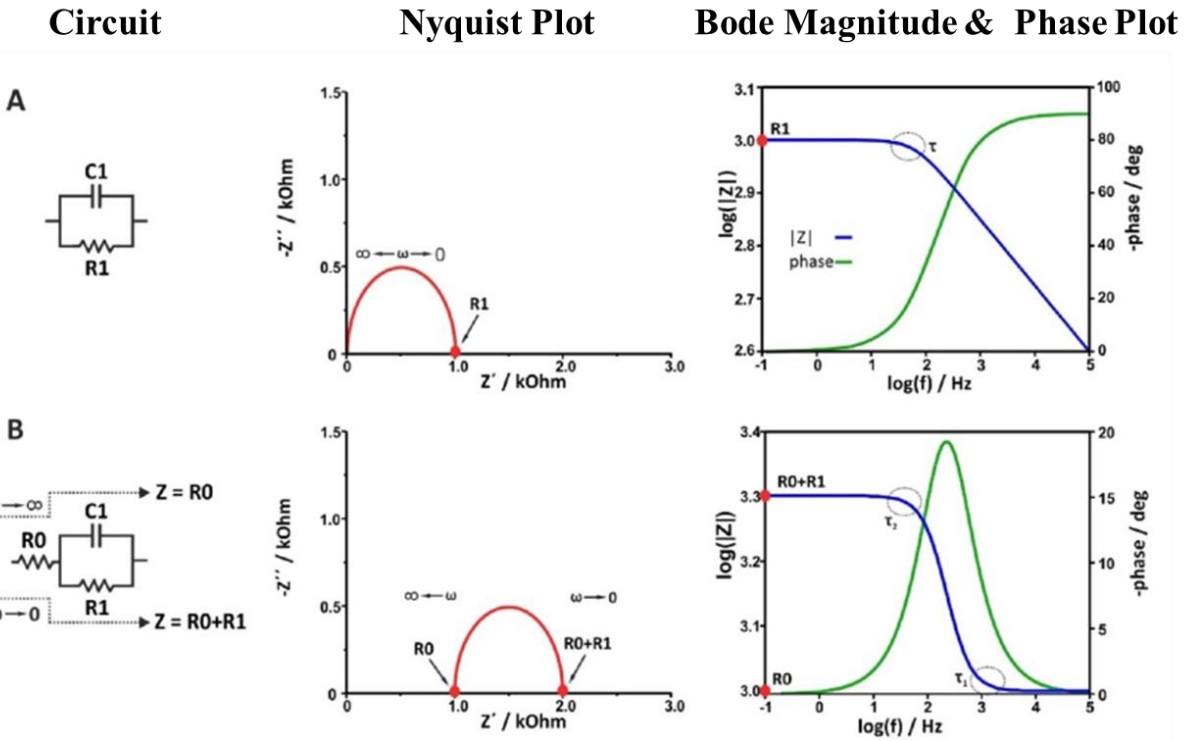


Figure 3.8. Nyquist, Bode magnitude, and phase angle plots of some model circuits (*collected from [2]*).

#### R is series with RC Parallel Circuit:

If a resistor  $R_0$  is connected in series with the circuit in Figure 3.8A, the equation of the impedance for the resulting circuit (Figure 3.8B).

At both very high and very low frequencies, the behaviour of the circuit is resistive and thus the semicircle is shifted to the real axis to a value equal to the ohmic resistance of  $R_0$ . As indicated in Figure 3.8B, at very high frequencies, ( $\omega \rightarrow \infty; X_C \rightarrow 0$ ),  $Z = R_0$ , while at very low frequencies ( $\omega \rightarrow 0; X_C \rightarrow \infty$ ),  $Z = R_0 + R_1$ . These boundary conditions are illustrated in the Nyquist plot as the first and the second crossing points of the semicircle on the axis of the real impedance, respectively. In contrast with the previous circuit (Figure 9A), this circuit has two time constants indicating the two breaking points appear at the Bode magnitude plot. The  $\tau_1$  at the high frequency domain is influenced by  $R_0$  and can be calculated as  $T_1 = [\frac{R_0 R_1}{R_0 + R_1}]C_1$ . The  $T_2$ , at lower frequencies, which as the slowest

one is considered as the characteristic time constant of the system, can be calculated from the Nyquist plot as in the case of the simple *RC* parallel circuit, as

$$wZ_{immax} = \frac{1}{T_2} = \frac{1}{R1C1}$$

Looking at the Bode magnitude and phase plot of this circuit, the change of  $|Z|$  and phase over a wide frequency range is described by an S-shaped and a bell-shaped curve, respectively.

### **3.4 The Real Lab Experiment Using The Iviumstat EIS Equipment**

In this section we will do real lab experiment using the IviumStat EIS . We will test an electrochemical equivalent circuit which is mainly used for analyse any fuel cell or any electrolyser or any other kind of electrochemical process from the point of a model that is made of electrical components.

From left to right, we can see some sections that are:

- a. Anode contact: 10 ohm.
- b. Anode reaction: 10 ohm R in parallel with 1uF capacitor.
- c. Electrolyte resistance: 100 ohm resistor in series with a 200 ohm Resistor
- d. Cathode reaction: 30ohm R in parallel with 10uF capacitor.
- e. Cathode contact: 10 ohms.

We will test this using impedance analyser called **IVIUMSTAT.XRi** . This is an electrochemical impedance operator and it's computer controlled.

1)To test any component we have to first connect two terminals/The first is Positive terminal which is red and the negative terminal is black.

2)At Ivium Software first we have to select **Impedance** from menu. The the option **Constatnt I** should be selected which means we are going to supply Sine wave to the equivalent Circuit with constant current. This is shown at Figure

3) To set some more parameters we will go to sub menu. We can see several things. They are'

Istat which is set to 0mA

The number of frequencies we are going to measure .

The current range etc.

This sub menu is presented at Figure

4)If we click the frequency options another submenu will be popped up. This shows how we can set up the frequency generator that we are going to supply. From this submenu we can select the start frequency ,end frequency and amplitude of the frequency. The all measured frequencies (61) that are going to be recorded can be observed here. So the frequencies are predetermined here.This all can be shown at Figure

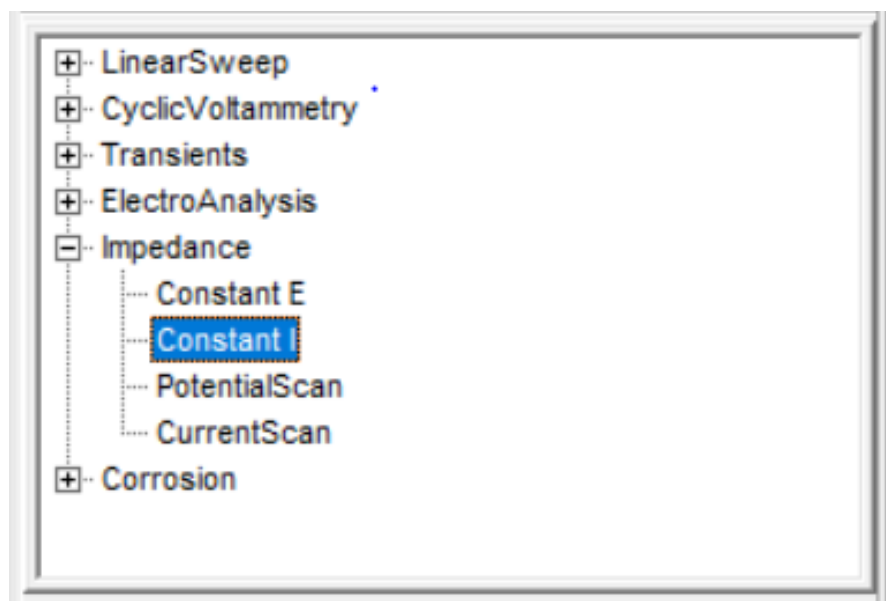


Figure 3.9. Impedance mode at IVIUMSTAT software.

	Value	Unit
Title	Scan 1	
+Redefine filename	<input type="checkbox"/> Off	
I start	0.000	mA
Equilibration time	0	s
I_Frequencies	5	
Current Range	10mA	
+Noise Reduction	<input type="checkbox"/> Off	
Filter	automatic	
Stability	automatic	
+Curr after meas	<input type="checkbox"/> Off	
IPretreatment	0	levels
Data Options		
+AUX	<input type="checkbox"/> Off	
+Anout2	<input type="checkbox"/> Off	
+Modules	<input type="checkbox"/> Off	
MeasConfig	standard	
Report		
Start		
Abort		

Figure 3.10. Submenu for selection of the Current

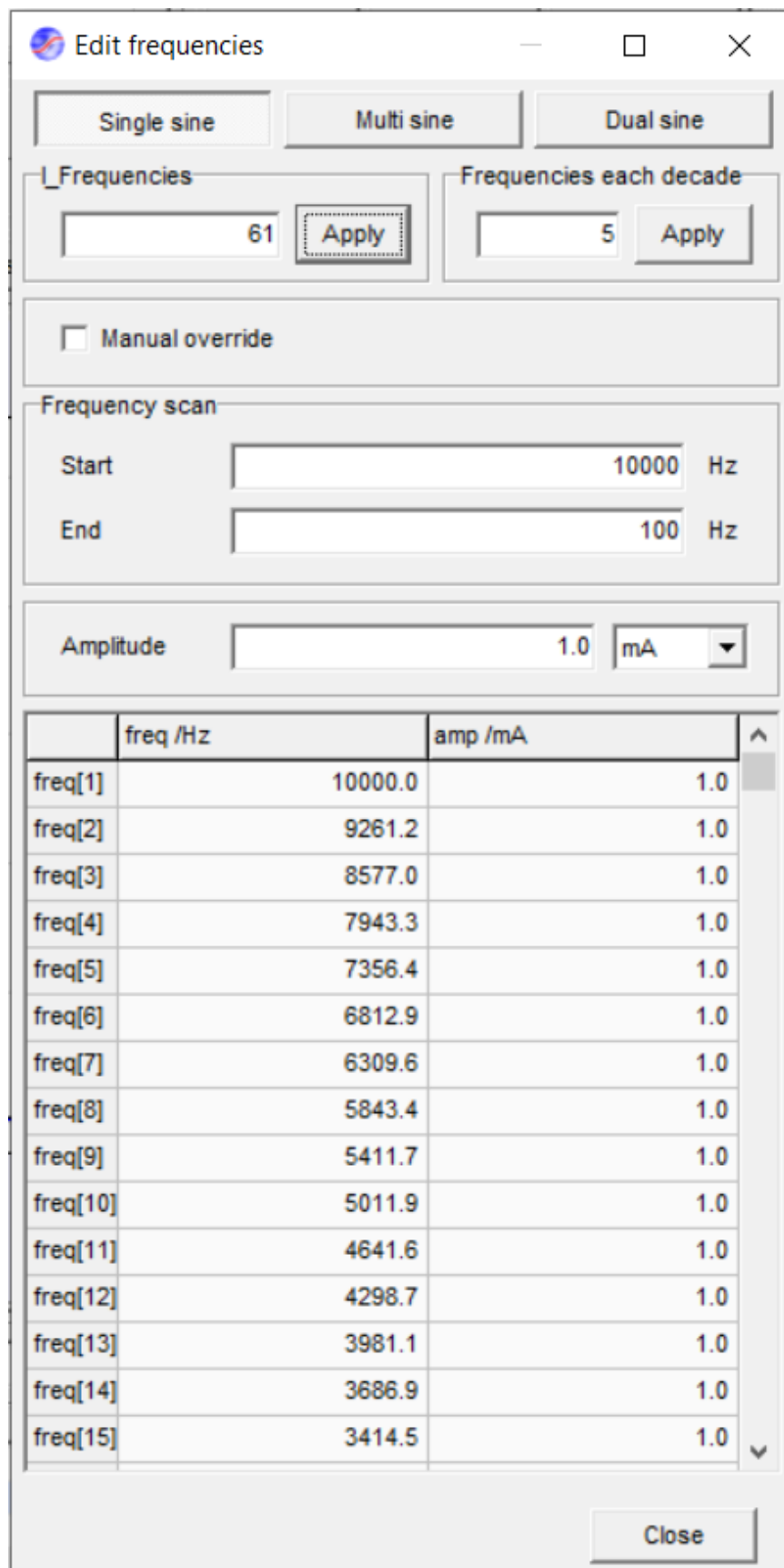


Figure 3.11. Frequency selection panel

5) We have to ensure the Ivium software is connected, then we can proceed into the next step, then we can start the testing

6) Now at the screen we can see the frequency response of the equivalent circuit. so for the whole circuit the curve will start from 50 ohm which is sum of all the resistors in high frequency and the curve will shaped like a semicircle. This is the high frequency semicircular arc or high frequency response for anode reaction. After that the frequency response for second equivalent circuit at low frequencies which represents the cathode reaction. It will take few moments to get down till the last frequency. When it reaches low frequencies, it takes longer time to record the spectrum. That's why we have to careful we should not select that much low frequency.

7) The menu has different dynamic plot options like

1. Nyquist plot of impedance

2. bode plot of impedance.

Now we will test each component one by one and try to find the frequency response for each of them. Later we will compare to the theoretical values for the following cases:

1. Cathode Contact Reaction Impedance
2. Cathode Contact Resistance:
3. Electrolyte Impedance:
4. Anode Contact Resistance
5. Capacitor Impedance
6. Capacitor in series with a Inductor

### 3.5 Results and Discussion

#### 3.5.1 Anode and Cathode Contact

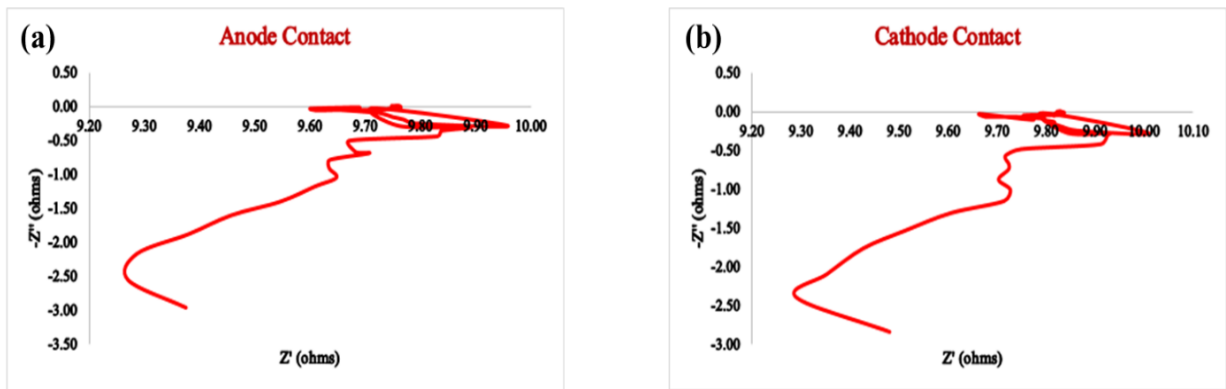


Figure 3.12. Anode and cathode contact resistances (a) Anode contact Nyquist plot (b) Cathode contact Nyquist plot.

Anode and cathode contacts are contact leads that are normally represented by resistances so, it reciprocates the condition of Figure 3.7A, where a resistance can be modelled through a dot in the Nyquist plot in the real axis. That is, the impedance values at all the excitation frequencies are exactly the same and equal to the value of the resistance of the resistor. However, experimentally a aberration on the behaviour is observed due to the associated inductances involved with the contact leads. That's why within the frequency region a trace has been found in place of a dot. However, the trace for both cases remained limited between  $9.2\Omega$  and  $10\Omega$  that closely resembles the nominal value of  $10\Omega$  for both the contacts.

#### 3.5.2 Electrolyte

According to Figure 3.13, a trace evolving around the imaginary axis has been shown. But the presence in the y-axis is too small compared to real axis value. Thus, it can be said that the electrolyte can be represented through a

resistance of  $32\Omega$ . This voltage loss is the straightforward resistance to the flow of electrons through the material of the electrodes and the various interconnections, as well as the resistance to the flow of ions through the electrolyte. The voltage drop is essentially linearly proportional to the current density and therefore is sometimes also called resistive losses.

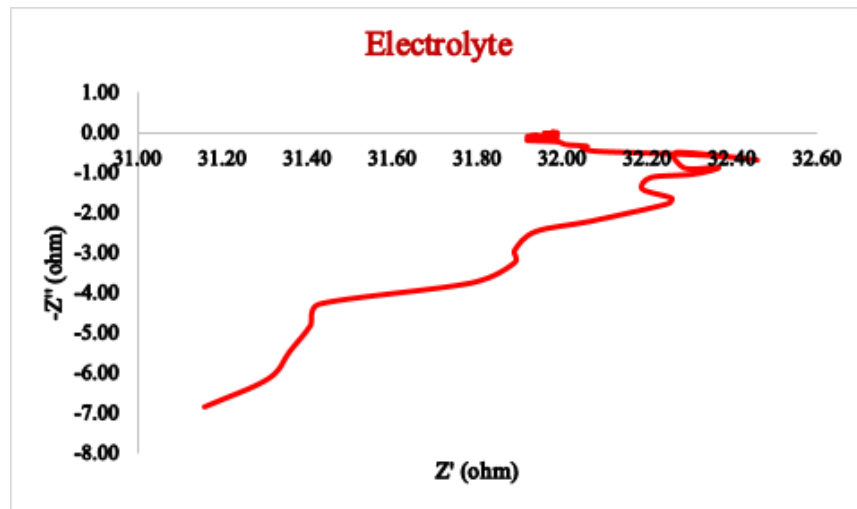


Figure 3.13. Nyquist plot for the electrolyte of the electrolyser.

### 3.5.3 Capacitor

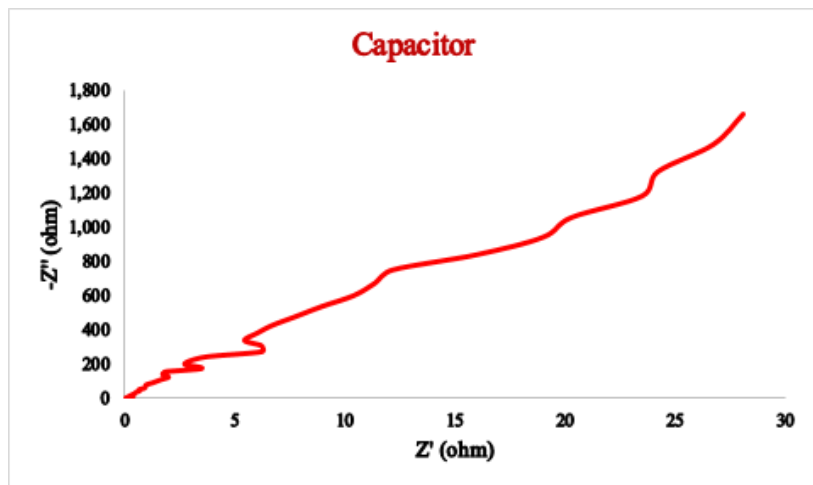


Figure 3.14. Nyquist plot for the  $1000\mu\text{F}$  capacitor.

As seen in Figure 3.7B, for capacitor, the real part of impedance is zero, while the imaginary part is reversely proportional to the capacitance and frequency. As a result, the Nyquist plot should be a straight line lies in positive side of  $y$ -axis (the real impedance is zero). Values close to zero corresponds to high frequencies, while at lower frequencies the impedance values are higher. However, from Figure 3.14 a variation is the  $x$ -axis is also visible while the deviation in real axis much smaller than that in imaginary axis. This is due to the involved resistance with the capacitor leads. The experimental value of the capacitor can be determined from the imaginary impedance at the lowest frequency (as the circuit is almost open) using the formula,

$$X_c = \frac{1}{2\pi f C}$$

The determined value of the Capacitance is found to be  $955\mu\text{F}$  whereas the nominal value is  $1000\mu\text{F}$ .

### 3.5.4 Inductor

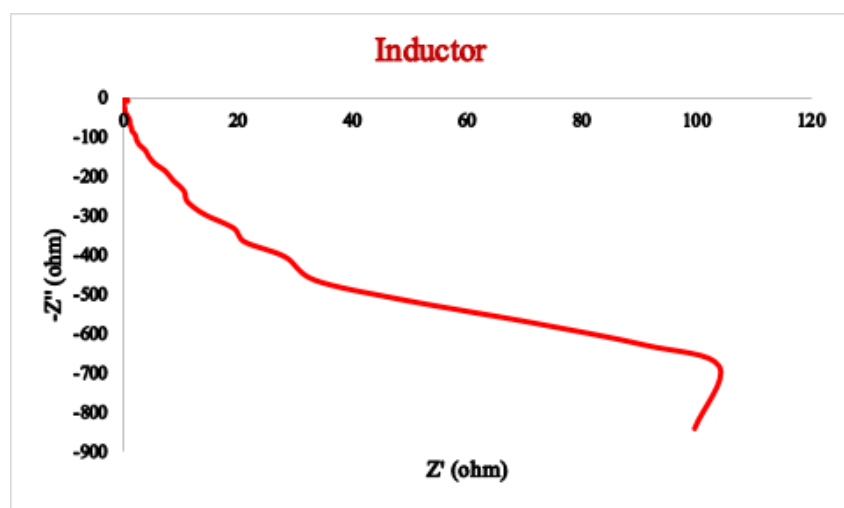


Figure 3.15. Nyquist plot for the  $150\mu\text{H}$  inductor.

When the circuit contains only an inductor, Figure 3.7C, the equation of the impedance is  $Z = 0 + j\omega L$ . The real part is zero, while the imaginary part is proportional to the inductance of the coil and frequency. As a result, the Nyquist plot shows a straight line lies in  $y$ -axis, below the real axis. Values close to zero corresponds to low frequencies, while at higher frequencies the impedance values become higher. In Figure 3.15, a variation is observed on the  $x$ -axis as well. This variation can be attributed to the resistance associated with the inductor leads. The experimental value of the inductor can be determined by analysing the imaginary impedance at the highest frequency, where the circuit is almost open. This can be done using the following formula:

$$X_L = 2\pi fL$$

The determined value of the inductance is found to be  $134\mu\text{H}$  whereas the nominal value is  $150\mu\text{H}$ .

### 3.5.5 Inductor and Capacitor

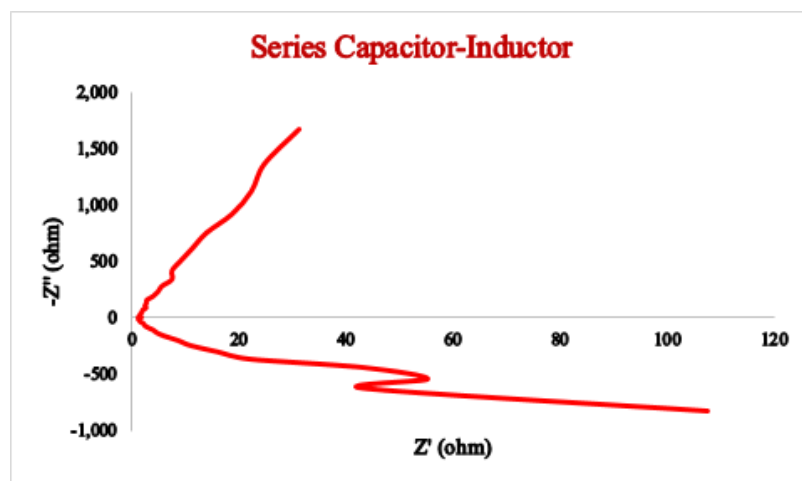


Figure 3.16. Nyquist plot for the series combination of inductor and capacitor.

When the circuit contains a series combination of an inductor and a capacitor, the equation of the impedance is  $Z = 0 + jwL - jwC$ . The real part is zero, while the imaginary part is proportional to the effect of inductance and capacitance for a

particular frequency. As a result, the Nyquist plot should be a straight line that lies in y-axis, below and above the real axis. However, from Figure 3.16 a variation is the x-axis is also visible while the deviation in real axis much smaller than that in imaginary axis. This is due to the involved resistance with the leads. The experimental value of the capacitor and inductor can be determined from the imaginary impedance at the lowest frequency and highest frequency using the formula employed in previous two cases.

The determined value of the inductance is found to be  $132.4 \mu\text{H}$  whereas the nominal value is  $150\mu\text{H}$  and the determined value of the capacitance is found to be  $953 \mu\text{F}$  whereas the nominal value is  $1000 \mu\text{F}$ .

### 3.5.6 Anode and cathode reaction

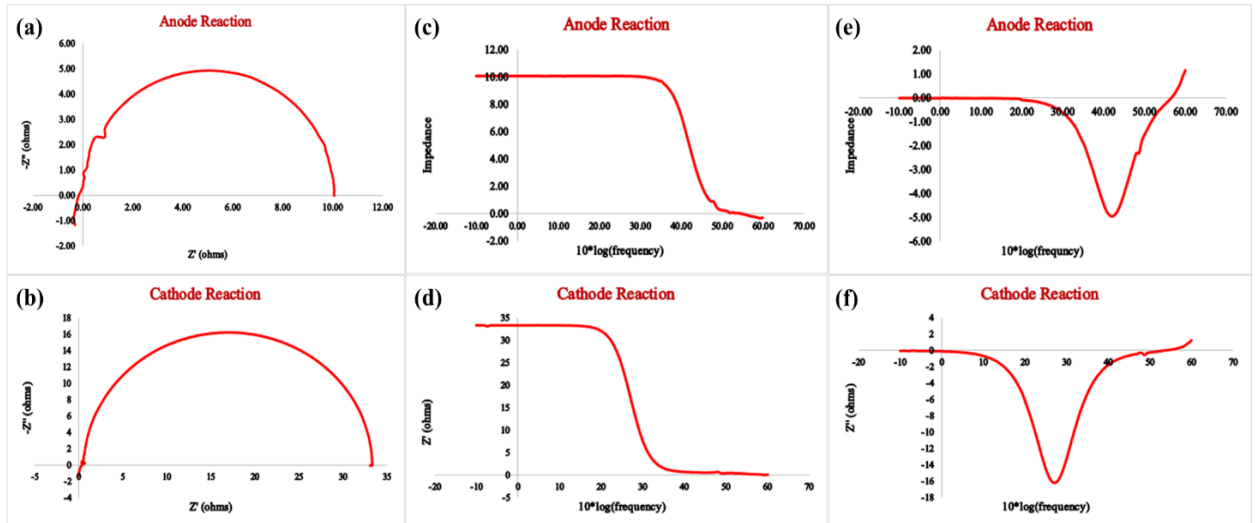


Figure 3.17. Nyquist plot for (a) Anode reaction, (b) Cathode reaction, bode plot – Real part of impedance for (c) Anode (d) cathode, Bode plot – Imaginary part of impedance for (e) Anode (f) cathode.

If Figure 3.17 and Figure 3.8A has been compared closely almost similar nature in the Nyquist plot can be observed as both the Nyquist plot corresponds to a

semicircle. Thus, it can be said that anode and cathode reaction correspond to a parallel RC circuit. In this case, at very high frequencies the capacitive reactance tends to zero, and thus, all the current passes through the capacitor. The circuit acts as a short circuit and the impedance is zero. At very low frequencies, the capacitive reactance tends to be infinite, and all the current passes through the resistor. So, at low frequency the impedance contains only the real part and  $Z' = R$ . Closely observing Figure 3.17 (a) and (b) it can be said that the resistive elements of the parallel branch have value of  $10\ \Omega$  and  $33.27\ \Omega$  for the anode and cathode reaction respectively. And the nominal values are  $10\ \Omega$  and  $30\ \Omega$  respectively.

The capacitive element of the parallel branch can be determined from the bode plot. Traversing from high to medium frequencies, the capacitive reactance becomes larger but remains still lower than the ohmic resistance ( $X_c < R$ ), which causes more alternating current to go through the capacitor while less constant current goes through the resistor. Thus, the relation between imaginary impedance and frequency is given by the equation,

$$X_c = \frac{1}{2\pi f C}$$

By closely inspecting Figure 3.17 (e) and (f), the capacitance values for the cathode and anode reactions are determined to be  $18.19\ \mu F$  and  $2.039\ \mu F$ , respectively. These experimentally derived values deviate significantly from the nominal values of  $10\mu F$  and  $1\mu F$ . It should be noted here that it is logical to have the experimental values larger than the nominal values.

### 3.5.7 Complete cell reaction

In the low frequency region, the capacitor acts like an open circuit, that's why the parallel resistance contributes to the total resistance value.

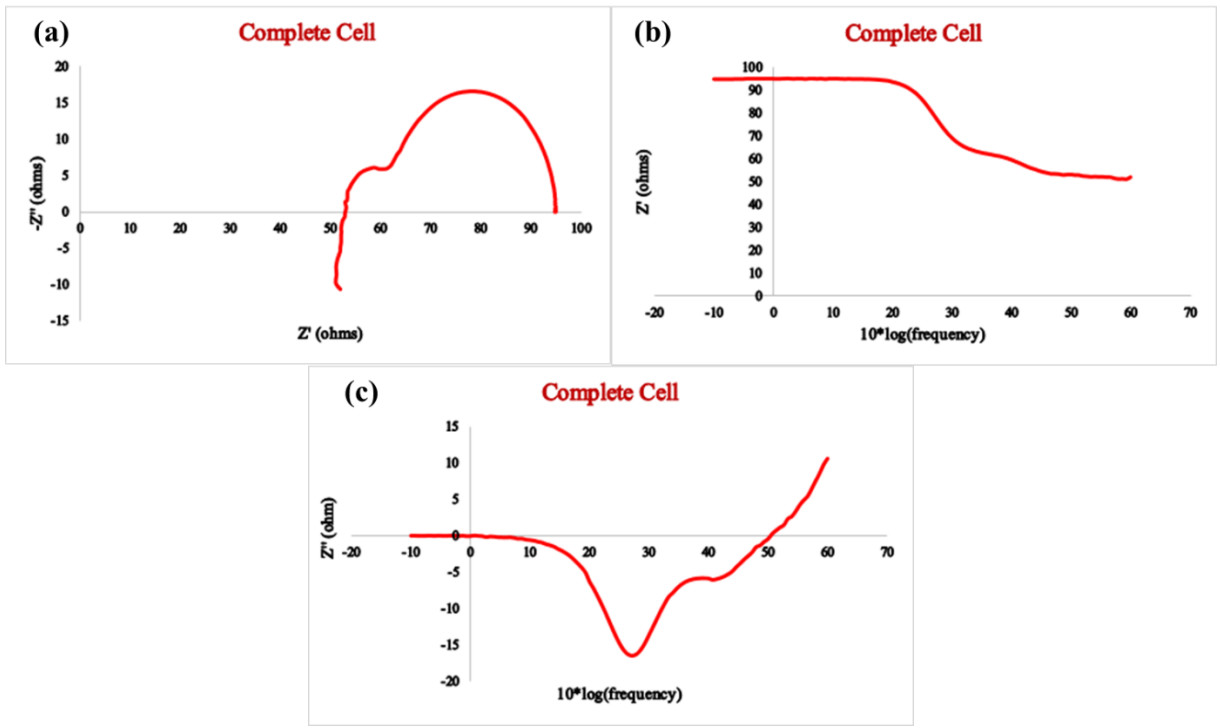


Figure 3.18. (a) Nyquist plot for the complete cell (b) Bode plot of real impedance (c) Bode plot of imaginary portion of impedance for the complete cell.

As seen in Figure 3.19a, the total resistance sums up to  $90\Omega$ . But at the high frequency region, the situation becomes exactly opposite and parallel resistors do not contribute to the total resistance. That sums up having total resistance of  $50\Omega$  as shown in Figure 3.19b.

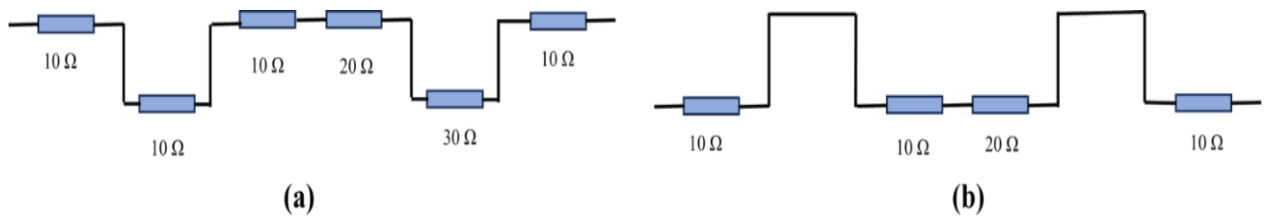


Figure 3.19. Circuit behaviour at low and high experimental frequency condition.

As close inspection of Figure 3.18a reveals the trace is offset by a real impedance value of  $52.84 \Omega$  which is explainable as the complete circuit exhibits impedance of  $50 \Omega$  at the high frequency. And the low frequency arc terminates at  $94.9 \Omega$  this resembles the impedance of the equivalent circuit at the lowest impedance when the capacitors act as open circuit.

Also, the distinguishable arcs at both the frequency region reveals that the cathode and anode reaction are represented by RC parallel circuits. The high frequency arc expands for almost  $10\Omega$  in the real axis, this suggests that in the parallel branch RC representation of anode reaction the charge transfer resistance is almost  $10\Omega$ . Where at low frequency region the expansion of the arc is about  $33\Omega$ . The existence of two parallel RC branch can be discovered from two visible valley that is present in the bode plot of imaginary impedance of Figure 3.18c. The value of the capacitance associated with the parallel branch can be determined from the relation of time constant to maximum imaginary impedance as employed in the previous cases. Identical analysis like the previous cases reveal that the values of the capacitances are  $2.2\mu F$  and  $17.3 \mu F$  for the high and low frequency arc respectively. These capacitances are also known as double layer capacitance as mentioned in Section 3.1 as they are associated with the capacitance formed due to the layer of charge on or near the electrode and electrolyte interface.

Apart from the cathode and anode reactions the electrolyte in the electrochemical systems is represented by resistance due to the ohmic losses. This voltage loss is the straightforward resistance to the flow of electrons through the material of the electrodes and the various interconnections, as well as the resistance to the flow of ions through the electrolyte. The voltage drop is essentially linearly proportional to the current density and therefore is sometimes also called resistive losses.

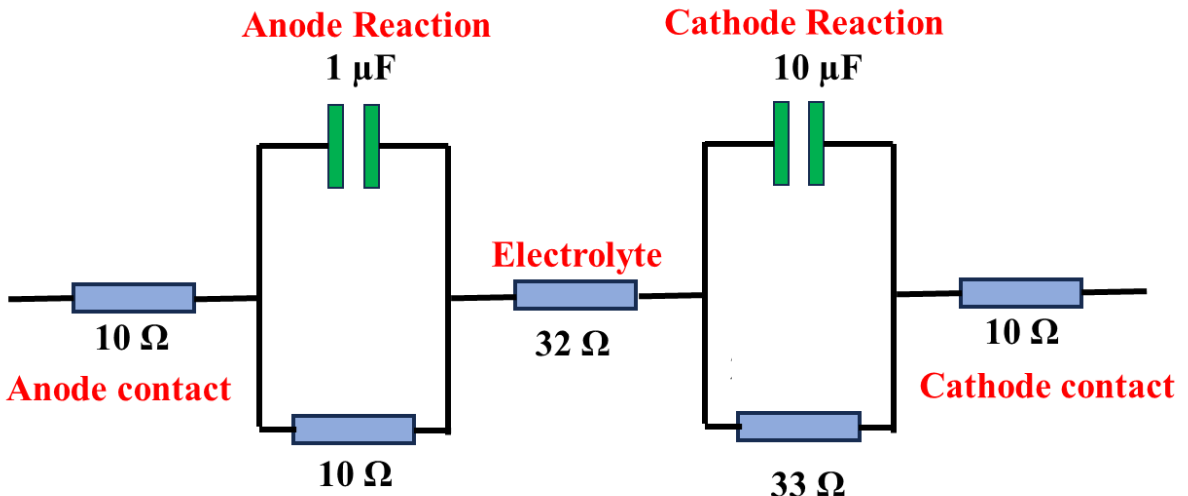


Figure 3.20. Complete equivalent representation of the electrochemical system.

Another resistive element that is visible in electrochemical systems is contact resistance. Contact resistance refers to the resistance encountered at the interfaces between different components, such as the electrode-electrolyte interface or the electrode-current collector interface. But the most dominant portion comes from the anode and cathode contact of the systems as external circuitry remains connected to these ports.

So, the complete representation of the equivalent circuit of the electrochemical system can be presented as Figure 3.20.

It is important to highlight that the measurement was conducted within an equivalent circuit comprising electrical components designed to emulate the electrical behavior of an electrolyzer. While these components may not precisely replicate the behavior, they do provide a reasonably close response. Furthermore, it is crucial to consider the experimental values as accurate and practical measurements for all conditions, rather than relying solely on the nominal values specified on the datasheet.

### 3.5.8 Determining the value of components from Ivium Software

The value that has been obtained from Ivium Software and there corresponding Nyquist plot are presented in Figure 3.21 to Figure 3.29.

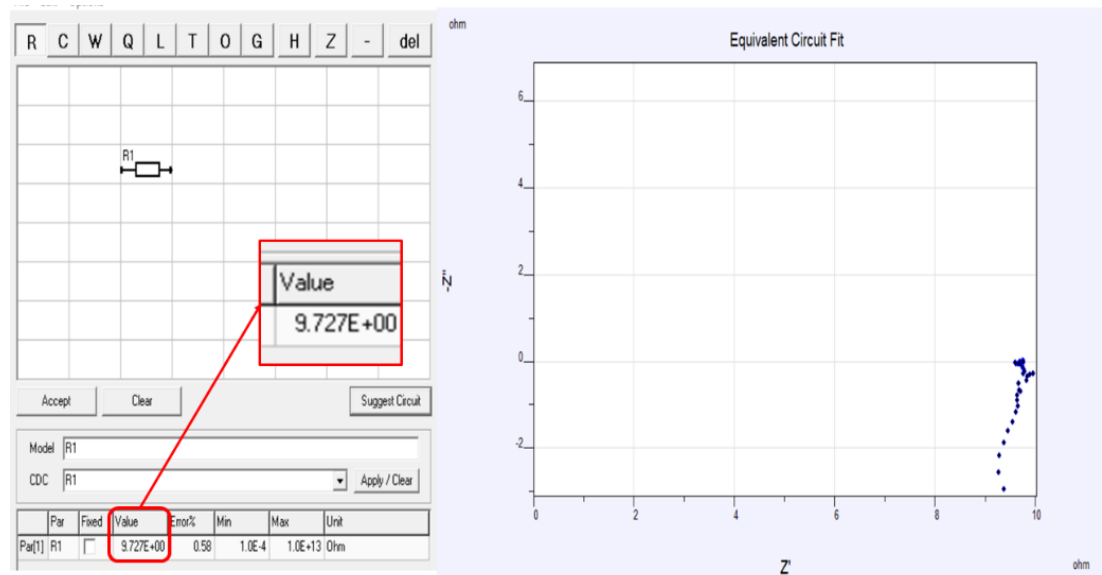


Figure 3.21 Determined value of resistance from Nyquist plot of Anode Contact.

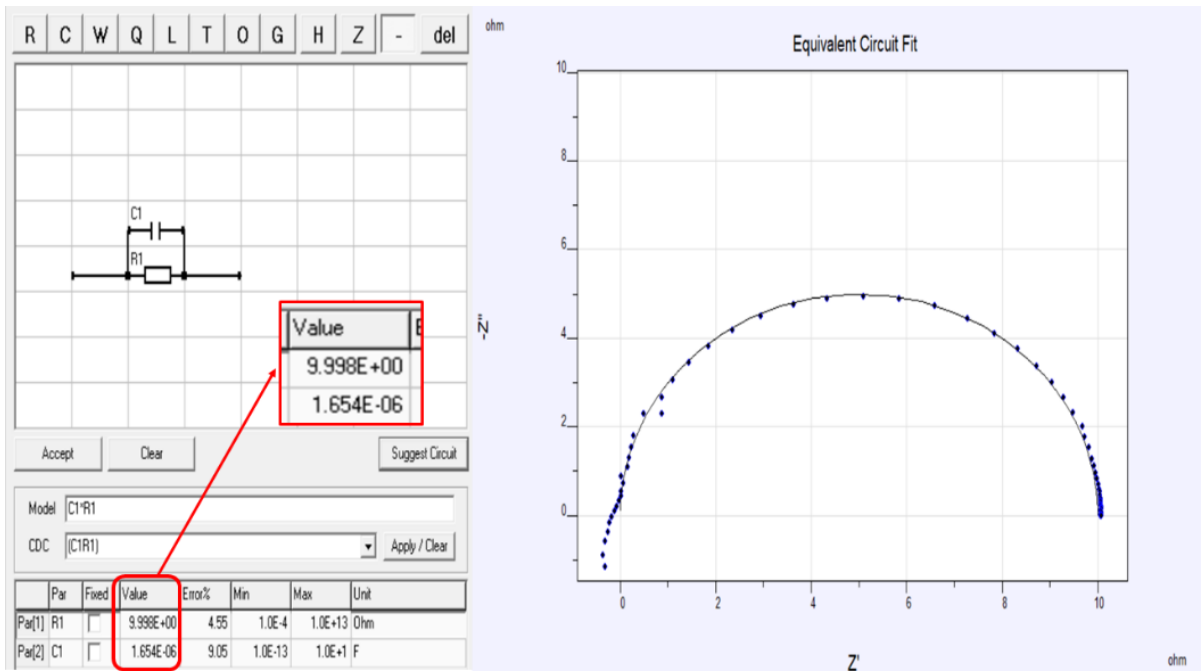


Figure 3.22 Determined value of resistance from Nyquist plot of Anode Reaction.

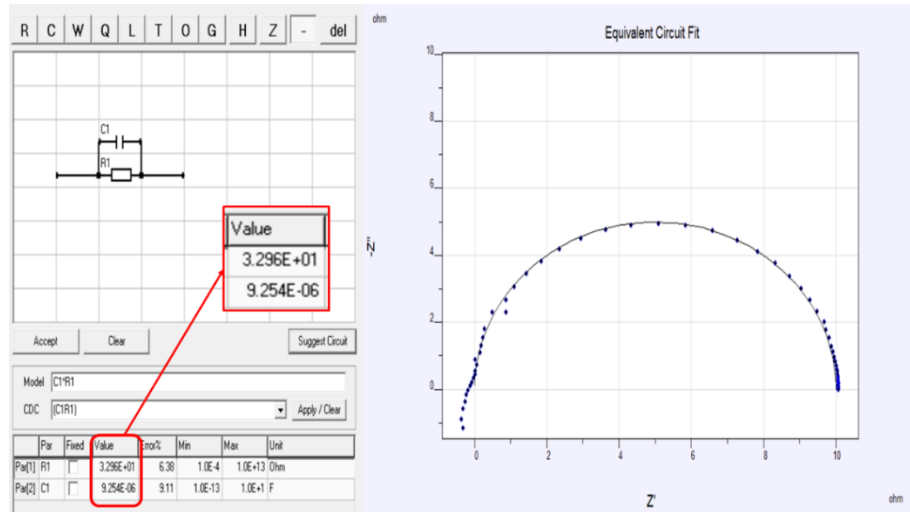


Figure 3.23 Determined value of resistance from Nyquist plot of Cathode Reaction.

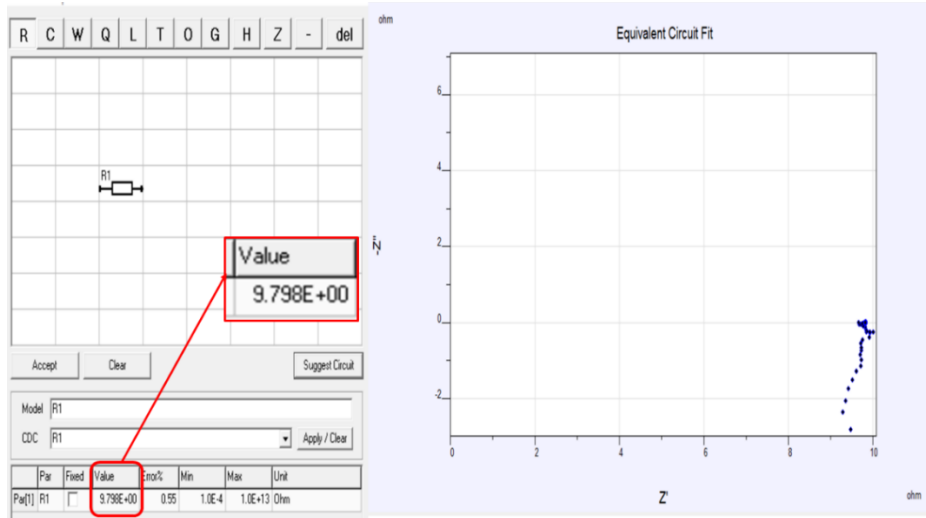


Figure 3.24 Determined value of resistance from Nyquist plot of Cathode Contact.

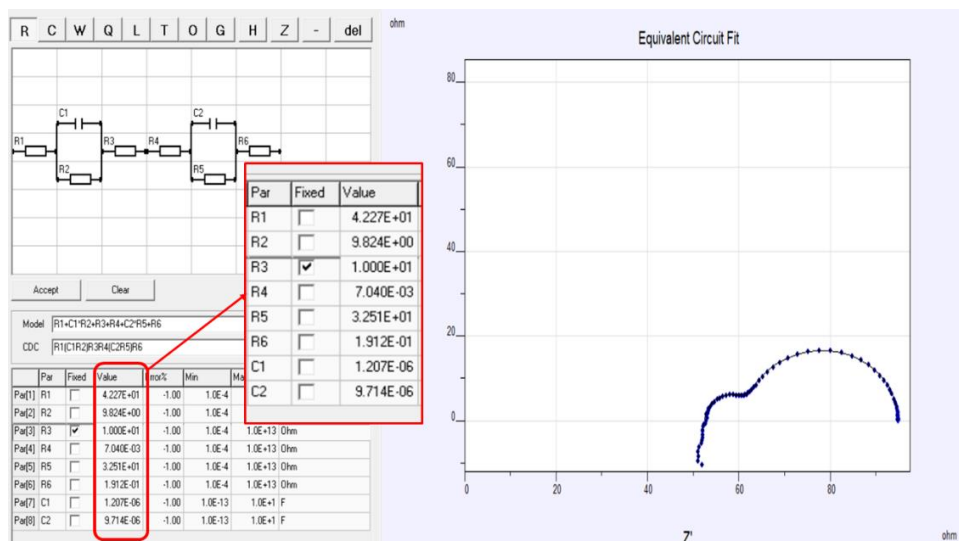


Figure 3.25 Determined value of resistance from Nyquist plot of Complete cell.

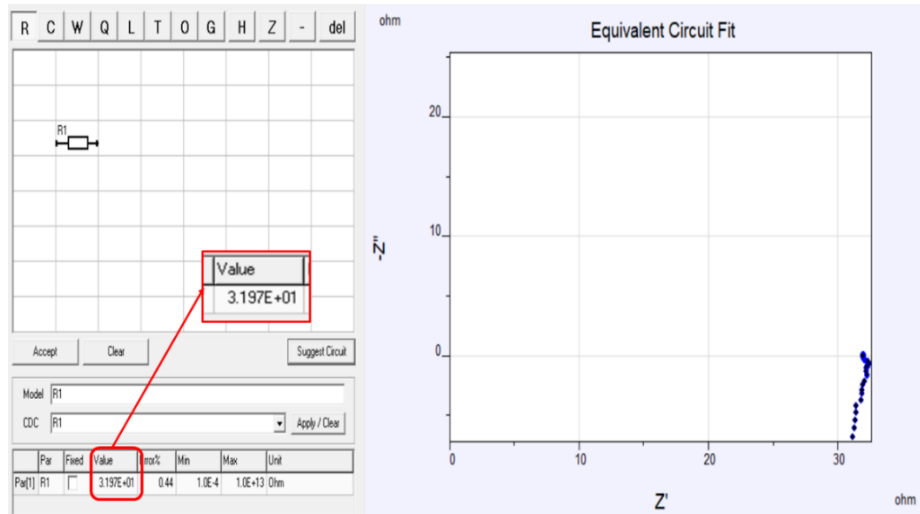


Figure 3.26 Determined value of resistance from Nyquist plot of Electrolyte.

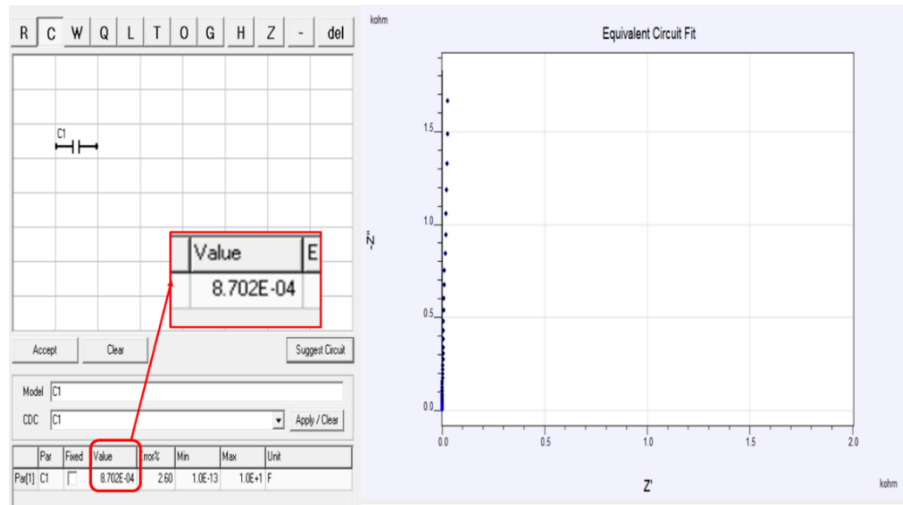


Figure 3.27 Determined value of resistance from Nyquist plot of Capacitor.

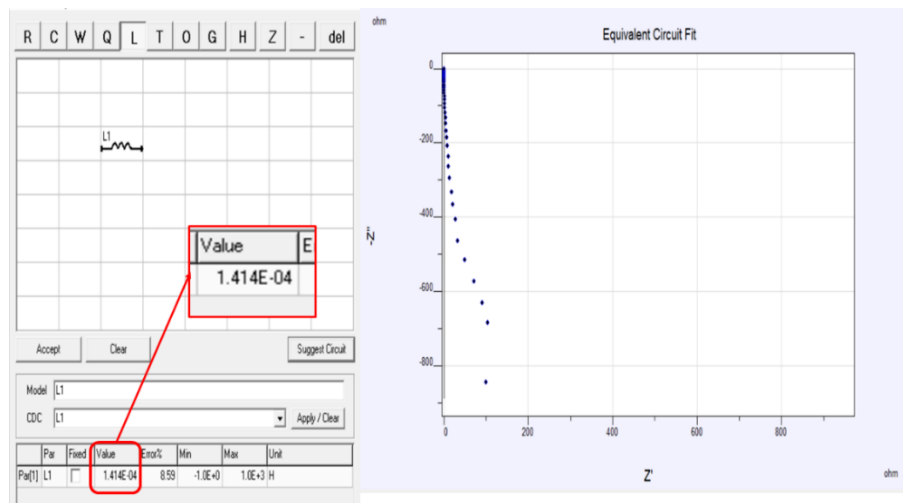


Figure 3.28 Determined value of resistance from Nyquist plot of Inductor.

The value of resistance for different components has been presented by the following table.

Parameters	Resistance (Ohm)	Capacitance (Faraday)	Inductor (Henry)
Anode Contact	9.727	-	-
Anode Reaction	9.998	-	-
Cathode Reaction	32.96	9.25e-6	-
Cathode Contact	9.79	-	-
Electrolyte	31.97	-	-
Capacitor	-	8.7e-5	-
Inductor	-	-	1.414e-4

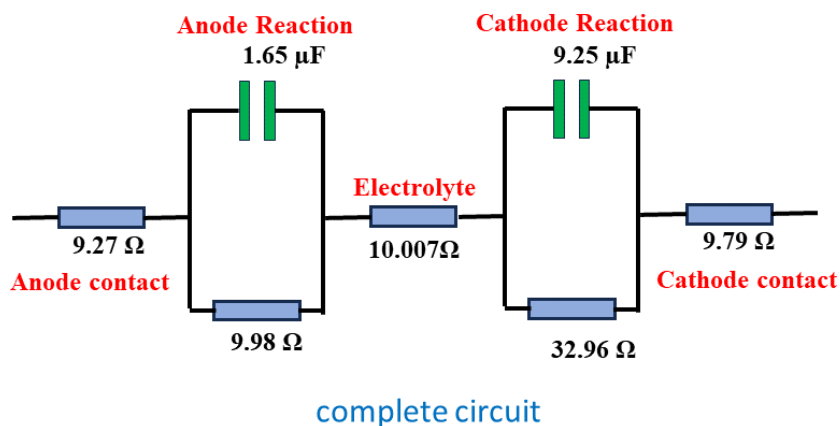


Figure 3.29 Complete Circuit measured resistance value by Ivium Software

# Chapter 4: Final Project

---

## 4.1 INTRODUCTION

In the current technological era, the global energy consumption landscape is undergoing dynamic changes. There is a growing emphasis on cleaner energy sources to mitigate greenhouse gas emissions. Within this context, hydrogen fuel-based sources are being considered as a significant alternative to meet the increasing energy demand. As a result, Polymer Electrolyte Membrane (PEM) fuel cell technologies have garnered widespread attention globally in recent years. This is primarily due to their high efficiency and low emissions, making them a promising solution in the pursuit of cleaner energy.

PEM fuel cells are distinguished by their construction utilizing polymer electrolyte membranes, notably Nafion, as the proton conductor, and electrochemical catalysts, typically Platinum-based materials, for facilitating electrochemical reactions at low temperatures. These fuel cells possess several notable features, including low operating temperatures, high power density, and ease of scalability. As a result, PEM fuel cells are considered promising candidates for the next generation of power sources in various applications such as transportation, stationary power generation, and portable electronics. Figure 1 illustrates the structure of a PEM fuel cell and its major components.

The history of fuel cells dates back to 1839 when Sir William Robert Grove demonstrated the first fuel cell. He showcased the nearly reversible electrochemical dissociation of water using platinized platinum electrodes in dilute sulfuric acid [3]. Another significant milestone occurred in 1962 when General Electric Company (GE) developed the first practical fuel cell for the

Gemini space mission. The 1-kW Gemini fuel cell system consisted of 31 cells in series, utilizing bi-porous nickel electrodes (anode porous Ni and cathode lithiated NiO) and a potassium hydroxide solution as the electrolyte. The system, enclosed in a thin metallic cylinder, provided electric power for life support and drinking water during the two-week lunar mission [4].

Notably, breakthrough techniques were introduced by Ian Raistrick *et al.* of Los Alamos National Laboratory (LANL) [5], who applied a solution containing dissolved Nafion material to the surface of a porous electrode, and by Wilson *et al.* [6], also of LANL, who invented methods for fabricating repeatable thin-film electrodes bonded to the proton-exchange membrane, resulting in a membrane electrode assembly (MEA). The combination of their techniques significantly reduced the required precious-metal catalyst loadings while improving performance. Gottesfeld *et al.*, also from LANL, proposed the injection of a small amount of oxygen-containing air into the fuel stream to oxidatively remove CO from the catalyst surface, enabling the direct use of hydrogen-rich gas streams derived from hydrocarbon fuels in PEM fuel cells [7]. Additionally, the concept of porous media flow fields was introduced to enhance reactant supply, byproduct removal, and fuel cell design [8].

Nowadays, PEM fuel cells find major applications in transportation, distributed/stationary power generation, and portable electronics. In 2017, Toyota launched its first commercial fuel cell vehicle, Mirai, at an affordable price with a total Platinum loading of  $0.365 \text{ mg/cm}^2$ . The Mirai fuel cells incorporate a carbon-coated titanium-based porous flow field in the cathode [9]. Despite significant advancements during the past decades, challenges such as cost reduction and durability improvement still need to be addressed for widespread deployment of PEM fuel cells. Another promising area is the utilization of PEM fuel cells for portable electronics and aircraft power, as the limited energy

capacity of batteries may not meet the growing energy demand of modern portable devices. PEM fuel cells provide continuous power as long as hydrogen fuel is available, and they can be fabricated in small sizes without efficiency loss. For aircraft power, PEM fuel cells offer advantages such as direct electrical power, high power density, and large energy capacity [10].

In this study, the fabrication, assembly, and testing of a basic single-cell PEM fuel cell are reported. Initially, a 3D structure of the cell was designed using SolidWorks software and then printed using a 3D printer available through UiA facility. The Nafion, Ni-foam, carbon paper, and gasket were collected and prepared in the Hydrogen lab. Subsequently, the assembled cell was subjected to experimental testing to characterize its behaviour.

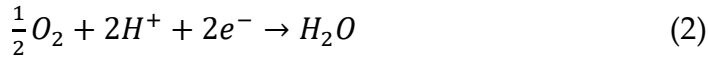
## 4.2 THEORETICAL BACKGROUND

### 4.2.1 Electrochemical Aspects

The Proton Exchange Membrane Fuel Cell (PEMFC) serves as an electrochemical system that converts hydrogen and oxygen into electricity while producing water as a by-product, operating efficiently at low temperatures. An integral element of the PEMFC is its membrane, facilitating the passage of protons while directing electrons into an external circuit.

In the initial stage, hydrogen undergoes oxidation at the anode/electrode interface, as described by Equation (1), where it is split into protons and electrons. Subsequently, protons and electrons travel along distinct pathways via the electrolyte and interconnect, respectively, to reach the cathode site. At this juncture, oxygen combines with protons and electrons, leading to the formation of water, as depicted in Equation (2). Notably, the oxygen reduction reaction

(ORR) kinetics occur concurrently on both sides of the anode and cathode membrane, culminating in the overall reaction outlined in Equation (3) [11].



However, the PEMFC faces multiple technical challenges, including challenges related to managing water within the gas channels, ensuring an adequate oxygen supply, and coping with high susceptibility to impurities, ultimately leading to the electrochemical deterioration of interconnectors.

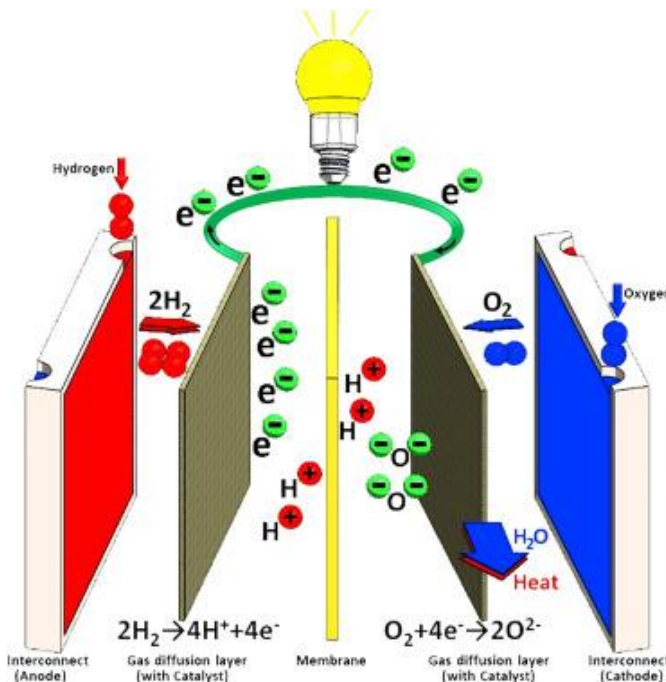


Figure 4.1. A typical single PEMFC schematic (recreated from [9]).

With the various operational factors impacting losses within the cell, the thermodynamic voltage (referred to as  $E_{thermo}$ ) stands as a critical influence on PEMFC output power. Essentially, the output voltage of a PEMFC relies on the potential difference between the anode and cathode, termed as  $E_{thermo}$  or cell

potential. The overall reaction for the formation of water (1 mol of H<sub>2</sub>O) results from combining 1 mol of H<sub>2</sub> with half a mole of O<sub>2</sub>. Consequently, estimating E<sub>thermo</sub> theoretically from this comprehensive reaction emerges as an important parameter affecting the performance of PEMFC output power.

Hence, Equation (4) and Equation (5) provide a means to measure the Gibbs free energy ( $\Delta G$ ) of water under standard conditions (25°C and 1 atm) utilizing pure H<sub>2</sub> and O<sub>2</sub> gases.

$$\Delta G = \Delta G \text{ of products} - \Delta G \text{ of reactants} \quad (4)$$

$$\Delta G = \Delta G^0 - RT \ln \left( \frac{a_{H_2} \times a_{O_2}^{\frac{1}{2}}}{a_{H_2O}} \right) \quad (5)$$

Here,  $\Delta G^0$  represents the standard Gibbs free energy associated with the overall reaction. R denotes the gas constant with a value of 8.314 J mol<sup>-1</sup> K<sup>-1</sup>, while T represents the temperature measured in Kelvin (K). Additionally, a<sub>H<sub>2</sub></sub>, a<sub>O<sub>2</sub></sub>, and a<sub>H<sub>2</sub>O</sub> denote the activities of H<sub>2</sub>, O<sub>2</sub>, and H<sub>2</sub>O, respectively.

Theoretically, it might be to assume that all of the standard Gibbs free energy,  $\Delta G^0$ , transforms into electrical energy in the absence of errors within the PEMFC system. However, when the reaction occurs within a single cell encompassing all reactants, the theoretical E<sub>thermo</sub> value of 1229 V can be determined under standard conditions using the Gibbs free energy, as detailed in Equation (6).

$$E_{thermo} = \frac{-\Delta G^0}{n.F} \quad (6)$$

In this equation, where n equals 2, it signifies the number of moles of electrons transferred during the cell reaction, while F stands for the Faraday constant, equivalent to 6.23 \* 10<sup>23</sup>. Due to various factors such as cell overpotential and irreversible losses (denoted as h), including activation (h<sub>act</sub>), ohmic (h<sub>ohmic</sub>),

and concentration ( $\eta_{conc}$ ) losses, the actual output potential ( $V$ ) of the operating PEMFC is notably lower than the  $E_{thermo}$ . Consequently, it can be deduced that the operating cell voltage ( $E$ ) represents a deduction from the reversible theoretical fuel cell voltage, in accordance with the Nernst equation (Equation (7)). Here,  $E_{rev}$  signifies the reversible fuel cell voltage, while  $E_{irrev}$  represents the irreversible voltage loss. Therefore, through the assessment of the actual voltage error, the output voltages ( $V$ ) of the PEMFC stack can be mathematically expressed using Equation (8) [11].

$$E = E_{rev} - E_{irrev} \quad (7)$$

$$V = E_{thermo} - \eta_{act} - \eta_{ohmic} - \eta_{conc} \quad (8)$$

#### 4.2.2 I-V Curve and Power Density Curve

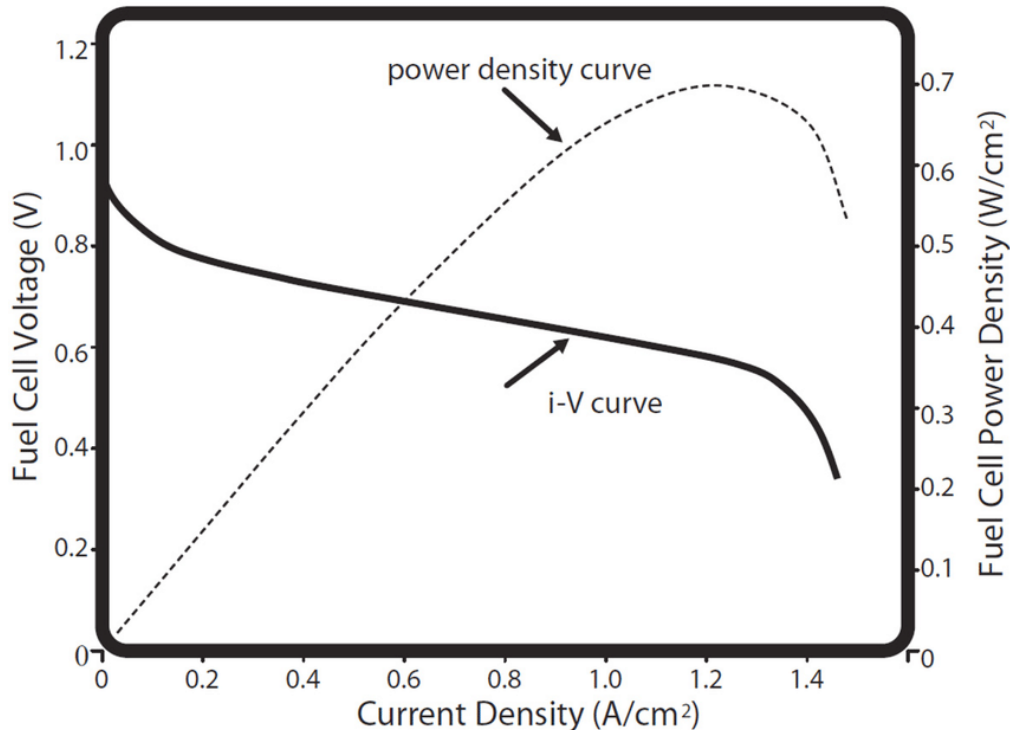


Figure 4.2. I-V Curve and Power Density Curve (collected from [10]).

The Figure 4.2 displays a graph depicting the relationship between voltage, power, and current for a PEM fuel cell. Notably, as the current density increases,

there is a corresponding reduction in the open circuit voltage. The maximum output current of the fuel cell is depending on the current density of the membrane multiplied by the membrane's surface area. Simultaneously, the fuel cell's output voltage is determined by the voltage of a single cell multiplied by the total number of stacked cells. Furthermore, it's crucial to recognize that the fuel cell's power output can be adjusted within a specified range, known as the load-following region, by regulating the rate of fuel flow. The power output of the fuel cell is intricately linked to factors such as temperature, pressure, and humidity. Consequently, dynamic control of these parameters is imperative to achieve optimal efficiency in fuel cell operation [12].

The power density curve is derived from the I-V curve by calculating the product of the voltage at each point along the I-V curve with its corresponding current density. The power density of a fuel cell tends to rise with the increment of current density, reaching a peak value before declining at higher current densities. Typically, fuel cells are constructed to function at or below this maximum power density threshold. When operating at current densities below the maximum power density, the voltage efficiency tends to improve; however, the power density decreases. Conversely, as current densities surpass the maximum power density level, both the voltage efficiency and power density exhibit a decline.

## 4.3 METHODOLOGY

### 4.3.1 Design Process: SolidWorks Steps

The initial design of the main housing for the PEM cell is carried out using SolidWorks, a widely used computer-aided design (CAD) software in industries like aerospace, automotive, and energy. SolidWorks offers a robust set of tools and features for creating 3D models and performing simulations. Although the

specific application of SolidWorks in fuel cell design may vary based on specific requirements and design considerations, it provides various features such as extruded boss/base, extruded cut, swept cut, and plate modeling that can be employed in the design process. Additionally, SolidWorks can be integrated with other simulation software like COMSOL Multiphysics to analyze and optimize fuel cell designs. However, for the purposes of this report, SolidWorks was solely used to obtain a 3D representation of the PEM cell structure.

During the design process, a hexagonal shape was chosen for the housing to represent the 3D structure. It is important to note that the shape of the geometry is not a significant aspect discussed in this report, as it is solely based on the preferences.

Once the hexagonal shape was established, a depth was created using the extruded cut feature to serve as the active region of the cell. Additionally, distinct passages were created on both sides of the housing to facilitate inlet and outlet functions. To ensure a compact base, a fillet was added to the bottom portion of both the inlet and outlet passages.

In the centre of the active region, a hole was introduced to accommodate a current collector screw. The area surrounding the hole was extruded to enlarge the screw thread. Furthermore, to securely connect both sections of the housing, six screw holes with an equivalent radius of M6 were implemented. Finally, in one of the housing components, a portion was extruded, and a corresponding hole was created in the other housing component to facilitate the assembly and connection of both parts.

The top view, side view and bottom view of the 3D designed housing has been reported in Figure 4.3 and Table 4.1 with sufficient labelling and dimensioning of the distinguishable structures.

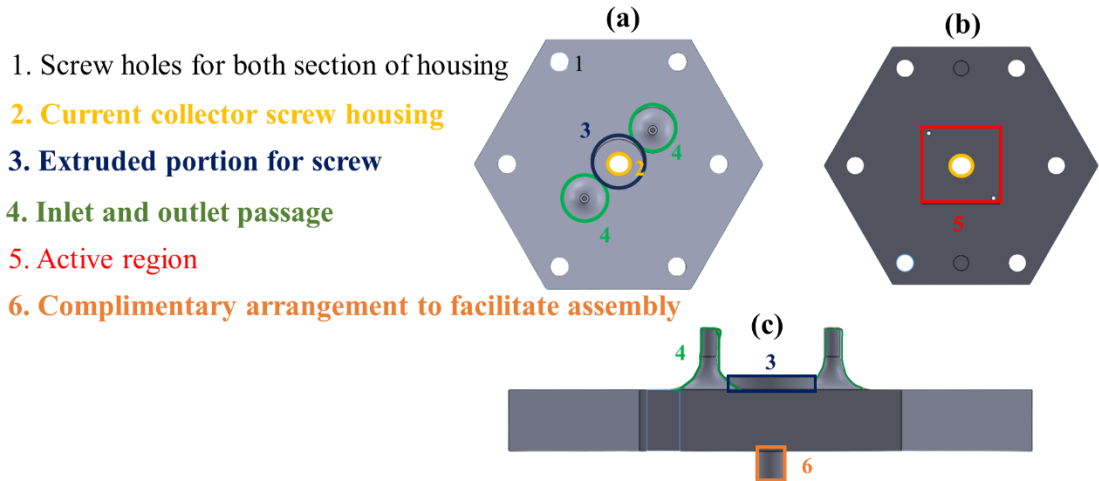


Figure 4.3. Distinguishable structures of the housing of PEM cell.

Table 4.1. DIMENSIONING OF THE DISTINGUISHABLE STRUCTURES OF THE HOUSING.

Structure features	Dimensions and Unit
Length of each arm of hexagonal shape	63.5 mm
Diameter of screw hole	8 mm
Diameter of current collector screw hole	10.5 mm
Extruded height for current collector screw	8 mm
Outer diameter of inlet and outlet	4 mm
Inner diameter of inlet and outlet	2 mm
Area of active region	1260.25 mm <sup>2</sup>
Depth of active region	5 mm
Height and depth of extruded portion of complementary arrangement of both segment	6 mm

## **4.3.2 Fabrication and Assembling**

### **4.3.2.1      *Base***

In a PEM fuel cell, the "base" is the foundation or structure that supports and contains the different parts of the fuel cell. This includes the proton exchange membrane, electrodes, catalyst layers, and gas diffusion layers. The base material must possess qualities such as strong mechanical properties, chemical stability, and electrically isolated to enable the fuel cell to operate efficiently. It is crucial for the base material to be compatible with the other components of the fuel cell, like the membrane and electrodes, to ensure proper functioning and prevent any issues such as leakage or deterioration. The design that has been made into Autocad was printed by using 3D printing. We used Artillery Sidewinder X2 3D Printer which was available in our lab. The Artillery Sidewinder X2 3D Printer is known to be compatible with a wide range of materials for 3D printing. Based on the available information, here is a list of materials that are commonly used and compatible with the Sidewinder X2 [13]:

1. PLA and Tough PLA
2. ABS
3. PETG and CPE
4. ASA
5. Nylon
6. TPU and TPE
7. Carbon fiber-infused NylonX filaments (with upgrades)

These materials provide a variety of properties and characteristics, making them suitable for different applications and requirements in 3D printing. However, it's important to note that the specific compatibility and optimal settings for each material may vary. For our experiment we have used Carbon fibre infused NylonX filaments. A picture of Artillery Sidewinder X2 3D in lab can be shown

in Figure 4.4 and the pictures of our experimental PEM fuel cell's bas is presented at Figure 4.5.



Figure 4.4. Artillery Sidewinder X2 3D Printer.

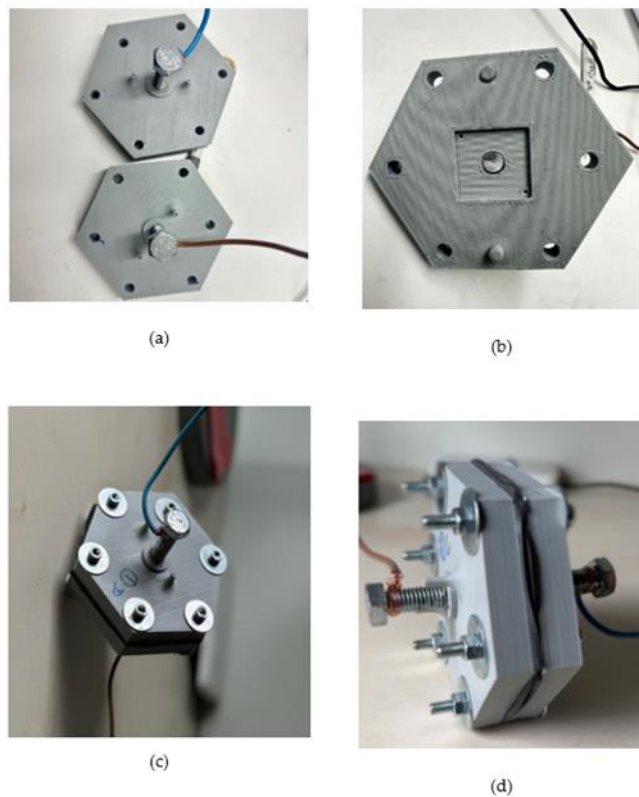


Figure 4.5. Different views of 3D printed base.

#### 4.3.2.2 Screw

We have used M-6 screw for coupling the both sides of the fuel cell and M-8 as current collector which can be shown at Figure



Figure 4.6. M-6 screw.

**Current Collector:** We have used a metallic plate to collect the electron from electrode. Here one thing should be noted the metallic plate should of same size of active region.

#### 4.3.2.3 *Carbon Paper*

The carbon paper electrode is an important component in a PEM fuel cell as it enables the movement of electrons during the fuel cell's operation. It acts as a conduit for the electrons generated at the anode to travel to the cathode, where they combine with protons and oxygen to generate water and release energy. The water content of this kind of membrane determines its ionic conductivity; a dry membrane has less ionic conductivity and hence more ohmic voltage loss. Practically speaking, external humidifiers are typically designed to increase membrane hydration by humidification Carbon paper, which is typically composed of carbon fibres or carbon nanotubes embedded in a matrix, is chosen as a conductive material for fuel cell electrodes due to its beneficial properties[14]. These include excellent electrical conductivity, strong mechanical properties, and a large surface area that allows for effective catalyst deposition.

To provide the carbon paper a catalyst support, it has been coated with mixer compromised of 5% Nafion Resin, and PTC 40% which was later liquifies by 2-Propoanol. These can be observed on Figure 4.7.

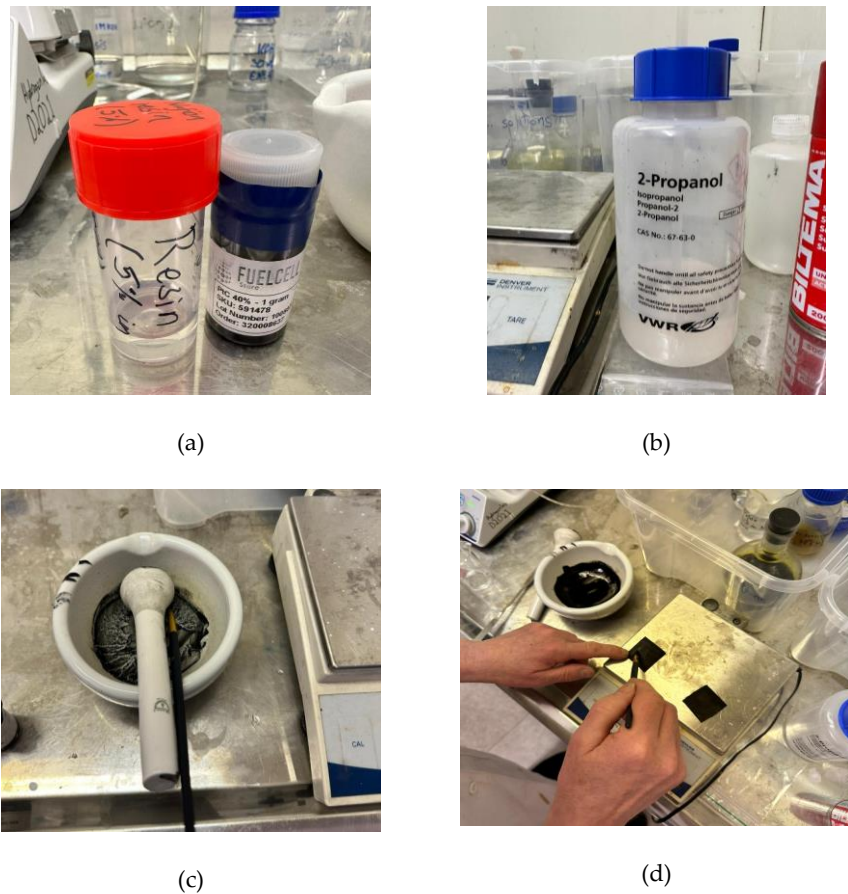


Figure 4.7. (a) 5% Nafion Resin and PTC 40% (b) 2-Propoanol (c) Mixer of 5% Nafion Resin and PTC 40% (d) Platinum Catalyst Coating of Carbon Paper.

#### 4.3.2.4 Nickel Foam

The utilization of nickel foam in PEM fuel cells serves various crucial purposes. Initially, it functions as a flow field structure, ensuring the uniform distribution of reactants over the electrode surface, thereby enhancing overall performance. Its thermal conductivity allows for efficient dissipation of heat, which is vital in maintaining the ideal operating temperatures and preventing overheating. Moreover, nickel foam plays a significant role in managing water within the fuel cell, facilitating the effective distribution and removal of excess water to prevent flooding and ensure optimal operation [15].



Figure 4.8. Current collector, Nickel Foam, Carbon Paper from left to right.

#### 4.3.2.5 *Nafion*

Nafion membranes are integral to the operation of PEM fuel cells as they serve as a crucial separator between the anode and cathode compartments. These membranes are highly preferred in fuel cell applications due to their desirable properties, including thickness, conductivity, strength, resistance to water uptake, and chemical durability. Nafion membranes are made into thin, flexible sheets, with a transparent appearance similar to kitchen film and a thickness of approximately 0.05 mm (50  $\mu\text{m}$ ). The original invention of Nafion was by Dupont. Overall, Nafion membranes play a critical role in PEM fuel cells by providing effective separation and contributing to their efficient and reliable operation [16].

We have humidified Nafion before using it in PEM cell. This process is crucial for maintaining the optimal water content within the membrane, consequently lowering the activation barrier. Water plays a pivotal role in promoting proton transfer across the membrane, facilitating efficient electrochemical reactions at the electrodes. We have used 1 molar  $\text{H}_2\text{SO}_4$  as protonic solution and the nafion was submerged into the solution. The solution was heated up to  $90^\circ$  for complete the whole process of humidification. Proper

humidification is necessary to ensure optimal performance and longevity. The process is shown at Figure 4.9.

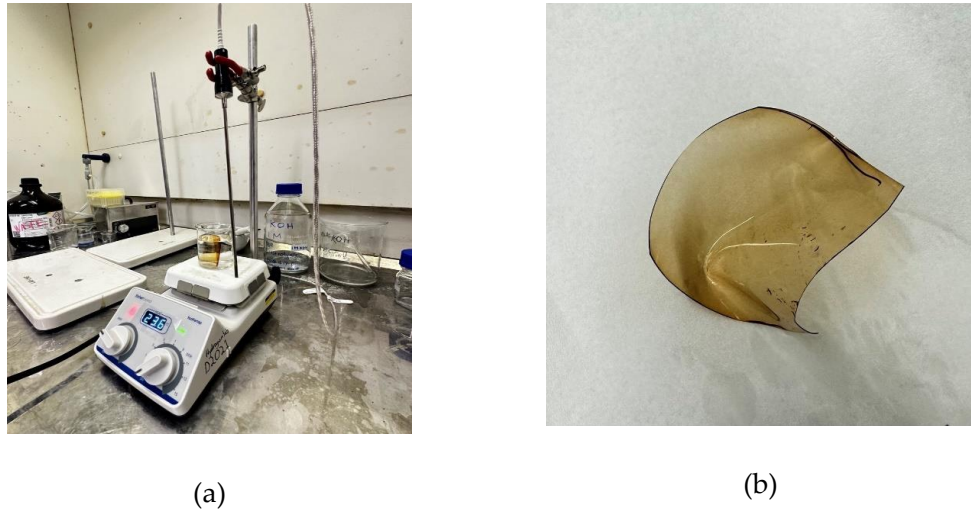


Figure 4.9. (a) Humidification process of Nafion (b) Nafion after humidification.

#### 4.3.2.6 Gasket

An insulation layer known as a gasket is utilized in a PEM (Proton Exchange Membrane) fuel cell stack to prevent fuel leakage. This component serves the purpose of sealing and maintaining the separation of different sections within the fuel cell, ensuring that the reactant gases remain within their designated areas. The gasket's primary role is to prevent gas leakage, thereby upholding the fuel cell stack's efficiency, reliability, and overall performance. It is typically positioned between various components of the fuel cell, including the membrane electrode assembly (MEA), bipolar plates, and end plates. By creating a secure seal, gaskets prevent the mixing of reactant gases, enabling the electrochemical reactions to take place solely within their intended regions. We have made our own Gasket at lab which can be shown at Figure 4.10.



Figure 4.10. Gasket

The complete structure of the PEM cell is presented in Figure 4.11,

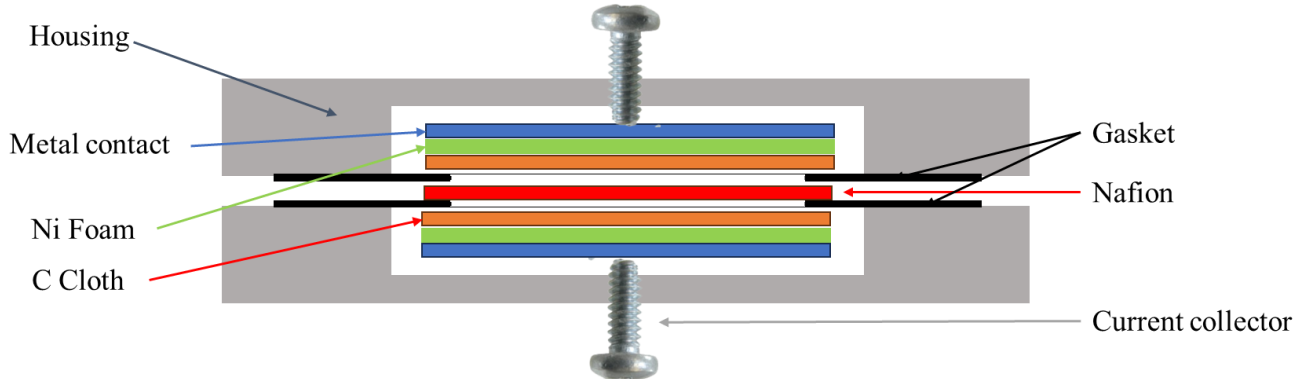


Figure 4.11. Complete structure of the PEM cell.

### 4.3.3 Experimental setup

1. For the experiment initially the Hydrogen fuel cell was supplied from a tank. The pressure of the fuel cell was controlled by a barometer.
2. Then at the table we set up our PEM fuel Cell.
3. A flow controller called Teledyne managed the flow rate and the supply of hydrogen and oxygen via the input and output passages.
4. The anode side of the system received a flow of hydrogen, while the cathode side received a flow of air.

5. The load that we employed was a resistance box. We have seen the fuel cell's I-V and I-P properties by changing the resistance.
6. The cell was further humidified with distilled to obtain a better Ion-Exchange behavior. To get rid of excess water the cell was injected with dried air.

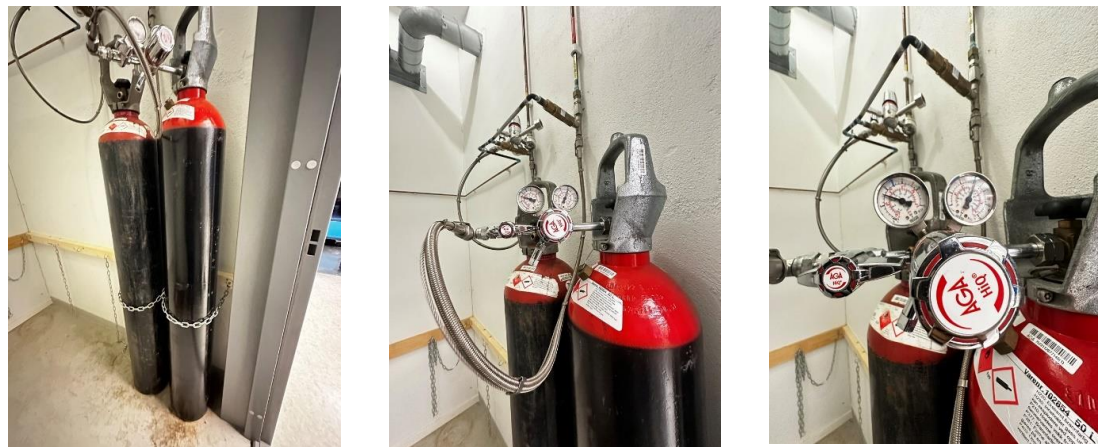


Figure 4.12. Hydrogen Fuel Tank

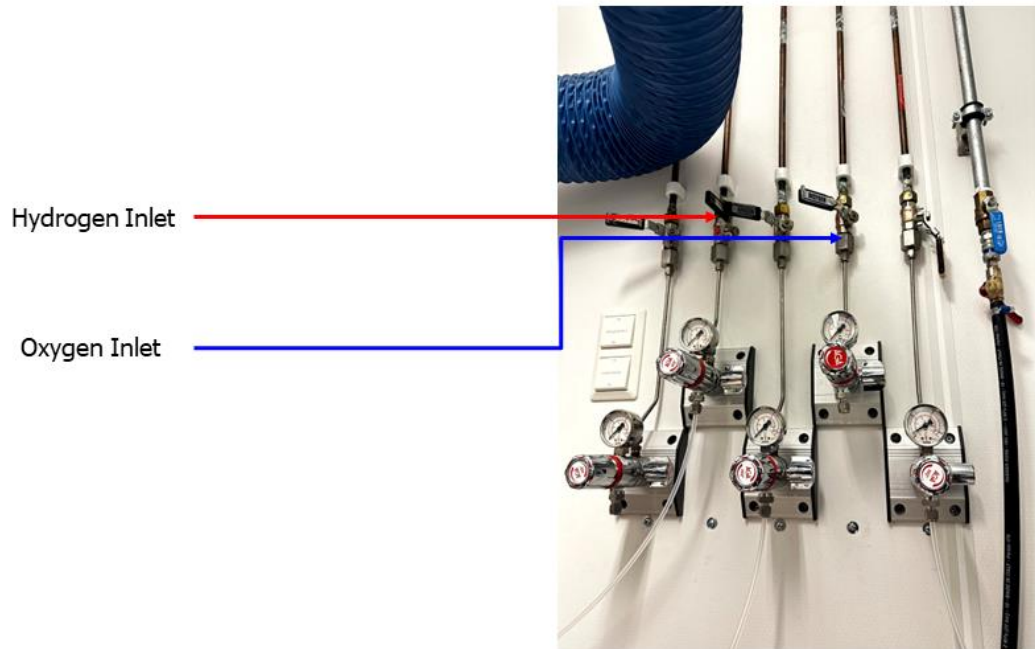


Figure 4.13. Hydrogen and Oxygen Inlet.

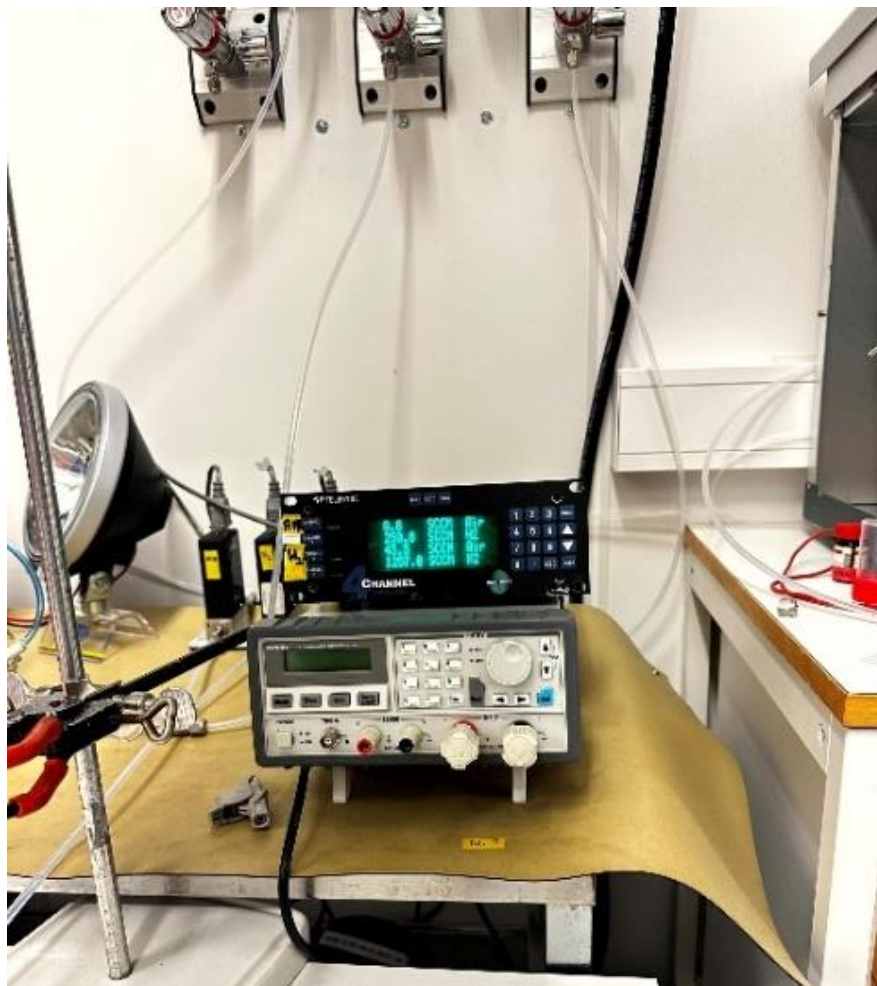


Figure 4.14. Control of H<sub>2</sub> and O<sub>2</sub> flow to the PEM cell.

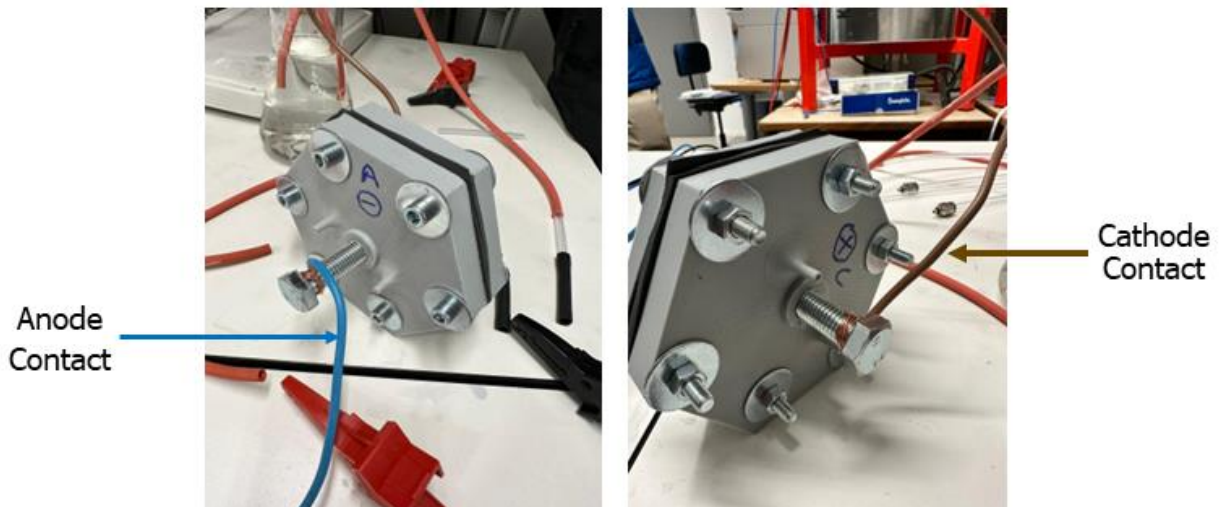


Figure 4.15. PEM fuel cell anode and cathode contact.

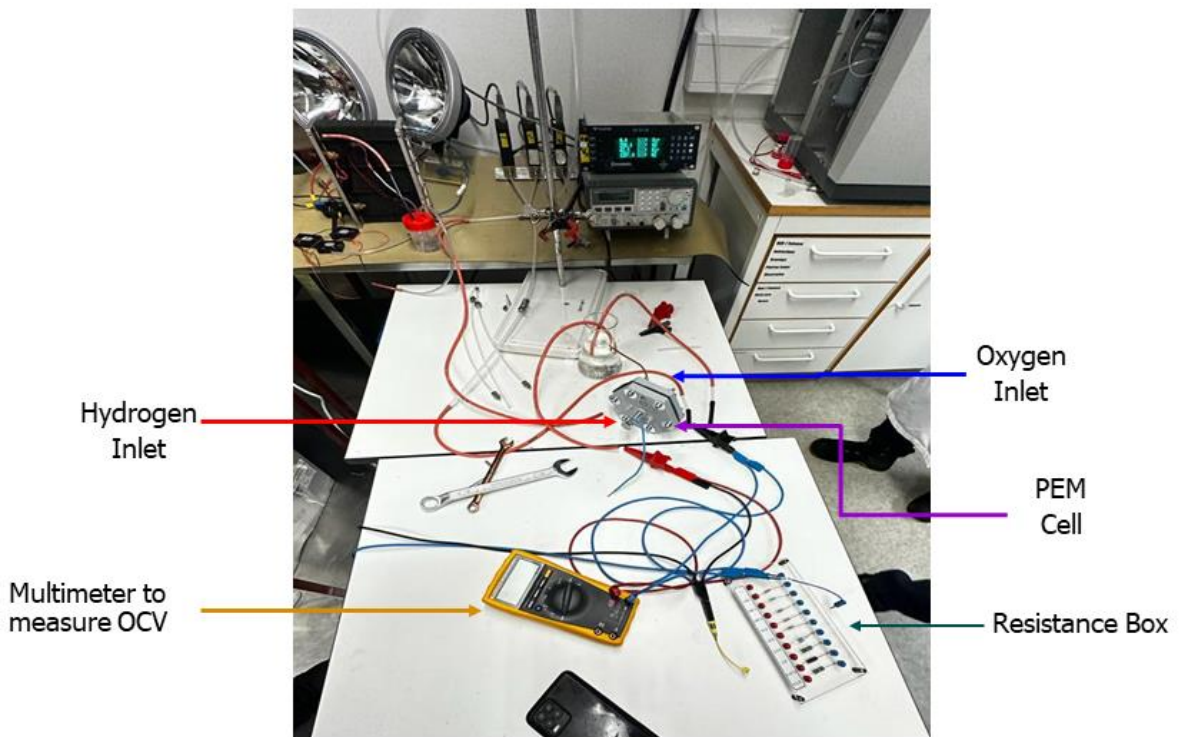


Figure 4.16. Experimental Setup.



Figure 4.17. Humidification of Fuel Cell.

#### 4.4 RESULT AND ANALYSIS

In the experiment, the fuel cell was tested three times with the identical test setup just under different test cases as stated below.

**Test 1:** Humidifying the Nafion with the 1M  $H_2SO_4$  solution.

**Test 2:** After the initial humidifying process the Nafion is further humidified with distilled water.

**Test 3:** Drying the Nafion by blowing air through the inlets.

The test results are tabulated in Table 4.2,

Table 4.2. TABULATED DATA OBTAINED FROM THE TEST CASES.

R	Test 1			Test 2			Test 3		
	V	I	P	V	I	P	V	I	P
inf	0.823	0	0	0.716	0	0	0.786	0	0
1000	0.738	0.000738	0.00054	0.71	0.00071	0.0005041	0.773	0.000773	0.00059752
330	0.689	0.00208	0.00143	0.698	0.0021151	0.001476376	0.751	0.002275758	0.00170909
100	0.622	0.00622	0.00386	0.667	0.00667	0.00444889	0.707	0.00707	0.0049984
33	0.54	0.01636	0.00883	0.608	0.0184242	0.011201939	0.644	0.019515152	0.01256775
10	0.413	0.0413	0.01705	0.5	0.05	0.025	0.544	0.0544	0.029593
3.3	0.266	0.08060	0.02144	0.366	0.1109090	0.040592727	0.419	0.126969697	0.05320030
1	0.138	0.138	0.01904	0.234	0.234	0.054756	0.242	0.242	0.058564
0.47	0.08	0.17021	0.01361	0.122	0.2595744	0.031668085	0.152	0.323404255	0.0491574
0.1	0.025	0.25	0.00625	0.037	0.37	0.01369	0.051	0.51	0.02601

The resulting IV (Current-Voltage) curves obtained from the three test cases are presented in Figure 4.18. Upon observation of Figure 4.18 and Table 4.2, it is evident that the highest Open Circuit Voltage (OCV) was obtained in test case 1 (0.83 volt), followed by a significant drop in test case 2 (0.71 volt), and a slight recovery in test case 3 (0.786 volt). The OCV provides an indication of the electrochemical potential of the fuel cell. It represents the voltage generated by the cell when there is no external load connected. The OCV is a key factor in determining the efficiency of the fuel cell. It represents the maximum voltage that can be obtained from the cell under ideal conditions. By comparing the OCV to

the actual voltage output during operation, the efficiency of the fuel cell can be assessed. However, it is important to note that the expected OCV should ideally be around 0.9-1 volt, as per theoretical expectations. It should be acknowledged that minute internal currents resulting from electron conduction can cause a slight reduction in cell voltage. Notably, in practical fuel cells, the diffusion of hydrogen from the anode to the cathode through the electrolyte can occur. This hydrogen reacts with oxygen present on the cathode catalyst, consuming it and resulting in no current generation from the cell. This migration of fuel through the electrolyte is known as "fuel crossover" and contributes to wasted fuel.

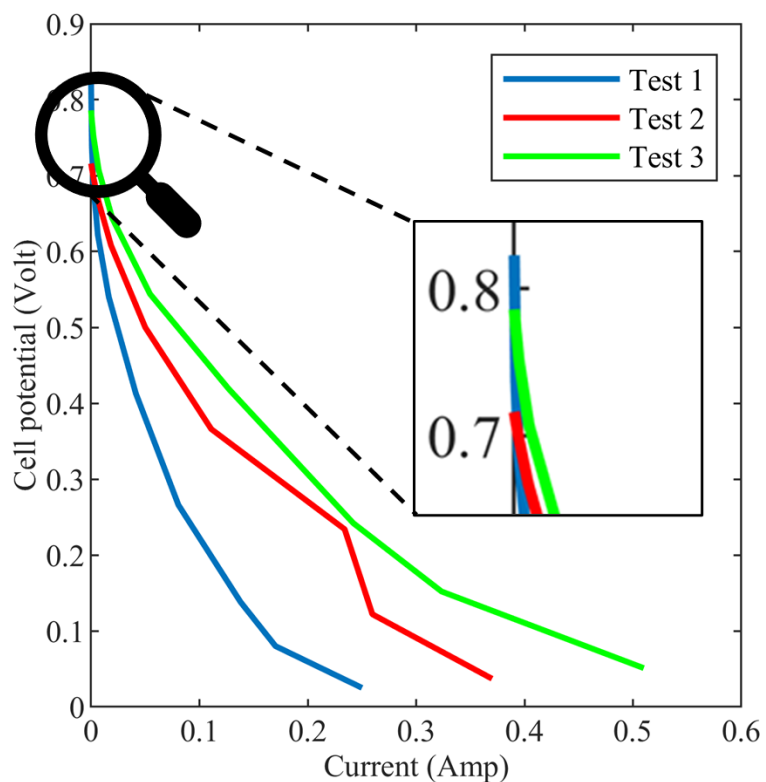


Figure 4.18. IV characteristics of the PEM cell under three different test cases.

Another factor that can contribute to the reduction in OCV is the flooding effect in PEM fuel cells. Flooding effect refers to the accumulation of excessive liquid water within the cell, primarily in the gas diffusion layer and catalyst layer regions. This accumulation hampers the flow of reactant gases and impedes the electrochemical reactions, leading to decreased performance and efficiency of the

cell. The presence of excess water blocks the reactant gas flow channels, limiting the availability of reactants at the catalyst sites. Consequently, this diminishes the supply of reactants required for the electrochemical reactions, resulting in reduced cell voltage and power output. Furthermore, the accumulation of excess water also increases the electrical resistance within the cell, further impacting its overall performance [1].

The flooding effect can be caused by various factors, including high humidity, excessive water production during electrochemical reactions, and inadequate water management within the fuel cell system. Operating conditions such as temperature, pressure, and gas flow rates can also influence the occurrence of flooding. Based on our assumption, the excessive flooding of water prior to test case 2 caused an overflooding effect in the tested cell. Additionally, there was some evidence of fuel crossover, possibly due to undesired leakage in the gasket or non-uniform pressure applied through the screws.

The resulting I-P (Current-Power) curves for the test cases are depicted in Figure 4.19. It is worth noting that a slight deviation in the behaviour of the I-P curves has been observed. As mentioned earlier, test case 1 exhibits the highest Open Circuit Voltage (OCV) among the test cases. Intuitively, one would expect test case 1 to demonstrate the most power-efficient behaviour. However, interestingly, as indicated in Table 4.2, the voltage drops in test case 1 decreases abruptly to a lower value.

This unexpected behaviour can potentially be attributed to the humidification of the cell prior to test case 2. It is possible that the internal resistances associated with the contact of layers were reduced, resulting in a lesser voltage drop. Consequently, this increased the rate of current flow through

the external lead and subsequently enhanced the power output in the latter two test cases.

However, it's worth noting that the maximum extractable power from the test cases is recorded as 0.021441-watt, 0.054756 watt, and 0.058564 watt, respectively.

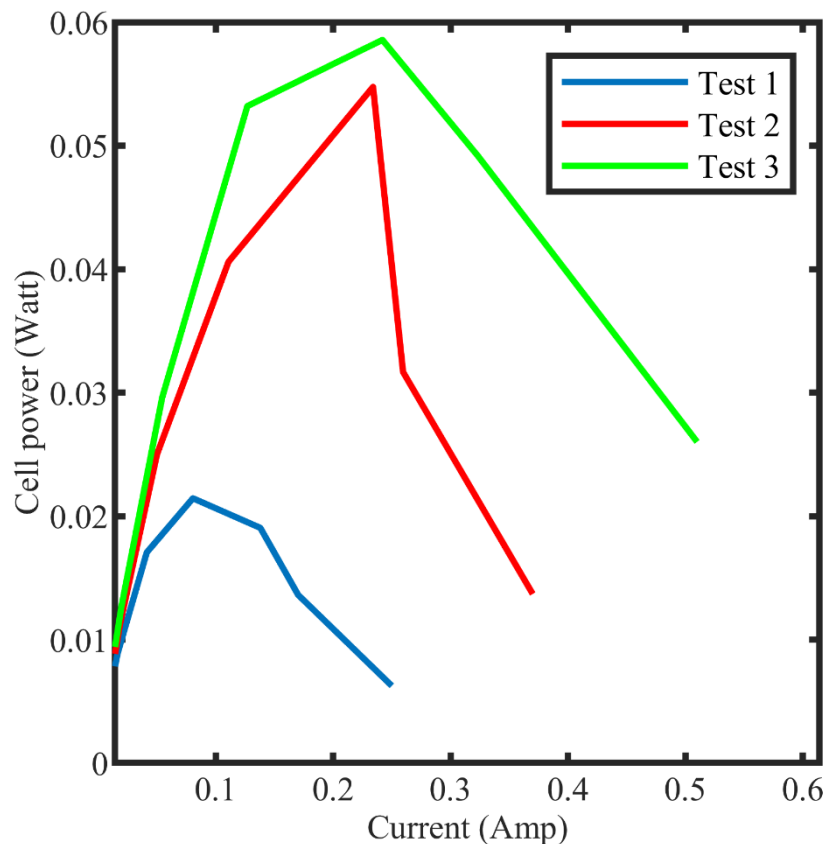


Figure 4.19. I-P characteristics of the PEM cell under three different test cases.

#### 4.5 CONCLUSION

In this report, from designing to fabrication, assembly, and testing of a basic single-cell PEM fuel cell is presented. Subsequently, the assembled cell underwent rigorous experimental testing to evaluate its performance and behavior.

Upon conducting IV testing with a resistance box, it was observed that the Open Circuit Voltage (OCV) of the cell exhibited fluctuations ranging from 0.7 volt to 0.83 volt during the testing phases. This fluctuation deviated from the expected OCV of approximately 0.9 volt. The detrimental characteristics displayed by the cell can be primarily attributed to two factors: fuel crossover and flooding effect. These issues arose due to inadequate prevention of leakage within the cell, leading to the undesirable mixing of reactants and excessive accumulation of liquid within the cell.

Additionally, an anomaly in the I-P (Current-Power) behavior of the cell was also observed. This anomaly was caused by the introduction of distilled water into the inlet and outlet passages, resulting in flooding within the cell. This excess water disrupted the reactant supply and hindered the electrochemical reactions, contributing to the observed irregularities in the I-P behavior. These findings underscore the importance of effective prevention of leakage and proper water management to ensure optimal performance and behavior of PEM fuel cells.

# Chapter 5: References

---

- [1] D. A. J. R. Andrew L. Dicks, *Fuel cell systems explained*, 3rd ed. Wiley, 2018.
- [2] A. C. Lazanas and M. I. Prodromidis, "Electrochemical Impedance Spectroscopy—A Tutorial," *ACS Meas. Sci. Au*, vol. 3, no. 3, pp. 162–193, 2023, doi: 10.1021/acsmeasuresciau.2c00070.
- [3] F. T. Bacon, "Fuel cells, past, present and future," *Electrochim. Acta*, vol. 14, no. 7, pp. 569–585, Jul. 1969, doi: 10.1016/0013-4686(69)87042-8.
- [4] A. J. Appleby, "Fuel cell technology: Status and future prospects," *Energy*, vol. 21, no. 7–8, pp. 521–653, Jul. 1996, doi: 10.1016/0360-5442(96)00030-8.
- [5] I. R.-P. of the S. on Diaphragms and undefined 1986, "Modified gas diffusion electrode for proton exchange membrane fuel cells," *books.google.comID RaistrickProceedings Symp. Diaphragms, Separators, Ion*, 1986•books.google.com, Accessed: Nov. 23, 2023. [Online]. Available: <https://books.google.com/books?hl=en&lr=&id=CcjAAAAMAAJ&oi=fnd&pg=PA172&ots=zub3oL2tX9&sig=VEpZqIEQ94IWvdA-MISIGRI42hg>.
- [6] M. S. Wilson, "Membrane catalyst layer for fuel cells," Dec. 20, 1991.
- [7] S. Gottesfeld and J. Pafford, "A New Approach to the Problem of Carbon Monoxide Poisoning in Fuel Cells Operating at Low Temperatures," *J. Electrochem. Soc.*, vol. 135, no. 10, pp. 2651–2652, Oct. 1988, doi: 10.1149/1.2095401/XML.
- [8] Y. Wang, "Porous-Media Flow Fields for Polymer Electrolyte Fuel Cells: II. Analysis of Channel Two-Phase Flow," *J. Electrochem. Soc.*, vol. 156, no. 10, p. B1134, Jul. 2009, doi: 10.1149/1.3183785.
- [9] Y. Wang, D. F. Ruiz Diaz, K. S. Chen, Z. Wang, and X. C. Adroher, "Materials, technological status, and fundamentals of PEM fuel cells – A review," *Mater. Today*, vol. 32, no. February, pp. 178–203, 2020, doi: 10.1016/j.mattod.2019.06.005.
- [10] B. Lee, P. Park, K. Kim, and S. Kwon, "The flight test and power simulations of an UAV powered by solar cells, a fuel cell and batteries," *J. Mech. Sci. Technol.*, vol. 28, no. 1, pp. 399–405, Jan. 2014, doi: 10.1007/S12206-013-0936-7.
- [11] M. M. Tellez-Cruz, J. Escorihuela, O. Solorza-Feria, and V. Compañ, "Proton exchange membrane fuel cells (Pemfcs): Advances and challenges," *Polymers (Basel.)*, vol. 13, no. 18, Sep. 2021, doi:

10.3390/POLYM13183064.

- [12] S. Haji, "Analytical modeling of PEM fuel cell i–V curve," *Renew. Energy*, vol. 36, no. 2, pp. 451–458, Feb. 2011, doi: 10.1016/J.RENENE.2010.07.007.
- [13] "Artillery Sidewinder X2 Review: A Refined Sidewinder X1? | 3D Print Beginner." <https://3dprintbeginner.com/sidewinder-x2-review/> (accessed Nov. 23, 2023).
- [14] S. Waseem, P. H. Maheshwari, S. Abinaya, A. K. Sahu, A. Saini, and S. R. Dhakate, "Effect of matrix content on the performance of carbon paper as an electrode for PEMFC," *Int. J. Energy Res.*, vol. 43, no. 7, pp. 2897–2909, Jun. 2019, doi: 10.1002/ER.4432.
- [15] S. Huo *et al.*, "Elucidating the operating behavior of PEM fuel cell with nickel foam as cathode flow field," *Sci. China Technol. Sci.*, vol. 64, no. 5, pp. 1041–1056, 2021, doi: 10.1007/s11431-020-1767-5.
- [16] P. C. Okonkwo, I. Ben Belgacem, W. Emori, and P. C. Uzoma, "Nafion degradation mechanisms in proton exchange membrane fuel cell (PEMFC) system: A review," *Int. J. Hydrogen Energy*, vol. 46, no. 55, pp. 27956–27973, Aug. 2021, doi: 10.1016/J.IJHYDENE.2021.06.032.

# Chapter 6: Acknowledgement

---

We would like to extend our heartfelt appreciation to Professor **Peter Hugh Middleton** and PhD researcher **Antoine de Padoue Shyikira** for their invaluable guidance and unwavering support throughout our inaugural course on Hydrogen fuel cells. It has been an extraordinary journey for us, and it is both of you who have truly made this journey unforgettable. Your expertise and dedication have profoundly contributed to our understanding and learning in this complex field.

Furthermore, we would like to express our gratitude to the exceptional lab facilities of UiA, which have provided us with the necessary resources to conduct experiments and gain practical experience. The opportunity to work in such well-equipped labs has enhanced our learning and enriched our understanding of Hydrogen fuel cells.



In closing, we would like to extend our heartfelt wishes to Professor Hugh Middleton for his future endeavors beyond teaching. His passion for education and unwavering commitment to nurturing students like us have been a constant source of inspiration. We are honored to have been the last group of students to experience the privilege of having our Carbon cloth coated with the catalyst under your academic guidance.

Once again, we express our deepest gratitude for your guidance and support, and we wish both of you continued success and fulfillment in all your future endeavors.

Sincerely,

Md Iftekher Hossain, Opy Das and Anfaj Islam